UNIVERSITY OF CALIFORNIA SAN DIEGO

Eastern Pacific bivalve shell calcification in a warming and acidifying ocean.

A Dissertation submitted in partial satisfaction of the requirements
for the degree Doctor of Philosophy

in

Biology

by

Elizabeth Marie Bullard

Committee in charge:

Kaustuv Roy Chair
Thomas Deméré
Olivia Graeve
Joshua Kohn
Carolyn Kurle
Jonathan Shurin

2022

The Dissertation of Elizabeth Marie Bullard is approved, and it is acceptable in quality and form for publication on microfilm and electronically.

University of California San Diego

2022

DEDICATION

To my father, Ted Bullard, who loved & revered the natural world more than anyone else. Thank you, Dad, for passing that wonder, awe, and curiosity onto me. I'll work hard to be a living legacy to our leader of the band.

TABLE OF CONTENTS

LIST OF FIGURES

Chapter 1

Chapter 2

Chapter 3

LIST OF TABLES

Chapter 1

Chapter 2

Chapter 3

ACKNOWLEDGEMENTS

Some people are blessed with money and beauty. I've been blessed with wonderful people. So many hands, minds, and hearts contributed to this work – whether directly or through their emotional support – and I will forever be grateful for it all.

I'd first like to thank all my committee members for their wisdom, insightful questions and support over the years. Thank you to Carolyn for giving me the affirmation to be my authentic, aligned self. To Jon for all of his time, advice, and support to help me make my projects that much more impactful. To Josh for standing up for me and cheering me on, to Tom for holding down the fort on paleo knowledge and providing me with access to samples to do my third chapter. Most especially a big thank you to Dr. Olivia Graeve for so many things – being the most phenomenal co-author, sharing her network and helping to expand my PhD, always making time for me to work through problems and get things done right, and for being an incredible role model and mentor as a powerful and empathetic woman in STEM on a mission to change the world. I have learned so much from watching you and being supported by you – thank you a million times over.

I'd also like to thank my other co-authors and people that I've worked with through the years. A huge thank you to Nick for all his support and knowledge on structural engineering as well as to Maroun and Florian for helping me carry out all my functional tests. Thank you to Arash, Ved, and Ivan for tirelessly helping me by running samples, Tianqi for more time than we ever thought we'd have to spend to figure out how to analyze XRD data, Garfield for all our experiment madness and for constantly cheering me on at every step of my PhD, and to all the

undergrads who helped me to collect data but most especially to Minerva & Andrea for your dedicated effort – thank you all.

Thank you to the three museums that opened their doors for me to collect data in. To the Santa Barbara Museum of Natural History, Natural History Museum of Los Angeles, and a huge thank you to the San Diego Natural History Museum & Pat and Kesler.

I'd like to also extend a big thank you to the other EBE students I had the pleasure of sharing space with over the years. Especially to Marika & her brilliance board wisdom, Steph, Liz, and Alena for being awesome cohort compatriots, Dillon, Hank, Ugbad, Hannah, and Dani for being absolutely amazing resources and support systems. I'd also like to thank Alyona and Joanna for all the work they did for all of us and to Sarah Stockwell for being the most incredible teaching mentor and person. Thank you also to the Roy Lab Fam members Kayla, Maddie, and Ian for everything from forming secret societies to blasting BTS and always being down to look for clams with me (and never getting upset when we didn't find any).

Thank you to all those at Engaged Teaching who have made me a better person and teacher. To Kirk, Rachel Fox, Avaneesh, and Abdullah – you all have become friends I am so grateful for and you made the pandemic more than bearable for me. To Erilynn – words will never be able to express what you have done for me – and for all of us – just by being the incredible human being that you are. Your kindness is beyond anyone else I know and you have created the safest space I have ever been in with the GTC community. Thank you for giving me a place to heal and be myself within academia.

Thank you to my friends who have been on this wild journey with me. To the Gal Pals – Julia, Jani, and Allison who have worked to pave a path forward for me and cheer me on as I follow after their monumental examples. You three ladies are a core part of why I was able to do

a PhD and were one of the greatest gifts I have received through this entire process. I love you all so much. To Brittany for being the best person to bemoan the state of the world with and for driving down from LA so often to see me, to Marina for introducing me to the world of astrology, to Shannon for being my favorite walking + sushi buddy & for inspiring me to be a better ally, to the BAM fam members Matt & Athina for weathering the hardest parts of the pandemic with me, and to Kelsey for not just being a friend but also sharing your family with me so I always had a place to go during the holidays. Special thank you to Madison for becoming one of my very favorite people ever during this long journey and of course the greatest thank you goes to Chandler – this ain't our first rodeo, it won't be our last, and I can't imagine ever doing this without you.

A big thank you to my family for all the love, support, and encouragement they have given me. To my mom, Nancy, for always telling me, 'The world is your oyster!' so I believed I was capable of anything. To Kathleen for always calling me her, 'rock star' and working to keep up with everything I am doing, to Graydon for reminding me every chance he got that I was a nerd…but also that he was proud of me. To Laura for your quiet but fervent cheering and belief in me, to Cody for the rain ponchos I ironically ended up needing when I moved to San Diego, and to Brad for always wanting to talk about nature. Thank you also to the kids: Jake, Ben, Megan, Lily, and Henry; I am the luckiest aunt in the world for having you all in my life. I'd also like to thank all the Polzers but especially my grandmother, Ruth, for instilling in all of us a love of the ocean and shells, to Aunt Kathy for sharing her love of birds with me and inspiring me to keep my eyes and ears open to the beauty of the natural world, to Aunt Elaine for her support and example, and to Aunt Mary for her deep love. Thank you also to my Aunt Linda & Uncle Leroy, but especially Aunt Linda, for constantly doing everything she could the last eight years to make

my life even a tiny bit easier. Thank you to Dana & Hailee for becoming like sisters and forming the best quad of all time. Finally, the greatest thank you goes to Anna and Ashley. If soulmates are a thing, you two are it for me. To Anna – for being the pancake to my sausage, for being able to communicate telepathically & through random sounds & pics, and even for pushing me out first so you could have your own 'womb' for a while, you have never failed to make me laugh, inspired me to be better and reach for more, and given the most sage and thoughtful advice. And to Ashley for being my person, for always being down to go on an adventure with me (even if it ends with us almost dying), for having the identical sense of humor, for weathering the harshest of storms together, and for being my Tohru – thank you for being you.

To the cornerstones of my PhD, Kaustuv & Alex - none of this would have been possible without you two. Beyond a thank you or acknowledgement, any success I had during my PhD was the result of both of you spending your time, effort, and energy to help me make it happen. To Kaustuv for always making time to talk through a random idea or work through a problem I was having, to encouraging me to be more assertive and confident, and to training me to be scientist & critical thinker beyond what I thought I was capable of – thank you for being the most incredible advisor. To Alex for becoming my family and being the best friend and lab mate anyone could ask for – I never would have made it without you.

My last blessing inspires this truth: I am a scientist because my father was a scientist. He may not have had a degree or letters after his name, but to this day, I have never met anyone who loved and pondered nature as much as my Dad. Whether it was following behind him and learning the names of birds, fish, and trees or forming hypotheses around how long it takes a drop of ocean water to circulate the planet, my Dad was always quietly and powerfully engaging with nature and encouraging us to treat her as a living entity that deserved our stewardship and

respect. I am beyond thankful for the sacrifices my father made for me, and for all four of us, so that we could live a life very different than his. I'm also thankful for the lessons he left behind, for being a phenomenal role model, and for the deep love he shared with all of us. As I end a journey he started me on and feel the loss of his presence even more than normal, I can only imagine the questions he would have asked about my work, the joy he would have found in visiting my field sites, and the insights he would have had. I bet though, if he was still here, after reading through everything I had done and receiving my PhD he would simply say, "Well, even a blind squirrel can find a nut".

Finally, I'd like to extend a thank you to the clams and mussels that made it possible for me to do my research. No offering I gave will ever equal what I was given, and I want to acknowledge that.

Chapter 1, in full, is a reprint as it appears in Bullard et al. 2021. Bullard, E.M, Torres, I., Ren, T., Graeve, O.A., Roy, K. 2021. Shell mineralogy of a foundational marine species, *Mytilus californianus*, over half a century in a changing ocean. *PNAS*, 118 (3), 1-5. The dissertation author was the primary investigator and author of this paper.

Chapter 2, in part, is currently being prepared for submission for publication of the material. Bullard, E.M., Abi Ghanem, M., Yazdani, A., Allein, F., Graeve, O.A., Boechler, N., Roy, K. Functional consequences of changing shell calcification traits in response to anthropogenic climate change in a foundational marine bivalve. The dissertation author was the primary researcher and author of this material.

Chapter 3, in part, is currently being prepared for submission for publication of the material. Bullard, E.M., & Roy, K. Temporal trends in shell calcification in the Veneridae: using

paleontological baselines to understand species-specific responses in a changing ocean. The dissertation author was the primary researcher and author of this material.

VITA

2012 Bachelor of Science in Biology & Geology, Muskingum University

2016 Master of Science in Geology, University of Cincinnati

2022 Doctor of Philosophy in Biology, University of California San Diego

PUBLICATIONS

Bullard, E.M, Torres, I., Ren, T., Graeve, O.A., Roy, K. 2021. Shell mineralogy of a foundational marine species, *Mytilus californianus*, over half a century in a changing ocean. *PNAS*, 118 (3), 1-5.

Bullard, E.M., Yanes, Y., Miller, A.I. 2017. Compositional variability of Pleistocene land snail assemblages preserved in a cinder cone volcano from Tenerife, Canary Islands. *Palaeogeography, Palaeoclimatology, Palaeoecology*, 471, 196-208.

ABSTRACT OF THE DISSERTATION

Eastern Pacific bivalve shell calcification in a warming and acidifying ocean.

by

Elizabeth Marie Bullard

Doctor of Philosophy in Biology

University of California San Diego, 2022

Professor Kaustuv Roy, Chair

Models suggest that marine calcifiers (organisms that precipitate a calcium carbonate exoskeleton) are especially vulnerable to anthropogenic ocean warming and acidification (Cooley and Doney 2009). Short-term experiments using marine calcifiers show that changes in these two stressors can affect physiology (Beniash et al. 2010), shell and soft body growth

(Kroeker et al. 2010), and shell function, (i.e., vulnerability of a shell to break under crushing predation (Fitzer et al. 2015b)). However, organism responses don't always have the same directionality (positive, negative, no change) or intensity (Ries et al. 2009) even when exposed to the same stressor. Furthermore, how short-term experiment results scale to longer time periods and across multiple generations remains poorly known.

My research evaluates how these traits associated with shell calcification vary across different climatic and environmental conditions at different temporal and spatial scales and what the functional cost of these trait shifts are. Specifically, I focus on traits associated with shell strength and dissolution prevention, such as mineralogy (Harper 2000), internal shell organics (Lopez et al. 2014, Telesca et al. 2019), and shell structure (Johnson 2020). I assess changes in these traits and their functional consequences across natural pH and temperature gradients both spatially and temporally. I do this in three distinct chapters: Chapter 1 assesses changes in shell mineralogy in response to warming and acidification over a 60 year period along the eastern Pacific in a foundational marine mussel (Bullard et al. 2021); Chapter 2 uses that same species to determine changes in internal shell organics and shell structure along a pH and temperature gradient and how these changing traits influence shell strength and toughness; and Chapter 3 evaluates long-term temporal changes (i.e., Pleistocene to today) in shell calcification of five closely related venerid species.

My research fills gaps in our knowledge about long-term responses of marine calcifiers to ocean warming and acidification. Additionally, it integrates multiple fields, such as paleontology and materials engineering, to fully capture trait changes and their functional consequences. Results of this work are useful for creating more accurate predictions about the responses of marine calcifiers to future conditions.

INTRODUCTION

Two threats to marine organisms under climate change are ocean warming and acidification (Cooley and Doney 2009, Kroeker et al. 2010). Ocean warming not only causes unpredictable movement of organisms into new regions as they respond to climatic changes (Jones et al. 2010), it also negatively impacts marine species' metabolic activity (Salas et al. 2014) and has been shown in some cases to synergistically augment the effects of ocean acidification (OA) (Findlay et al. 2010, Lischka and Riebesell 2012). OA results from the increase in dissolved anthropogenic carbon dioxide (pCO_2), and is of particular concern for marine calcifiers, such as bivalves, whose calcium carbonate skeletons are potentially vulnerable to reduced pH (Cooley and Doney 2009, Findlay et al. 2010, Kroeker et al. 2010).

The vast majority of studies on the impacts of climate warming and OA involve short-term experiments (Kroeker et al. 2010). These experiments have been carried out on a diverse assemblage of calcifying marine organisms (Kroeker et al. 2010) and have found that elevated levels of pCO_2 impact organism physiology (Beniash et al. 2010), inhibit both shell and soft body growth (Kroeker et al. 2010), and can negatively impact shell functionality traits such as strength and toughness (Fitzer et al. 2015b). Studies looking at the impact of both increasing temperature and OA have found a variation of responses with some organisms showing a higher sensitivity to OA when exposed to higher temperatures (Findlay et al. 2010, Kroeker et al. 2010, Lischka and Riebesell 2012), suggesting that these two changes may have a negative, synergistic effect on organisms in the future, but some studies showing no impact of temperature (Cross et al. 2019), or even have shown that temperature can offset the negative impacts of OA (Waldbusser et al. 2011).

While these short-term experiments can provide us with information on responses of species to one or two specific stressors, these studies are primarily conducted on individuals (Kroeker et al. 2010). To address this short-coming, there has been an influx of studies conducting multi-population and longer-term evaluations of OA and temperature impacts on marine calcifiers, and these studies, similar to some short-term tank evaluations (Ries et al. 2009), have shown variable results. For example, an archaeological assessment on shell calcification of a foundational mussel, *M. californianus*, showed significant shell thinning through time, potentially in response to OA (Pfister et al. 2016), while a centennial study on the brachiopod *Calloria inconspicua* showed no thinning even under changing environmental conditions (Cross et al. 2018).

While the knowledge gained from these longer-term assessments has been valuable, three main gaps still remain: i) There has been a dearth of studies focusing on changes in shell biomaterials, like the mineralogy of the skeleton and shell organics, which have immense potential to change and impact an organism's ability to survive (but see [(Fitzer et al. 2015b, McCoy et al. 2018))., ii) We have a limited understanding of how multiple traits change simultaneously in response to shifting environmental conditions and what the functional consequences of these trait changes may be (Fitzer et al. 2015b)., and iii) We still lack robust information on the long-term response of species to these stressors and how general calcification responses through time and space are.

My research attempts to fill these gaps of multiple populations and species, time, simultaneously changing traits and impact on function, and testing of general calcification responses by utilizing fossil and historical samples paired with large-scale sampling of natural

populations. The results will further inform our understanding of the responses of marine calcifiers under future warming and OA.

To do all this, I have focused on eastern Pacific bivalves, primarily the foundational species *M. californianus*, and five related venerid species. Eastern Pacific bivalves serve as an excellent system to study changes in intraspecific trait variation in shell calcification in response to anthropogenic change from the Pleistocene to present. Bivalves are well-known to be impacted by different anthropogenic effects that change their traits, such as human harvesting which can negatively affect body size (Fenberg and Roy n.d.) and the onset of OA which has been shown to influence mineralogy and calcification (Pfister et al. 2016, McCoy et al. 2018, Bullard et al. 2021). Additionally, the main trait of interest for many short-term tank experiments looking at OA and warming, calcification, is easily tractable in the historical and fossil record. Thus, utilizing bivalves with historical baselines and extensive interglacial fossil records can not only give us the ability to test how shell calcification has been impacted by different anthropogenic drivers, and serve as tools for assessing species risk under current and future change.

Chapter Summaries

In Chapter 1 I ask how shell mineralogy, namely the ratio of aragonite to calcite, in M. californianus shells has changed under 60 years of ocean warming and acidification (Bullard et al. 2021). Utilizing a baseline of mussels collected along the eastern Pacific and analyzed in the 1950's, I compare modern mineralogy measurements to the past and test whether mineralogy has been responding to changes in temperature or if modern measurements are in line with potential

response to decreasing pH and carbonate saturation state. My results suggest that mineralogy is not responding to temperature, as had been the standing idea in the literature since the 1950's, but instead is responding in ways more aligned to OA.

In Chapter 2 I expand my evaluation of shell biomaterials and evaluate changing shell organics as well as shell structure and function of twelve populations of *M. californianus* along the eastern Pacific. I tested changes in shell strength and toughness and how they related to three structural measurements: shell volume, elongation index, and compacity index, as well as internal shell organics. I found that shell organics was not changing along *M. californianus* range and that shell structure, namely shell volume and compacity index, are the main drivers of shell strength and toughness. I also document that southern populations are stronger than northern populations despite having lower shell volume measurements, potentially due to increased compacity index and less endolithic parasites. This work highlights the importance of evaluating multiple traits and biotic interactions when thinking about marine calcifier response to current and future environmental change.

Finally, in Chapter 3 I focus on evaluating whether or not the long-term response of shell calcification in closely related species is variable. I test hypotheses about shell calcification response generated from short-term experiments and millennial scale assessments by assessing changes in size and shell calcification for five venerid species from the Pleistocene to present. I show that despite evolutionary relatedness, there is no one shell calcification response through time for the five species. Additionally, for two species, *Chione californiensis* and *Tivela stultorum*, I assess how their shell calcification patterns change through space. I show that while *C. californiensis* has southern populations where traits are similar to those recorded in the

Pleistocene fossil assemblage, *T. stultorum* shows significant thinning along even its southern range today.

Combined, my dissertation chapters work to provide a more holistic view of how shell calcification, and additional traits associated with it, change on different temporal and spatial scales. Using an interdisciplinary approach of combining paleontology, ecology, material and structural engineering as well as a diverse array of collaborations has allowed me to fill key knowledge gaps in the OA field and provide us with important information to understand how these important molluscan species are responding to anthropogenic changes.

CHAPTER 1

Shell mineralogy of a foundational marine species, *Mytilus californianus*, over half a century in a changing ocean

Elizabeth M. Bullard[a,1], Ivan Torres[b], Tianqi Ren[b], Olivia A. Graeve[b], and Kaustuv Roy[a]

[a]Section of Ecology, Behavior and Evolution, University of California San Diego, La Jolla, CA 92093-0116; and [b]Department of Mechanical and Aerospace Engineering, University of California San Diego, La Jolla, CA 92093-0411

Edited by Jeremy B.C. Jackson, American Museum of Natural History, New York, NY, and approved November 10, 2020 (received for review March 13, 2020)

Anthropogenic warming and ocean acidification are predicted to negatively affect marine calcifiers. While negative effects of these stressors on physiology and shell calcification have been documented in many species, their effects on shell mineralogical composition remains poorly known, especially over longer time periods. Here, we quantify changes in the shell mineralogy of a foundation species, *Mytilus californianus*, under 60 y of ocean warming and acidification. Using historical data as a baseline and a resampling of present-day populations, we document a substantial increase in shell calcite and decrease in aragonite. These results indicate that ocean pH and saturation state, not temperature or salinity, play a strong role in mediating the shell mineralogy of this species and reveal long-term changes in this trait under ocean acidification.

ocean acidification | foundational marine species | mineralogy

There is increasing concern about the effects of anthropogenic stressors, particularly warming and ocean acidification (OA), on marine calcifiers (organisms that precipitate a calcium carbonate ($CaCO_3$) exoskeleton). Short-term experimental studies, spanning days to months (1, 2), have shown negative impacts of OA on the physiology of calcifiers (3), inhibition of shell and soft body growth (3), and decreased functionality of the shell (4). Some experiments also suggest that rising temperatures can synergistically augment the effects of OA (5), while others show no impact on shell calcification (2) or even an increase in calcification rate with increasing temperature (6). Although an increasing number of experimental studies are investigating the biological effects of OA and warming, very little information is available on the long-term responses of calcification for wild populations of marine calcifiers to these stressors. Additionally, the few studies available that assess changes in calcification in response to warming and OA on decadal to centennial time scales show contrasting results. For example, comparison of specimens of the intertidal mussel, *Mytilus californianus*, from archeological middens (~1000 to 2420 y BP) with those from living populations showed a significant thinning of the shell (7) and loss of mineralogical control (8). In contrast, an analysis of shell thickness over a 120-y period in a brachiopod (*Calloria inconspicua*) from New Zealand showed no change in thickness through time (9). Furthermore, effects of anthropogenic stressors on the mineralogical composition of the shell, a key functional trait, still remain poorly quantified on both short and long time scales (but see ref. 4 for a short-term assessment). Here, we use historical measurements in conjunction with field sampling to quantify the impact of half a century of ocean warming and OA on the shell mineralogy of multiple populations of *M. californianus*, a foundational marine bivalve species along the northeastern Pacific coast.

The shells of marine mollusks are composed of two different polymorphs of $CaCO_3$, namely aragonite and calcite (10). Of these two polymorphs, aragonite is more soluble than calcite (11), though differences in crystal size and organic content of the shell can also play a role in mediating dissolution rates of mollusk shells (12–14). While most molluscan species tend to have shells that are predominantly made of either aragonite or calcite, others have shells that contain both polymorphs. It has long been hypothesized that the ratio of aragonite to calcite (in this study represented as the percentage of aragonite) in the shells of species with mixed mineralogy is mediated by the temperature and/or $CaCO_3$ saturation state of seawater (13, 15). This is supported by the observation that aragonite content of molluscan shells in species with mixed mineralogy changes predictably along a latitudinal gradient, with an enrichment of aragonite as compared to calcite in warmer waters (13, 15). Furthermore, larvae of a marine mussel with mixed mineralogy (*M. edulis*) grown under high partial pressure of carbon dioxide (pCO_2) conditions were enriched in calcite compared to those grown under lower pCO_2 conditions (16). Given that aragonite is preferentially precipitated in warmer waters compared to calcite in species with mixed mineralogy, anthropogenic warming by itself should favor higher aragonite content in shells of species that use both polymorphs, while the decrease in carbonate ions and saturation state of $CaCO_3$, primarily aragonite, in conjunction with increasing pCO_2 and decreasing ocean pH should favor calcite.

Along the northeastern Pacific coast, sea surface temperatures (SSTs) have increased significantly since the 1950s (*SI Appendix*, Table S1). Over this time, anthropogenic CO_2 emissions have also increased substantially (17, 18), leading to decreases in ocean pH and saturation state (18), although the exact magnitude of such

Significance

Anthropogenic ocean acidification (OA) is a potential threat for marine calcifying organisms. While much experimental work has been done to assess the impacts of OA on marine calcifiers, studies over long temporal scales and across multiple populations still remain limited. Here, we combine historical data with recent field surveys to quantify the plasticity in shell mineralogy, a key functional trait, of a foundational marine bivalve, *Mytilus californianus*. Our data suggest that mineralogy in this species is responding more to pH and saturation state changes than warming or decreasing salinity. This study highlights the importance of utilizing long-term data sets and large spatial comparisons to understand and test predictions about species responses to a changing world.

Author contributions: E.M.B. and K.R. designed research; E.M.B. and I.T. performed research; O.A.G. contributed new reagents/analytic tools; E.M.B., T.R., O.A.G., and K.R. analyzed data; and E.M.B., I.T., T.R., O.A.G., and K.R. wrote the paper.

The authors declare no competing interest.

This article is a PNAS Direct Submission.

[1]To whom correspondence may be addressed. Email: embullar@ucsd.edu.

This article contains supporting information online at https://www.pnas.org/lookup/suppl/doi:10.1073/pnas.2004769118/-/DCSupplemental.

published January 11, 2021.

decreases along the northeastern Pacific remains unknown. We quantified how the aragonite content of shells of *M. californianus* populations have changed in response to these opposing forces by comparing baseline measurements of aragonite content of shells collected in 1952 [hereafter referred to as sample S52 (10)] and 1958 to 1960 [sample S58-60 (19)] with those from samples collected in 2017 and 2018 (sample S17-18) (*SI Appendix*, Table S2). Specifically, we sampled five populations of *M. californianus* along a spatial gradient spanning 15° of latitude along the northeastern Pacific coast (Fig. 1), a transect similar to that from the late 1950s (19). Three of our sites in Southern California are the same as those from the late 1950s (19), and one matched site, La Jolla, additionally has data from 1952 (S52) (10); the other two sites further north are in the same regions sampled in the late 1950s study (19) but are not exact matches (Fig. 1 and *SI Appendix*, Fig. S1). Although the northern sites are not exact spatial matches with our baseline data, by sampling the same regions as in the 1950s (19), they allow us to investigate whether the latitudinal gradient in shell aragonite content of this species has changed over time. For two of our matched sites (La Jolla and Corona Del Mar), samples from 2010 (hereafter S10) were also available, providing an additional baseline that further allows us to assess decadal responses of shell mineralogy to warming and ocean acidification. For all of the comparisons, individuals of *M. californianus* sampled live in 2017-2018 (S17-18) were matched to the same body-size range as in the baseline studies to avoid any impact of size on shell aragonite content, and all samples were prepared following the same procedures described in the baseline studies (10, 19) and analyzed using X-ray diffraction (XRD) (see *Materials and Methods*).

Results and Discussion

At all three of our matched sites, large temporal changes in shell aragonite content are evident. At La Jolla, the shell aragonite content decreased significantly from the 1950s (S58-60) to 2010 (S10) and has been stable since (Fig. 1 and *SI Appendix*, Fig. S1 and Tables S3 and S4). Avila Beach shows a similar trend with a significant decrease in aragonite content from the 1950s (S58-60) to 2017-2018 (S17-18) (Fig. 1 and *SI Appendix*, Fig. S1 and Tables S3 and S4). At Corona del Mar, the trend is more complex, with a significant decline in aragonite content from the 1950s to 2010, but with subsequent recovery, so that the aragonite content of S17-18 is not significantly different from that of S58-60 (Fig. 1 and *SI Appendix*, Fig. S1 and Table S3).

Further north at Crescent City, only one sample from 1959 (S59) is available, making statistical comparisons impossible, but qualitative assessment is still feasible and informative. At this site, there has been an increase in temperature through time (*SI Appendix*, Tables S1 and S5) and a corresponding change in shell aragonite content, from 42.90% aragonite in sample S59 to a median value of 16.82% and a maximum of 23.38% in sample S17-18 (*SI Appendix*, Table S6). Thus, the 42.90% measured in 1959 is well outside the current range of our data despite a substantially larger sample ($n = 9$; *SI Appendix*, Tables S2 and S6).

The temporal decrease in shell aragonite content seen at each of our matched sites is also evident over a wider latitudinal gradient (Fig. 1*E* and *SI Appendix*, Fig. S1*E*). Regression models that take in to account spatial and temporal autocorrelations as well as potential effects of shell size and weight (lagged-mixed simultaneous autoregressive models, generalized least squares models, and linear mixed effect models with locality added as a random effect; see *Materials and Methods*) all show a significant difference in the latitudinal trends in shell aragonite content between the late 1950s and 2017-2018 (Fig. 1*E* and *SI Appendix*, Table S4). Specifically, there was a significant latitudinal trend in shell aragonite content during the 1950s, with higher latitudes being preferentially enriched in calcite (*SI Appendix*, Table S4). In contrast, latitude is not a significant predictor of aragonite content in 2017-2018 (*SI Appendix*, Table S4), suggesting an overall shallowing of the slope of this relationship through time, driven by larger decreases in shell aragonite content at our southern sites compared to northern ones. Overall, shell aragonite content has decreased substantially across the range of this species. The difference in percentage of aragonite is more pronounced if S52 and S10 data are added to the analyses with the slopes becoming significantly different between the past (S52 and S58-60) and recent times (S10 and S17-18) (*SI Appendix*, Table S3 and Fig. S1). Because temperature varies substantially with latitude, we also assessed changes in the relationship between shell aragonite

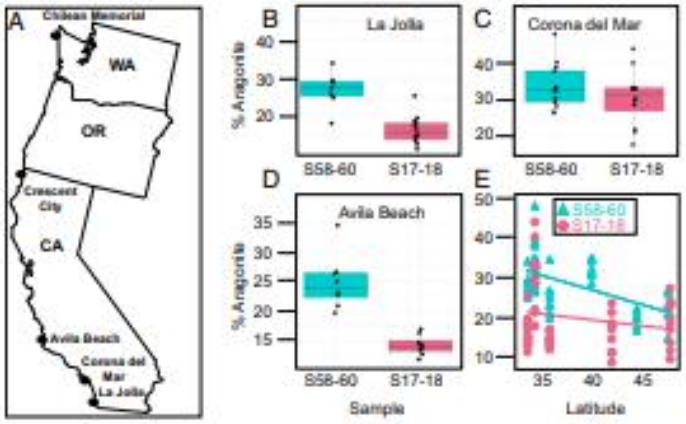

Fig. 1. (*A*) Locality map showing the five sites for samples S17-18. Three of the sites, Avila Beach ($n = 8$ for both S58-60 and S17-18), Corona del Mar ($n = 14$ for S58-60 and $n = 12$ for S17-18), and La Jolla ($n = 7$ for S58-60 and $n = 12$ for S17-18), in California, are the same as those in the late 1950's. The other two, Crescent City, California, and Chilean Memorial, Washington, are in the same region as northern sites sampled in 1958-1960 (see main text, *Materials and Methods*). The box plots show comparisons of the percentage of aragonite for S58-60 and S17-18. The samples S17-18 are significantly more enriched in calcite compared to those from the past (*SI Appendix*, Table S3). (*B*) La Jolla comparison. (*C*) Corona del Mar comparison. (*D*) Avila Beach comparison. (*E*) Relationship between percentage of aragonite in individual *M. californianus* shells and latitude for S58-60 ($n = 50$) and S17-18 ($n = 51$). The slopes are not significantly different between the two time periods (*SI Appendix*, Table S3).

content and SST (*SI Appendix*, Fig. S2). Similar to the difference in latitudinal trends, temperature is a significant predicter of percentage of aragonite in our most conservative spatial autocorrelation models controlling for size and weight for the late 1950s, but this relationship is not significant for our 2017-2018 samples (*SI Appendix*, Table S4 and Fig. S3).

In addition to SST and pH, an inverse relationship between salinity and shell aragonite content in Eastern Pacific mussels (*M. californianus* and *Mytilus gallogrovincialis*) has also been hypothesized (10, 15). This is in contrast to recent observations of *M. edulis* and *Mytilus trossulus* in the Baltic, where a decrease in aragonite content was evident with decreasing salinity (13). This potential difference in salinity response provides an interesting comparative framework for looking at how species with different evolutionary histories and different environmental regimes respond to the same stressor. In this case, *M. californianus* has evolved in a very different oceanographic regime (i.e., upwelling system) compared to *M. edulis*, the focus of the Baltic study. Furthermore, changes in salinity have also been shown to affect the metabolic cost of shell calcification (20), highlighting the importance of understanding how salinity changes affect shell mineralogy of species with different evolutionary and environmental histories. At all three of our southern matched sites, both SST and salinity has changed since the 1950s. SST has increased from the 1950s to 2017-2018, but the magnitude of this change varies across sites, with the largest temporal change in our warmest site, La Jolla (*SI Appendix*, Table S1). Over this time, salinity has decreased at each of our sites but, again, by different magnitudes (*SI Appendix*, Tables S1 and S5). Although the temporal data on temperature and salinity are too sparse for quantitative analyses at the level of individual sites given there are just two time points for Avila Beach and three for Corona del Mar and La Jolla, qualitatively, the directionality of the observed trends do not support the predicted relationships between temperature, salinity, and shell aragonite content for Eastern Pacific *Mytilus* species at any of the three sites analyzed here.

Overall, our results indicate that the aragonite content of *M. californianus* shells has declined significantly over the last half century. While the magnitude of this decrease varies across our sites, it is clear that most populations of this species incorporate much more calcite in their shells now than in the past. Our results also show that these decreases are not due to temperature or salinity change. Other factors such as predation pressure, wave exposure, and food availability are also known to affect shell calcification (7, 21), but whether they have any influence on shell mineralogy remains unclear. In fact, selection due to increased predation pressure and/or wave exposure should lead to an increase in shell aragonite content since it is the stronger of the two polymorphs (10). Age and growth rates of individuals can potentially also affect the proportion of aragonite/calcite within the shell. Individuals of *M. californianus* are extremely difficult to age from shell growth lines (10, 22), so we cannot rule out the possibility of some age-related effects, such as decreased longevity or changing growth rates, in our data. However, size and age are tightly and positively correlated in this species (19), and the lack of any significant size effects in our regression models suggest that temporal differences in age are unlikely to be a major driver of our results. One aspect of anthropogenic change that affects both shell calcification and mineralogy is changes in sea water saturation state and ocean pH (4, 16). Long-term measurements of these variables are not available at any of our sites, making it impossible to directly test the role of OA in driving the temporal changes seen here. However, multiple indirect lines of evidence suggest a major role of OA. For example, short-term experiments have shown a decrease in shell aragonite content in *M. edulis* larvae of parents grown under higher pCO_2 conditions (1,000 microatmospheres, or µatm) compared to offspring of parents grown under lower pCO_2 conditions (380, 550, and 750 µatm) (16). Similarly, the eastern oyster, *Crassostrea virginica*, shows an increase in the calcite laths within the shells of juveniles grown under treatments of 3,500 µatm as compared to those grown under 380 µatm, suggesting in both cases a response to elevated pCO_2 and decreased pH (23). On a larger spatial scale, the Atlantic mussels *M. edulis* and *M. trossolus* show an increase in the thickness of the calcitic prismatic layer in the shell from temperate to polar regions (13). Finally, long-term changes in the crystallographic structure of the shell of *M. californianus* has also been attributed to changing ocean pH (8). Thus, our results are consistent with experimental evidence of preferential precipitation of the less soluble calcite over aragonite under OA. While preferential dissolution of precipitated aragonite in response to more corrosive waters (21) can also affect the calcite/aragonite ratio of shells, we did not see any clear signs of dissolution such as substantial pitting of the shells in samples S10 and S17-18, and since those shells do not weigh significantly less than those from the 1950s (S58-60), it is likely that differential precipitation of calcite, rather than dissolution of aragonite due to OA, is the primary driver of our results.

Regardless of the exact cause(s) of the change in mineralogy of *M. californianus*, our results clearly demonstrate that shells of this species, across most of its geographic range, have significantly more calcite today compared to the 1950s. This suggests that marine calcifiers with mixed mineralogy may have considerable plasticity to adjust the ratio of different polymorphs of $CaCO_3$ in their shells in response to global change. While such plasticity may be advantageous in future ocean environments, as pH is expected to drop even more and higher latitudes are predicted to be undersaturated with respect to aragonite by the end of this century (24), there may also be functional trade-offs in decreasing shell aragonite content. For example, *M. edulis* larvae precipitating only calcite when born from parents raised in the highest pCO_2 treatment tend to show loss of crystallographic control (4). Calcite precipitated under these higher pCO_2 conditions (1,000 µatm) may also be more brittle (4), potentially making shells more prone to fracturing under durophagous predation. Further investigation of such functional trade-offs is needed to better predict the potential for adaptation of *M. californianus*, a foundation species, and other marine calcifiers with mixed mineralogy to future OA. Finally, the work presented here highlights the importance of long-term comparisons to better understand the responses of marine calcifiers to anthropogenic global change. Such comparisons not only document how wild populations are responding to changing conditions but also help test predictions derived from short-term experiments.

Materials and Methods

Collecting Localities and Historical Data. We extracted historical information about collecting locality, environmental variables, morphometric measurements, and shell mineralogical compositions of *M. californianus* along the northeastern Pacific from two primary sources, namely Lowenstam (10) (552) and Dodd (19) (558-60) (*SI Appendix*, Table S5). From ref. 10, we only used data for live-collected individuals from La Jolla, California, collected on December 26, 1952, and within the same size range as the samples collected by Dodd (19). The exact location of where samples were collected by Lowenstam (10) is unknown but is most likely from around the Scripps Institution of Oceanography (SIO) campus, where we collected our live samples. Dodd (19) collected his samples between 1958 and 1960 (558-60) from six localities (19) but provided a specific date of collection (month/day) only for the Corona del Mar site. This site is also the only locality accompanied by a detailed explanation of sample collection. The other sampling sites in ref. 19 are described as locality names without information about their latitude and longitude. However, we were able to confirm that the La Jolla, California, samples were collected from the pier pilings at SIO. The Avila Beach, California, samples were also very likely to have been collected from the pier pilings there. The name associated with the northern (Washington) locality in ref. 19 is somewhat ambiguous (see below). Thus, we directly matched

three of the sites from ref. 19, while for Washington, we sampled the same region as Dodd.

To compare mineralogical changes (specifically shell aragonite content) through time, we collected *M. californianus* in 2017 and 2018 (517-18) at the three sites that we were able to match from ref. 19, La Jolla (32.8663°N, 117.2546°W), Corona del Mar (33.5979°N, 117.8730°W), and Avila Beach (35.1800°N, 120.7319°W) in California. Additionally, we collected from two other sites, the Battery Point Lighthouse in Crescent City, California (41.7441°N, 124.2031°W), and Chilean Memorial, Washington (47.9643°N, 124.6635°W), to construct a latitudinal gradient comparable to that from ref. 19 (Fig. 1*A*). Crescent City is actually a site included in ref. 19, but the exact location of the collection within this city is unknown, and only data for one individual is included in ref. 19. Therefore, this site is a partial match where statistical analyses of temporal trends are not possible; only qualitative comparisons are provided here. Dodd's (19) northernmost site ("Hoh, Washington") could potentially refer to three different locations, so we chose Chilean Memorial, a site in the same region, as our northernmost site. More detailed information on each site can be found in *SI Appendix*.

At each locality, we collected individuals of *M. californianus* within the same size range as those from ref. 19 (*SI Appendix*, Table S6) from wave-exposed sites in the middle portion of the mussel zone. Exact replication of each individual's size was only possible at Avila Beach, where the populations were plentiful and a myriad of size classes existed at time of collection. Exactly matching the entire size range was not feasible at other sites, such as Corona del Mar, primarily because the largest individuals (>100 mm) are no longer present intertidally at these locations, most likely due to human harvesting [e.g., (25)]. To address this problem, we excluded any individuals from samples 558-60 that were too large to be found intertidally today. While age of individuals can also potentially affect the aragonite/calcite ratios of their shells, we focus on size (i.e., length) and weight (as a proxy for thickness) in our analyses here for multiple reasons: 1) information about the age of the specimens from the 1950s is not available, but sizes of those specimens are known; 2) qualitative aging of *M. californianus* is difficult if not impossible at many locations where we sampled this species [e.g., (22)], but in localities where aging is possible, a positive relationship between size and age has been documented for *M. californianus* (19, 26, 27); 3) recent analyses of shell calcification have largely used specimen size as a proxy for age (13, 28).

In addition to 2017-2018 (517-18) samples, we also used samples collected in 2010 (510) at two of the matched sites, La Jolla and Corona del Mar. These samples were also size matched to samples 558-60 with a similar cutoff for the largest individuals, as explained above.

We used the environmental data from refs. 10 and 19 for our comparison, though ref. 10 only contains temperature data. In addition, ref. 19 explicitly states that temperature data listed in the study is a 10-y average, but whether such averaging also applies to ref. 10 is unclear. Since the majority of our data came from ref. 19, we chose to use the 10-y mean annual temperature collected from the nearest buoy station (29, 30) for 2017-2018 (*SI Appendix*, Table S1). For 2010 at Corona del Mar, a 5-y average was used because data did not cover the whole 10-y average range (29). The late 1950s data from ref. 19 only records salinity "at time of collection," so we used the average salinity measurement for the day of collection for our 2010 and 2017-2018 samples (29, 30).

Shell Mineralogy Quantification Using XRD. We followed the methods stated in ref. 19 to quantify the shell mineralogical compositions of our samples so that our values are directly comparable to those from the 1950s studies. Note that the methods described in Dodd's Ph.D. thesis (19) also apply to ref. 10, since the work was completed under Lowenstam's supervision. The percentage of aragonite data in ref. 19 represents a mixture of single valve, whole individual, and multiple individuals. For this study, we only use the data from ref. 19 that are from single valves and use the relevant analytical method. Briefly, we first cleaned the shells of *M. californianus* of epibionts. We then placed a single valve from each individual in commercial Clorox bleach with a concentration of 5.25% sodium hypochlorite for 3 to 7 d to remove the periostracum as described in refs. 19 and 10. We then rinsed the valve with deionized water and dried it in a fume hood at ambient temperature until the weight of the valve did not change from water loss. Once dry, we ground each valve in its entirety by hand in an agate mortar and pestle until a grain size of less than No. 200 (75 μm) mesh was achieved (19). To avoid any possible conversion of aragonite to calcite, we first broke the shell into pieces and slowly ground them in small batches with continuous removal of the finer grains passing through the No. 200 mesh sieve (75 μm) (10, 19).

The powder for each individual valve was analyzed using a D2 Phaser X-ray diffractometer (Bruker AXS, Madison, WI). For each individual sample, the resulting powder was divided into three parts in order to run independent measurements, which were then averaged. The procedure consisted of passing the powdered samples through a No. 100 mesh (150 μm) sieve onto a silicon crystal zero-background disk, as described by ref. 19. The surface of the zero-background disk was covered in a thin layer of petroleum jelly, which allowed the fragments to randomly adhere upon the platform and minimize any effect of preferred orientation (19). Prior to any subsequent runs, the sieve was rinsed with water and fully dried, and the silicon disk was cleaned with ethanol in order to ensure each sample was unaffected by previous runs. The XRD runs were carried out using copper K-alpha (CuK_α) radiation with a step size of 0.01° 2θ ranging from 20° to 60°, with each sample run lasting ~37 min. We used *Littorina keenae* collected from the rocky intertidal area near SIO and commercially raised *Crassostrea gigas* as our pure biogenic aragonite and calcite standards, respectively. XRD patterns for both *L. keenae* and *C. gigas* were obtained to confirm their purity. We ground the *L. keenae* and *C. gigas* standards to the same grain size as the test samples (i.e., <75 μm) and followed the procedure above to create a calibration curve. We analyzed the diffraction peaks using TOPAS 4.2 software (DIFFRAC^{Topas}, Bruker AXS) and determined percentage of aragonite by means of Rietveld refinement. This methodology allows refinement through a least-squares algorithm by evaluating user-defined parameters that minimize the difference between an experimental pattern and a model based on crystal structure and instrumental parameters. These latter parameters help constrain peak positions and peak intensities, respectively (31). In accordance with this technique, each raw diffraction pattern per individual run was loaded into TOPAS and compared with the calibration curve and standard calcite and aragonite values. These values were made accessible via the Inorganic Crystal Structure Database (ICSD) (32, 33). With respect to the instrumental parameters, a CuK_α emission profile was loaded, along with a fourth-order Chebychev polynomial background function to filter the data. The goniometer radii of our specific system were set to 141 mm, while the zero-error correction was utilized in order to account for any peak shifts that could arise due to systematic error. This correction ensures all peaks are shifted by a constant value, independent of θ angle (34). Calcite and aragonite structures were added accordingly, with the respective lattice parameters taken via ICSD, along with the atomic sites necessary for each structure. During the process, it is also safe to assume that there is no preferred orientation, that is, the orientation of the crystallites is considered to be random. This random orientation otherwise indicates that all possible orientations of crystallites within the sample occur with the same probability (34). All parameters (i.e., overall intensities, background, peak positions, peak shapes, and structures) were set to be refined during the calculation. The Rietveld refinement was then run for three iterations to obtain consistent R values as the phase composition is carried out. The resulting values are a final phase ratio indicating the amount of calcite and aragonite within each individual measurement as a percentage.

Statistical Analyses. We first tested for a significant difference in percentage of aragonite between left and right valves at each of our 2017-2018 (517-18) localities using Wilcoxon rank sum tests. Since there was no significant difference (*SI Appendix*, Fig. S4 and Table S3), we did not differentiate data from left and right valves for subsequent analyses.

We used Kruskal–Wallis rank sum tests to determine if percentage of aragonite had significantly changed at our three matched sites through time. Kruskal–Wallis was used instead of a Student's *t* test because percentage of aragonite is a ratio, and assessing statistical changes in the median is more informative than the mean in such cases. Additionally, we conducted *F*-tests to determine significant changes in variation for matched sites through time.

We tested for temporal and spatial autocorrelation using the Durbin–Watson test (35) and Moran's I (36), respectively. Durbin–Watson tests were run using the lmtest package in R (37) and Moran's I using the Ape package (38). Data were temporally and spatially autocorrelated (*SI Appendix*, Table S3), so we ran multiple models to account for such autocorrelation and selected the best model using Akaike information criterion (AIC) scores. To account for temporal autocorrelation, we used the Cochrane–Orcutt method (39) using the Orcutt package in R (40). The base of the model was a linear regression model comparing percentage of aragonite as a function of time, latitude, temperature, length, and weight (*SI Appendix*, Table S4). We used the temperature data associated with 558 -60 (19) and 517-18 (29, 30) for our main comparison. In addition, we compared all past data (552 (10) and 558-60 (19) combined) with all recent samples [510 (29, 30) and 517-18 (29, 30) combined] for our full analyses. To control for spatial autocorrelation, we

ran three different types of models, each of which evaluated percentage of aragonite as a function of latitude and temperature as well as length and weight to account for potential size effects on the mineralogical composition. The three different models we tested were 1) generalized least square models, 2) linear mixed effect models (LME) with locality as a random effect, and 3) simultaneous autoregressive models with a mixed lagged effect and locality as a random effect to account for spatial autocorrelation in multiple directions using the spatialreg package in R (41). All models used restricted maximum likelihood. Regardless of which model we used, the results were qualitatively the same. However, model comparison using AIC suggested that the best-performing model was an LME with locality as a random effect. We thus used LME with locality as a random effect to test for differences in slopes between samples 558-60 and 517-18, as well as the slope between combined past (552 and 558-60) and combined recent (510 and 517-18). To further control for any potential nonlinear effect of size on our latitudinal or temperature trends, we used the residuals from a linear regression of percentage of aragonite and length against latitude and temperature (*SI Appendix*, Fig. S5 and Table S4). All analyses were carried out in R (42).

Data Availability. All study data are included in the article and *SI Appendix*.

ACKNOWLEDGMENTS. We thank A. Nau for aiding in sample collection and helpful discussions about this work. This work was partially supported by a grant from the NASA (to K.R.) and the Jeanne Marie Messier Memorial Endowment Fund (to E.M.B.).

1. K. J. Kroeker *et al.*, Impacts of ocean acidification on marine organisms: Quantifying sensitivities and interaction with warming. *Glob. Change Biol.* **19**, 1884–1896 (2013).
2. E. L. Cross, E. M. Harper, L. S. Peck, Thicker shells compensate extensive dissolution in brachiopods under future ocean acidification. *Environ. Sci. Technol.* **53**, 5016–5026 (2019).
3. K. J. Kroeker, R. L. Kordas, R. N. Crim, G. G. Singh, Meta-analysis reveals negative yet variable effects of ocean acidification on marine organisms. *Ecol. Lett.* **13**, 1419–1434 (2010).
4. S. C. Fitzer *et al.*, Ocean acidification alters the material properties of *Mytilus edulis* shells. *J. R. Soc. Interface* **12**, 1–8 (2015).
5. H. S. Findlay, M. A. Kendall, J. I. Spicer, S. Widdicombe, Relative influences of ocean acidification and temperature on intertidal barnacle post-larvae at the northern edge of their geographic distribution. *Estuar. Coast. Shelf Sci.* **86**, 675–682 (2010).
6. G. G. Waldbusser, E. P. Voigt, H. Bergschneider, M. A. Green, R. I. E. Newell, Biocalcification in the eastern oyster (*Crassostrea virginica*) in relation to long-term trends in the Chesapeake Bay pH. *Estuaries Coasts* **34**, 221–231 (2011).
7. C. A. Pfister *et al.*, Historical baselines and the future of shell calcification for a foundation species in a changing ocean. *Proc. Biol. Sci.* **283**, 1–8 (2016).
8. S. J. McCoy, N. A. Kamenos, P. Chung, T. J. Wootton, C. A. Pfister, A mineralogical record of ocean change: Decadal and centennial patterns in the California mussel. *Glob. Change Biol.* **24**, 2556–2562 (2018).
9. E. L. Cross, E. M. Harper, L. S. Peck, A 120-year record of resilience to environmental change in brachiopods. *Glob. Change Biol.* **24**, 2262–2271 (2018).
10. H. A. Lowenstam, Factors affecting the aragonite: Calcite ratios in carbonate-secreting marine organisms. *J. Geol.* **62**, 284–322 (1954).
11. J. D. Currey, J. D. Taylor, The mechanical behavior of some molluscan hard tissues. *J. Zool.* **173**, 395–406 (1974).
12. E. M. Harper, Are calcitic layers an effective adaptation against shell dissolution in the Bivalvia? *J. Zool. (Lond.)* **251**, 179–186 (2000).
13. L. Telesca *et al.*, Biomineralization plasticity and environmental heterogeneity predict geographic resilience patterns of foundation species to future change. *Glob. Change Biol.* **25**, 1–15 (2019).
14. M. Chadwick, E. M. Harper, A. Lemasson, J. I. Spicer, L. S. Peck, Quantifying susceptibility of marine invertebrate biocomposites to dissolution in reduced pH. *R. Soc. Open Sci.* **6**, 190252 (2019).
15. J. R. Dodd, Paleoecological implications of shell mineralogy in two pelecypod species. *J. Geol.* **71**, 1–11 (1963).
16. S. C. Fitzer, M. Cusack, V. R. Phoenix, N. A. Kamenos, Ocean acidification reduces the crystallographic control in juvenile mussel shells. *J. Struct. Biol.* **188**, 38–45 (2014).
17. H. A. Keeling *et al.*, "Atmospheric CO2 and 13CO2 exchange with the terrestrial biosphere and oceans from 1978 to 2000: Observations and carbon cycle implications" in *A History of Atmospheric CO2 and Its Effects on Plants, Animals, and Ecosystems*, M. D. Ehleringer, J. R. Cerling, T. E. Dearing, Eds. (Springer Verlag, 2005), pp. 83–113.
18. R. A. Feely, S. C. Doney, S. R. Cooly, Ocean acidification – present conditions and future changes. *Oceanography (Wash. D.C.)* **22**, 36–47 (2009).
19. J. R. Dodd, *Paleoecological Implications of the Mineralogy, Structure, and Strontium and Magnesium Contents of Shells of the West Coast Species of the Genus Mytilus* (California Institute of Technology, Pasadena, CA, 1961).
20. T. Sanders, L. Schmittmann, J. C. Nascimento-Schulze, F. Melzner, High calcification costs limit mussel growth at low salinity. *Front. Mar. Sci.* **5**, 1–9 (2018).
21. F. Melzner *et al.*, Food supply and seawater pCO2 impact calcification and internal shell dissolution in the blue mussel *Mytilus edulis*. *PLoS One* **6**, e24223 (2011).
22. T. H. Suchanek, The role of disturbance in the evolution of life history strategies in the intertidal mussels *Mytilus edulis* and *Mytilus californianus*. *Oecologia* **50**, 143–152 (1981).
23. E. Beniash, A. Ivanina, N. S. Lieb, I. Kurochkin, I. M. Sokolova, Elevated level of carbon dioxide affects metabolism and shell formation in oysters *Crassostrea virginica*. *Mar. Ecol. Prog. Ser.* **419**, 95–108 (2010).
24. S. Doney, W. Balch, V. Fabry, R. Feely, Ocean acidification: A critical emerging problem for the ocean sciences. *Oceanography (Wash. D.C.)* **22**, 16–25 (2009).
25. K. Roy, A. G. Collins, B. J. Becker, E. Begovic, J. M. Engle, Anthropogenic impacts and historical decline in body size of rocky intertidal gastropods in southern California. *Ecol. Lett.* **6**, 205–211 (2003).
26. C. A. Blanchette, B. Helmuth, S. D. Gaines, Spatial patterns of growth in the mussel, *Mytilus californianus*, across a major oceanographic and biogeographic boundary at Point Conception, California, USA. *J. Exp. Mar. Biol. Ecol.* **340**, 126–148 (2007).
27. H. L. Ford *et al.*, Evaluating the skeletal chemistry of *Mytilus californianus* as a temperature proxy: Effects of microenvironment and ontogeny. *Paleoceanography* **25**, 1–14 (2010).
28. A. Piwoni-Piórewicz *et al.*, Size effect on the mineralogy and chemistry of *Mytilus trossulus* shells from the southern Baltic Sea: Implications for environmental monitoring. *Environ. Monit. Assess.* **189**, 157 (2017).
29. Data from, "Southern California Coastal Ocean Observing System". https://sccoos.org/regions/sccoos/. Accessed 4 January 2019.
30. Center of Excellence in Marine Technology, Data from "National Oceanic and Atmospheric Administrations' national data buoy center". https://www.ndbc.noaa.gov/. Accessed 2 February 2019.
31. G. Will, *Powder Diffraction: The Rietveld Method and the Two Stage Method to Determine and Refine Crystal Structures from Powder Diffraction Data* (Springer, 2006).
32. E. N. Maslen, V. A. Strahtsov, N. R. Strelnkova, X-ray study of the electron density in calcite, $CaCO_3$. *Acta Crystallogr. B* **49**, 636–641 (1993).
33. T. Pilati, F. Demartin, C. M. Gramaccioli, Lattice-dynamical estimation of atomic displacement parameters in carbonates: Calcite and aragonite $CaCO_3$, dolomite $CaMg(CO_3)$ and magnesite $MgCO_3$. *Acta Crystallogr. B* **54**, 515–523 (1998).
34. H. W. King, E. A. Payzant, Error corrections for x-ray powder diffractometry. *Can. Metall. Q.* **40**, 385–394 (2001).
35. J. Durbin, G. S. Watson, Testing for serial correlation in least squares regression III. *Biometrika* **58**, 1–19 (1971).
36. C. F. Dormann *et al.*, Methods to account for spatial autocorrelation in the analysis of species distributional data: A review. *Ecography* **30**, 609–628 (2007).
37. A. Zeileis, T. Hothorn, Diagnostic checking in regression relationships. *R. News* **2**, 7–10 (2002).
38. E. Paradis, K. Schliep, Ape 5.0: An environment for modern phylogenetics and evolutionary analyses in R. *Bioinformatics* **35**, 526–528 (2019).
39. W. D. Koenig, A. M. Liebhold, Temporally increasing spatial synchrony of North American temperature and bird populations. *Nat. Clim. Chang.* **6**, 614–617 (2016).
40. S. Stefano, M. Quartagno, M. Tamburini, D. Robinson, *orcutt*: Estimate procedure in case of first order autocorrelation (2018).
41. R. Bivand, G. Piras, Comparing implementations of estimation methods for spatial econometrics. *J. Stat. Softw.* **63**, 1–36 (2015).
42. R Core Team, R: A Language and Environment for Statistical Computing. R Foundation for statistical computing (2018).

Supplemental Material

Detailed description of sampling sites

Below we provide more detailed descriptions of each of the sampling sites used in this study.

Chilean Memorial: The northernmost sampled site was Chilean Memorial, Washington (WA), a site not from Dodd 1961 (19), but included here as a substitute for the elusive Hoh, WA locality of Dodd 1961 (19). We collected *M. californianus* about 5.6 km north of the Rialto Beach parking lot (47°56′31″N, 124°37′52″W, Fig. S6b). Approximately 56 m from the south entrance to the bay is a flat step (Fig. S6a) that sits about 2.5 m over the sand. We sampled individuals of *M. californianus* from the vertical wall at the west end of this step. The mussel beds are dense in this area, and the small rock pools are covered in algae and contain other molluscan species such as *Tegula funebralis, Littorina plena, L. sitkana, L. subrotundata, Lottia pelta,* and *Nucella sp*. Samples were collected in the dark around 5:00 AM making it difficult to get clear photographs of the mussel beds at the time of sampling; so no photos of the mussel beds from this site are included here.

Crescent City: Moving southward down the Eastern Pacific coast, we find our next northern site, Crescent City, California (CA). Here we collected *M. californianus* from the southwest side of the Battery Point Lighthouse (41°44′39″N, 124°12′07″W) which is located west of the B Street Pier (Fig. S7). On the southwest side of the lighthouse where a cement path begins to incline towards the Lighthouse there is a large pool to the west side of a large rock outcrop (Fig. S7a) and samples were collected from here. This mussel bed also housed many *Nucella sp,* commonly found on individual mussel shells. Other common rocky intertidal mollusks at this site include *L. keenae, L. plena,* and *T. funebralis*. Interestingly, *L. plena* and *T. funebralis* at this site were quite small in size compared to other sites from which our mussel samples were collected.

Avila Beach: Avila Beach, CA marks the northernmost of our three replicated sites from Dodd 1961 (19). Samples were collected from the Avila Beach Pier (35°10′42″N, 120°44′03″W) at low tide around 2 AM so clear photographs of the sampled mussel beds are not available. We collected *M. californianus* from the ocean-facing side of the two pilings in the 14th row of pier pilings counted from the beginning of the pier at the beach. The mussels here were the most varied in terms of ontogeny making it possible for us to directly match the size of each individual collected by Dodd (19).

Corona del Mar: Our second matched site as we move down the coast is Corona del Mar, CA. We collected *M. californianus* from the first large rock (Fig. S8a) approximately 640 m to the south of the Kerckhoff Marine Laboratory and 200 m north of the tide pools and Inspiration Point on Corona del Mar State Beach (Fig. S8b, 33°35′33″N, 117°52′23″W).

La Jolla: Our southernmost matched site is the Ellen Browning Scripps Memorial Pier (32°51′58″N, 117°15′15″W) on the Scripps Institution of Oceanography campus. We collected

M. californianus from the ocean-facing side of the two pilings in the 8th row of pier pilings counted from the landward end of the pier (Fig. S9a). At this site *M. californianus* occupies the wave exposed ocean-facing side of pier pilings while introduced Mediterranean mussel, *M. galloprovincialis*, is found on the beach facing side of the piling, protected from the waves. Gooseneck barnacles, crabs, and limpets such as *L. pelta*, and *L. scabra* are also common on these pilings. *L. gigantea* can also be found on the pilings, but they are not as common as the other limpets. Note that the mussel beds that we collected our samples from were decimated by illegal harvesting of intertidal species from this Marine Protected Area (MPA) during the Covid - 19 lockdown in California (Fig. S9b). This was a phenomenon occurring in many areas of southern California and elsewhere, as widely reported by the media (e.g. (SAHAGÚN 2020)).

Figures S1-S9

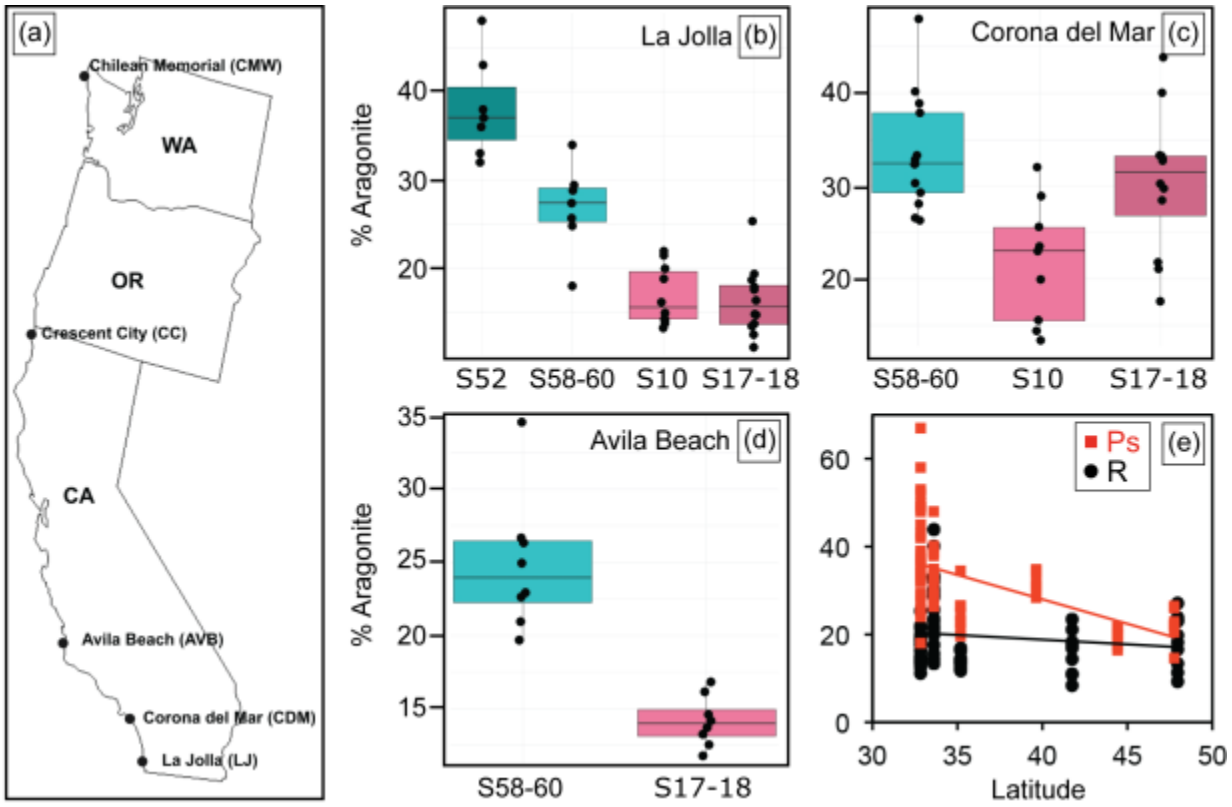

Figure S1. (a). Locality map showing the five sampled sites from S17-18. Three of the sites, Avila Beach (n=8 both time periods), Corona del Mar (n = 14 S58-60, n = 9 S10, n=12 S17-18), and La Jolla (n = 7 S52, n = 7 S58-60, n = 10 S10, n = 12 S17-18), are sites where direct matching of sampling location to S58-60 were possible, and two of the sites, La Jolla and Corona del Mar also include S10 data. Comparisons of the percent aragonite for S52, S58-60, S10, and S17-18 are included as boxplots. Significance of each comparison for each site is included in *SI Appendix*, Table S3. (b). La Jolla comparison including data from S52 (Lowenstam 1954) as well as S10. (c). Corona del Mar comparison including data from S10. (d). Avila Beach Comparison. (e). Relationship between percent aragonite in individual *M. californianus* from combined S52 (Lowenstam 1954) and S58-60 (Dodd 1961) (Ps, n = 57) and combined S10 and S17-18 (R, n = 70). A comparison of LME with locality as a random effect and using restricted maximum likelihood slopes between Ps and R is significantly different (*SI Appendix*, Table S3), with no

relationship between percent aragonite and latitude for combined S10 and S17-18 data (*SI Appendix*, Table S4).

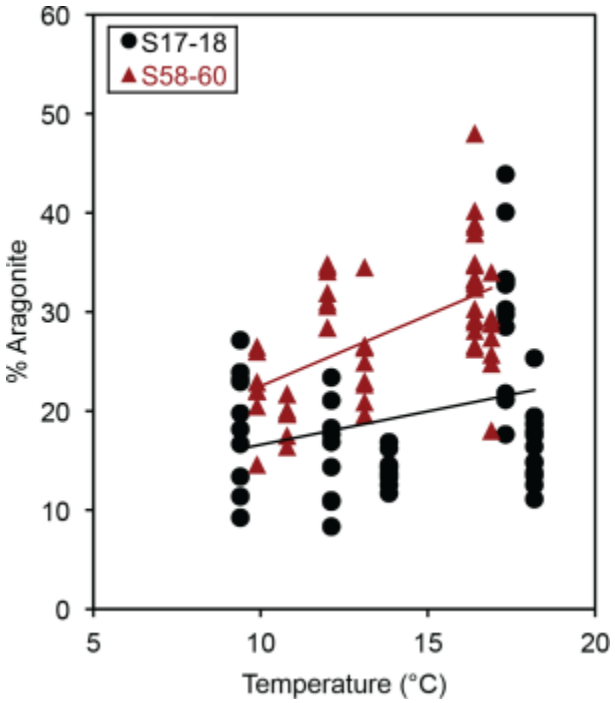

Figure S2. Relationship between temperature and percent aragonite through time for S58-60 (n=50) and S17-18 (n=51). Slopes are not significantly different (*SI Appendix*, Table S3).

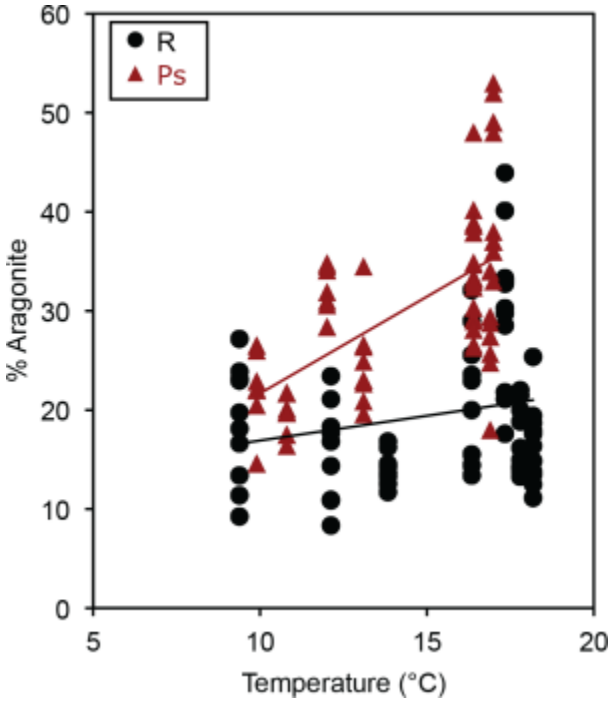

Figure S3. Relationship between temperature and percent aragonite for all of the data. Past data is composed of S52 and S58-60 (Ps, n = 57) while recent data includes S10 and S17-18 (R,

n=71). When all of the data are included in the analyses, the slopes are significantly different (*SI Appendix*, Table S3).

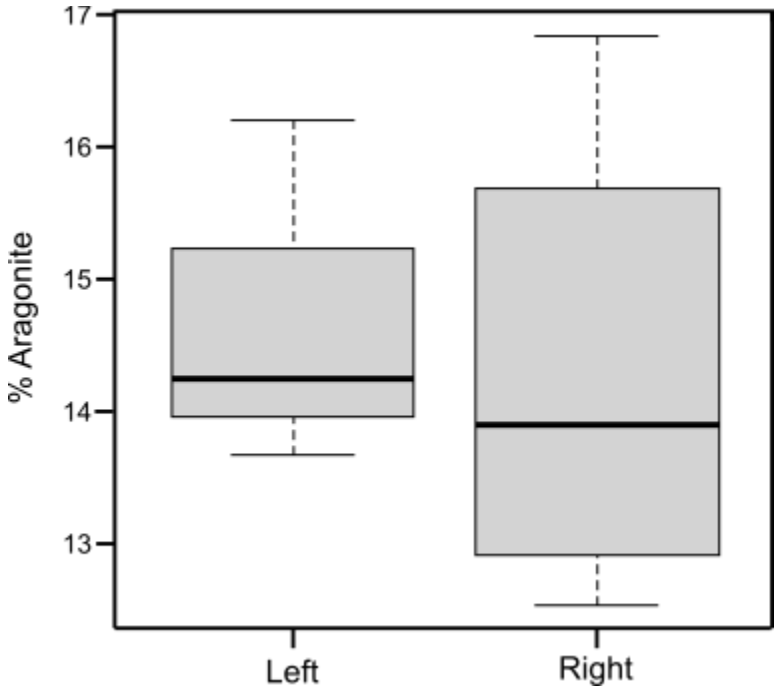

Figure S4. Figure showing percent aragonite for 2017-18 left (n=4) and right (n=4) valves at Avila Beach, California.

.

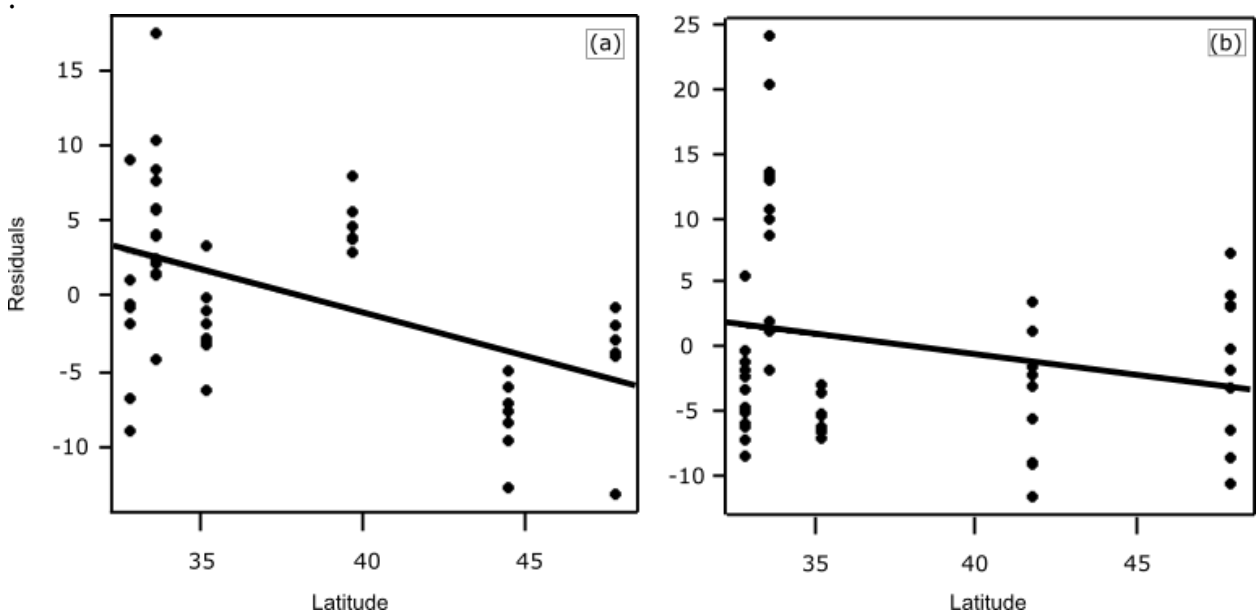

Figure S5. Residuals of percent aragonite ~ length plotted against latitude for a) S58-60 (n=50) and b) S17-18 (n=51).

Figure S6. Chilean Memorial, WA sampling site. Cardinal directions and arrows are included on image to assist with orientation at the site. a) Southern part of the bay leading up to the edge of the ocean. The gray arrows indicate where the flat step allows access to the vertical rock wall that forms the rock edge above the sand and the bay itself. b) Google Earth map showing the Rialto beach parking lot (southernmost white arrow) and the bay where the mussels were sampled ~5.6 km north (northernmost white arrow).

Figure S7. Crescent City, CA sampling site. Cardinal directions and arrows are included on image to assist with orientation at the site. a) Edge of lighthouse (indicated by white arrow) and rocky outcrops forming the pool from which mussels were collected. b) Mussel bed. c) Google Earth photo with white arrow indicating where the samples came from.

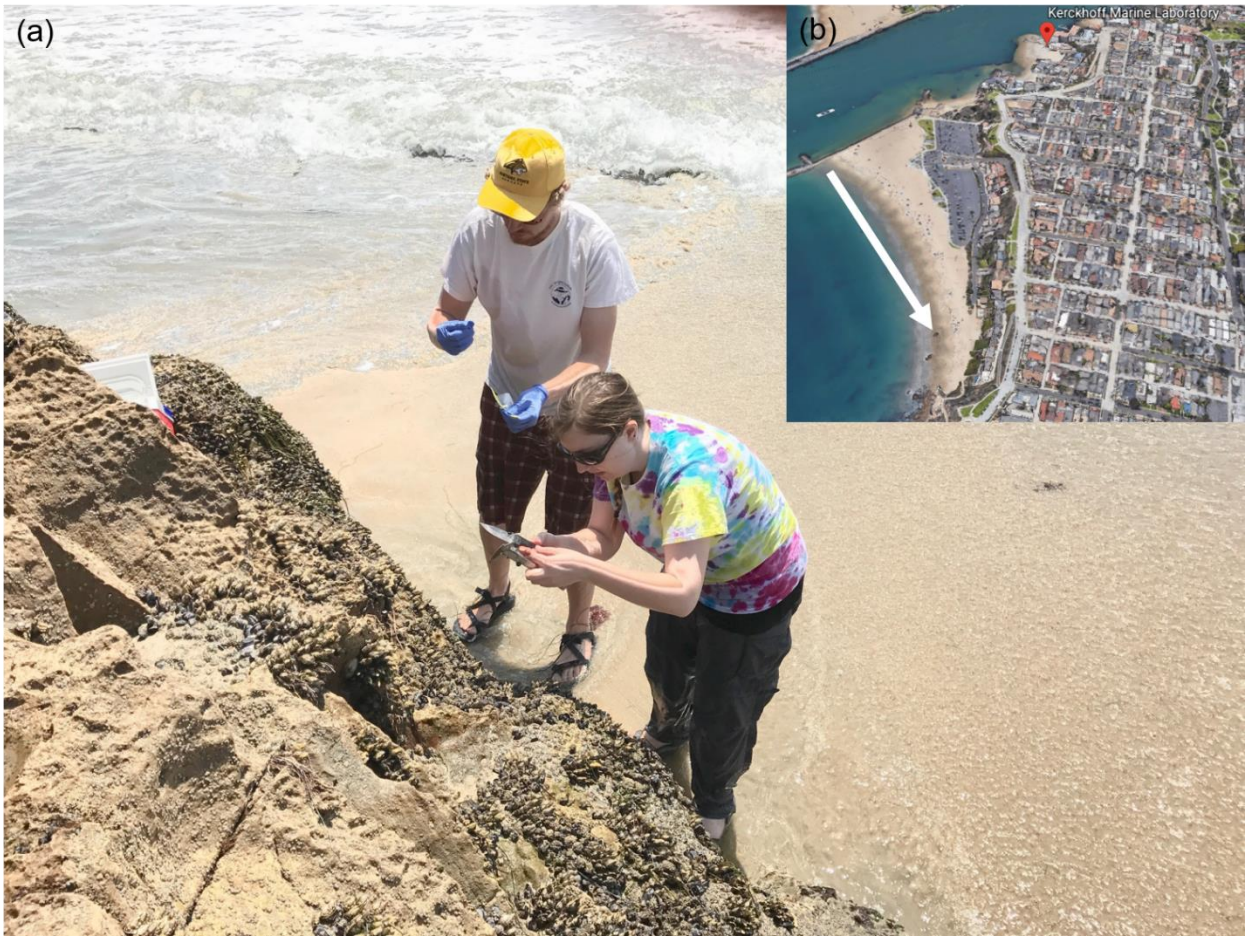

Figure S8. Corona del Mar, CA sampling site. a) Large rock and mussel beds that we collected from. b) Google Earth image of Corona del Mar State Beach with Kerckhoff Marine Laboratory indicated by the red pin and the sampling site indicated by the white arrow.

Figure S9. La Jolla, CA sampling site. a) SIO pier. *M. californianus* were collected from mussel beds attached to the pier pilings. b) Pier pilings after illegal harvesting of mussels and barnacles during the Covid-19 lockdown.

Tables S1-S6

Table S1. Environmental data for S58-60 [(Dodd 1961) and references therein], S10 samples ("National Oceanic and Atmospheric Administration's National Data Buoy Center. Center of Excellence in Marine Technology." n.d., "Southern California Coastal Ocean Observing System" n.d.) and S17-18 samples ("National Oceanic and Atmospheric Administration's National Data Buoy Center. Center of Excellence in Marine Technology." n.d., "Southern California Coastal Ocean Observing System" n.d.).

Locality	**10 YR Avg. SST S58-60 °C**	**10 YR Avg. SST S10 °C**	**10 YR Avg. SST S17-18 °C**	**Collecting Time Salinity S58-60 (‰)**	**Collecting Time Salinity S17-18 (‰)**
La Jolla, CA	16.9°C	17.8°C	18.18°C	34.40 ‰	33.09 ‰
Corona del Mar, CA	16.4°C	16.35°C	17.33°C	34.63‰	33.47‰
Avila Beach, CA	13.1°C	N/A	13.84°C	34.01‰	33.67‰
Westport, CA	12.0°C	N/A	N/A	34.02‰	N/A
Crescent City, CA	11.6°C	N/A	12.12°C	30.48‰	N/A
Waldport, OR	10.8°C	N/A	N/A	34.33‰	N/A
Hoh, WA	9.9°C	N/A	N/A	33.66‰	N/A
Chilean Memorial, WA	N/A	N/A	9.39°C	N/A	N/A

Table S2. Table indicating the number of samples from each locality used in the analyses. A full compilation of details for each individual is available in the supplemental materials (*SI Appendix*, Table S6). See Fig. 1 for time codes and S17-18 abbreviations. Additional abbreviations are as follows: WC = Westport, California; WO = Waldport, Oregon; HW = Hoh, Washington.

Date	LJ	CDM	AVB	WC	CC	WO	HW	CMW
1952	**7**	**-**	**-**	**-**	**-**	**-**	**-**	**-**
1958-60	**7**	**14**	**8**	**7**	**1**	**7**	**7**	**-**
2010	**10**	**9**	**-**	**-**	**-**	**-**	**-**	**-**
2017-18	**12**	**12**	**8**	**-**	**9**	**-**	**-**	**10**

Table S3. Statistical analyses used and the results. Significant results are marked with *.

Comparison	Statistical Analysis	Significance
% Aragonite left valve to right valve at AVB	Wilcoxon Rank Sum Test	$p = 0.72$
% Aragonite S58-60 LJ to S17-18 LJ	Kruskal-Wallis Test	$p = 0.0013$*
% Aragonite S10 LJ to S17-18 LJ	Kruskal-Wallis Test	$p = 0.55$
% Aragonite S58-60 CDM to S17-18 CDM	Kruskal-Wallis Test	$p = 0.25$
% Aragonite S10 CDM to S17-18 CDM	Kruskal-Wallis Test	$p = 0.016$*
% Aragonite S58-60 AVB to S17-18 AVB	Kruskal-Wallis Test	$p < 0.001$*
% Aragonite ~ Latitude S17-18	Moran's I Test for Spatial Autocorrelation	$p < 0.001$*
% Aragonite ~ Time S58-60 to S17-18	Durbin-Watson Test for Temporal Autocorrelation	$p < 0.001$*
Slope of % Aragonite ~ Latitude S58-60 to S17-18	LME Comparison	$p = 0.79$
Slope of Residuals of % Aragonite and Length ~ Latitude S58-60 to S17-18	GLS Comparison	$p = 0.23$
Slope of % Aragonite ~ Latitude Ps to R	LME Comparison	$p = 0.035$*
Slope of Residuals of % Aragonite and Length ~ Latitude Ps to R	GLS Comparison	$p = 0.0082$*

Table S4. Model equations and statistical results.

Equation	Estimate ± SE	T or Z value	P value or Pr(>|z|) (approx.)	AIC
gls(% Aragonite ~ Time + Latitude * Temperature + Length (mm) + Weight (g))				682.39
(Intercept)	5.85 ± 24.01	0.24	0.99	
Time	-8.41 ± 1.63	-5.16	<0.001*	
Latitude	0.19 ± 0.39	0.48	0.73	
Temperature	1.24 ± 0.73	1.70	0.62	
Length	-0.086 ± 0.12	-0.71	0.47	
Weight	0.38 ± 0.59	0.64	0.52	
Latitude:Temperature	-0.027 ± 0.13	-0.20	0.84	
S58-60 gls(% Aragonite ~ Latitude * Temperature + Length (mm) + Weight (g))				318.37
(Intercept)	130.86 ± 51.70	2.53	0.015*	
Latitude	-4.21 ± 1.76	-2.39	0.021*	
Temperature	-13.35 ± 5.98	-2.23	0.31	
Length	-0.41 ± 0.14	-2.87	0.0063*	
Weight	1.75 ± 0.78	2.24	0.032*	
Latitude:Temperature	0.50 ± 0.20	2.48	0.017*	
S17-18 gls(% Aragonite ~ Latitude * Temperature + Length (mm) + Weight (g))				354.69
(Intercept)	-17.31 ± 69.92	-0.25	0.81	
Latitude	-0.53 ± 2.51	-0.21	0.83	

Temperature	-3.04 ± 9.79	-0.31	0.76	
Length	0.29 ± 0.25	1.15	0.26	
Weight	-1.28 ± 1.65	-0.78	0.44	
Latitude:Temperature	0.17 ± 0.33	0.53	0.60	
lme(% Aragonite ~ Time + Latitude + Temperature + Length (mm) + Weight (g), random=Locality)				638.02
(Intercept)	43.50 ± 64.71	0.67	0.50	
Time	-6.73 ± 2.35	-2.87	0.005*	
Latitude	-0.36 ± 1.01	-0.35	0.74	
Temperature	0.03 ± 2.01	0.016	0.99	
Length	-0.13 ± 0.10	-1.20	0.23	
Weight	0.48 ± 0.59	0.82	0.41	
Locality	5.56 ± 5.16			
S58-60 lme(% Aragonite ~ Latitude * Temperature + Length (mm) + Weight (g), random = Locality)				305.84
(Intercept)	135.96 ± 149.33	0.91	0.37	
Latitude	-4.00 ± 5.17	-0.77	0.52	
Temperature	-12.40 ± 17.69	-0.70	0.56	
Length	-0.30 ± 0.12	-2.57	0.014*	
Weight	0.98 ± 0.65	1.51	0.14	
Latitude:Temperature	0.44 ± 060	0.74	0.54	
Locality	5.52 ± 4.15			
S17-18				328.56

lme(% Aragonite ~ Latitude * Temperature + Length (mm) + Weight (g), random = Locality)				
(Intercept)	-64.58 ± 201.35	-0.32	0.75	
Latitude	1.33 ± 5.60	0.24	0.85	
Temperature	4.03 ± 19.68	0.20	0.87	
Length	0.12 ± 0.18	0.67	0.50	
Weight	-0.062 ± 1.16	-0.054	0.96	
Latitude:Temperature	-0.057 ± 0.65	-0.086	0.95	
Locality	11.02 ± 5.46			
Cochran-Orcutt Analysis of Temporal Autocorrelation: S58-60 to S17-18 lm(% Aragonite ~ Time+ Latitude + Temperature + Length (mm) + Weight (g))				
Intercept	5.04 ± 54.09	0.093	0.93	
Time	-8.17 ± 2.60	-3.14	0.0023*	
Latitude	0.47 ± 1.62	0.29	0.77	
Temperature	2.42 ± 5.56	0.44	0.66	
Length	-0.14 ± 0.14	-1.00	0.32	
Weight	0.52 ± 0.71	0.73	0.47	
Cochran-Orcutt Analysis of Temporal Autocorrelation: Ps to R lm(% Aragonite ~ Time+ Latitude + Temperature + Length (mm) + Weight (g))				
Intercept	-1.94 ± 35.28	-0.055	0.96	
Time	-11.74 ± 2.28	-5.15	<0.001*	

Latitude	0.28 ± 0.56	0.50	0.62	
Length	-0.04 ± 0.08	-0.46	0.65	
Weight	0.13 ± 0.21	0.62	0.56	
SAR (Mixed Lag Effect) *S58-60* lagsarlm(% Aragonite ~ Latitude * Temperature + Length (mm) + Weight (g), Random = Locality)				315.39
Intercept	118.97 ± 50.08	2.38	0.018*	
Latitude	-3.83 ± 1.70	-2.25	0.024*	
Temperature	-12.21 ± 5.74	-2.13	0.033*	
Length	-0.42 ± 0.13	-3.20	0.001*	
Weight	1.78 ± 0.73	2.47	0.014*	
Latitude:Temperature	0.45 ± 0.19	2.37	0.018*	
SAR (Mixed Lag Effect) *S17-18* lagsarlm(% Aragonite ~ Latitude * Temperature + Length (mm) + Weight (g), Random = Locality)				349.76
Intercept	-12.83 ± 58.81	-0.22	0.83	
Latitude	-0.41 ± 2.11	-0.2	0.85	
Temperature	-1.85 ± 8.23	-0.23	0.82	
Length	0.29 ± 0.21	1.36	0.17	
Weight	-1.07 ± 1.38	-0.78	0.44	
Latitude*Temperature	0.11 ± 0.28	0.41	0.68	
Residual Linear Model			< 0.001*	316.88

S58-60 Residuals: lm(% Aragonite ~ Length) Model: lm(residuals ~ latitude)				
Intercept	21.63 ± 5.50	3.93	< 0.001*	
Latitude	-0.57 ± 0.14	-3.97	<0.001*	
Residual Linear Model *S17-18* Residuals: lm(% Aragonite ~ Length) Model: lm(residuals ~ latitude)			0.12	353.07
Intercept	11.44 ± 7.34	1.56	0.13	
Latitude	-0.30 ± 0.19	-1.58	0.12	
Ps to R lme(% Aragonite ~ Time + Latitude * Temperature + Length (mm) + Weight (g), random=Locality)				869.01
Intercept	-41.31 ± 83.01	-0.50	0.62	
Time	-12.71 ± 1.96	-6.50	<0.001*	
Latitude	1.51 ± 2.41	0.63	0.55	
Temperature	5.95 ± 8.16	0.73	0.47	
Length	-0.16 ± 0.12	-1.28	0.20	
Weight	1.28 ± 0.7	1.83	0.07	
Latitude:Temperature	-0.13 ± 0.26	-0.50	0.62	
Locality	5.08 ± 6.56			
Ps lme(% Aragonite ~ Latitude * Temperature + Length (mm) + Weight (g), random=Locality)				403.63
Intercept	55.42 ± 115.03	0.48	0.63	

Latitude	-2.69 ± 3.99	-0.67	0.54	
Temperature	-8.27 ± 13.64	-0.61	0.55	
Length	-0.34 ± 0.18	-1.92	0.061	
Weight	1.96 ± 0.96	2.06	0.045*	
Latitude:Temperature	0.39 ± 0.46	0.85	0.40	
Locality	3.70 ± 6.55			
R lme(% Aragonite ~ Latitude * Temperature + Length (mm) + Weight (g), random=Locality)				449.82
Intercept	-144.13 ± 169.73	-0.85	0.40	
Latitude	1.66 ± 5.02	0.33	0.76	
Temperature	1.66 ± 16.99	0.098	0.92	
Length	-0.03 ± 0.16	-0.19	0.85	
Weight	0.61 ± 1.07	0.57	0.57	
Latitude:Temperature	0.14 ± 0.52	0.28	0.78	
Locality	9.84 ± 5.44			
Residual linear model *Ps* Residuals: lm(% Aragonite ~ Length) Model: lm(residuals ~ latitude)			<0.001*	406.40
Intercept	33.31 ± 6.68	4.98	<0.001*	
Latitude	-0.89 ± 0.18	-5.03	<0.001*	
Residual Linear Model *R* Residuals: lm(% Aragonite ~ Length)			0.13	475.01

Model: lm(residuals ~ latitude)				
Intercept	9.05 ± 6.02	1.50	0.137	
Latitude	-0.25 ± 0.16	-1.52	0.13	
Residual Linear Model S58-60 Residuals: lm(% Aragonite ~ Length) Model: lm(Residuals ~ Temperature			< 0.001*	317.60
Intercept	-15.50 ± 4.10	-3.78	<0.001*	
Temperature	1.14 ± 0.30	3.85	<0.001*	
Residual Linear Model S17-18 Residuals: lm(% Aragonite ~ Length) Model: lm(Residuals ~ Temperature			0.04*	351.19
Intercept	-9.94 ± 4.85	-2.05	0.046*	
Temperature	0.68 ± 0.33	2.10	0.041*	

Table S5. Change in temperature from S52 to S17-18 ("National Oceanic and Atmospheric Administration's National Data Buoy Center. Center of Excellence in Marine Technology." n.d., "Southern California Coastal Ocean Observing System" n.d., Lowenstam 1954, Dodd 1961), median percent aragonite, standard deviation (SD), *p*-value for a Kruskal-Wallace rank sum test assessing changes in median percent aragonite from past samples to present. *Unknown if this reported value is a 10 year mean average or a one year mean average (Lowenstam 1954). **S58-60 only has one individual for this site (Dodd 1961), so rigorous statistics are not possible, but qualitative assessments are feasible.

Sample	**Δ 10 YR Avg. T (°C) Compared to S17-18**	**Median % Aragonite**	**SD of % Aragonite**	**Significance of Δ in Median % Aragonite Compared to S17-18**
La Jolla, S52	+ 1.18°C	37.00 %	5.64	$p < 0.001$*

La Jolla, S58-60	+ 1.28°C	27.40 %	4.93	$p = 0.0013$*
La Jolla, S10	+0.38°C	15.58%	3.34	$p = 0.55$
La Jolla, S17-18	N/A	15.62%	3.83	N/A
Corona del Mar, S58-60	+ 0.93°C	33.20 %	5.33	$p = 0.25$
Corona del Mar, S10	+ 0.98°C	22.98 %	6.54	$p = 0.016$*
Corona del Mar, S17-18	N/A	31.50 %	7.58	N/A
Avila Beach, S58-60	+ 0.74°C	23.95 %	4.63	$p < 0.001$*
Avila Beach, S17-18	N/A	13.97 %	1.74	N/A
Westport, S58-60	N/A	31.90 %	2.39	N/A
Crescent City, S58-60	+ 0.52°C	42.90 % **	N/A	N/A
Crescent City, S17-18	N/A	16.82 %	5.02	N/A
Waldport, S58-60	N/A	19.80 %	1.99	N/A
Hoh, S58-60	N/A	22.10 %	3.96	N/A
Chilean Memorial, S17-18	N/A	18.93 %	5.90	N/A

Table S6. Sample ID, locality, collection year, tidal position, substrate type, percent aragonite, size, and weight of each specimen in these analyses.

Sample	Locality	Year Collected	Tidal Position	Substrate	% Aragonite	Length (mm)	Weight (g)
SIO1	La Jolla	2017	Pier pilings (mid portion)	Concrete	19.41	34.36	0.961
SIO2	La Jolla	2017	Pier pilings (mid portion)	Concrete	25.32	54.72	4.347
SIO3	La Jolla	2017	Pier pilings (mid portion)	Concrete	14.79	55.15	3.033
SIO4	La Jolla	2017	Pier pilings (mid portion)	Concrete	18.69	49.57	2.964
SIO5	La Jolla	2017	Pier pilings (mid portion)	Concrete	17.9	41.2	1.521
SIO6	La Jolla	2017	Pier pilings (mid portion)	Concrete	16.39	32.29	0.748

SIO7	La Jolla	2017	Pier pilings (mid portion)	Concrete	13.77	35.07	0.936
SIO8	La Jolla	2017	Pier pilings (mid portion)	Concrete	17.58	54.73	2.928
SIO9	La Jolla	2017	Pier pilings (mid portion)	Concrete	13.46	36.23	1.281
SIO10	La Jolla	2017	Pier pilings (mid portion)	Concrete	12.51	34.1	0.792
SIO11	La Jolla	2017	Pier pilings (mid portion)	Concrete	11.11	29.78	0.556
SIO12	La Jolla	2017	Pier pilings (mid portion)	Concrete	14.85	26.49	0.595
SIOK1	La Jolla	2010	Pier pilings (mid portion)	Concrete	14.26	32.73	0.991
SIOK2	La Jolla	2010	Pier pilings (mid portion)	Concrete	19.96	28.59	0.649
SIOK3	La Jolla	2010	Pier pilings (mid portion)	Concrete	18.82	29.15	0.733
SIOK4	La Jolla	2010	Pier pilings (mid portion)	Concrete	14.25	37.94	1.597
SIOK5	La Jolla	2010	Pier pilings (mid portion)	Concrete	14.96	37.72	1.782
SIOK6	La Jolla	2010	Pier pilings (mid portion)	Concrete	21.99	30.76	0.782
SIOK7	La Jolla	2010	Pier pilings (mid portion)	Concrete	13.28	50.26	3.005
SIOK8	La Jolla	2010	Pier pilings (mid portion)	Concrete	21.46	37.99	1.61
SIOK9	La Jolla	2010	Pier pilings (mid portion)	Concrete	16.19	40.85	1.772
SIOK10	La Jolla	2010	Pier pilings (mid portion)	Concrete	13.81	51.16	2.839
LJD1	La Jolla	1958	Pier pilings (mid portion)	Concrete	34	53.5	4.99
LJD2	La Jolla	1958	Pier pilings (mid portion)	Concrete	25.7	45.3	3.21
LJD3	La Jolla	1958	Pier pilings (mid portion)	Concrete	18	41.3	1.79
LJD4	La Jolla	1958	Pier pilings (mid portion)	Concrete	27.4	35.4	1.4
LJD5	La Jolla	1958	Pier pilings (mid portion)	Concrete	29.4	34.8	1.69
LJD6	La Jolla	1958	Pier pilings (mid portion)	Concrete	28.8	26.1	0.577
LJD7	La Jolla	1958	Pier pilings (mid portion)	Concrete	24.8	23.1	0.435
LJL1	La Jolla	1952	Pier pilings (mid portion)	Concrete	36	22.4	0.33
LJL2	La Jolla	1952	Pier pilings (mid portion)	Concrete	48	26.7	0.53
LJL3	La Jolla	1952	Pier pilings (mid portion)	Concrete	37	31.1	0.91
LJL4	La Jolla	1952	Pier pilings (mid portion)	Concrete	38	33.1	0.99

LJL5	La Jolla	1952	Pier pilings (mid portion)	Concrete	33	41	2.03
LJL6	La Jolla	1952	Pier pilings (mid portion)	Concrete	36	50.6	3.77
LJL7	La Jolla	1952	Pier pilings (mid portion)	Concrete	52	56.4	5.4
CDM1	Corona del Mar	2017	Mid-Intertidal	Rock	33.3	44.5	2.758
CDM2	Corona del Mar	2017	Mid-Intertidal	Rock	32.73	47.17	2.744
CDM3	Corona del Mar	2017	Mid-Intertidal	Rock	43.89	46.2	3.286
CDM4	Corona del Mar	2017	Mid-Intertidal	Rock	32.95	50.62	4.061
CDM5	Corona del Mar	2017	Mid-Intertidal	Rock	33.22	36.73	1.606
CDM6	Corona del Mar	2017	Mid-Intertidal	Rock	21.79	52.4	3.722
CDM7	Corona del Mar	2017	Mid-Intertidal	Rock	29.73	49.39	3.197
CDM8	Corona del Mar	2017	Mid-Intertidal	Rock	40.08	46.62	4.018
CDM9	Corona del Mar	2017	Mid-Intertidal	Rock	21.09	53.32	3.305
CDM10	Corona del Mar	2017	Mid-Intertidal	Rock	28.49	49.31	3.173
CDM11	Corona del Mar	2017	Mid-Intertidal	Rock	30.26	28.91	0.839
CDM12	Corona del Mar	2017	Mid-Intertidal	Rock	17.62	20.5	0.469
BROC1	Corona del Mar	2010	Mid-Intertidal	Rock	23.55	23.24	0.356
BROC2	Corona del Mar	2010	Mid-Intertidal	Rock	28.94	65.78	6.7
BROC3	Corona del Mar	2010	Mid-Intertidal	Rock	13.42	54.5	4.32
BROC4	Corona del Mar	2010	Mid-Intertidal	Rock	32.07	52.93	3.695
BROC5	Corona del Mar	2010	Mid-Intertidal	Rock	14.44	49.79	2.826
BROC6	Corona del Mar	2010	Mid-Intertidal	Rock	25.57	50.26	3.604
BROC7	Corona del Mar	2010	Mid-Intertidal	Rock	19.97	50.37	2.667
BROC8	Corona del Mar	2010	Mid-Intertidal	Rock	22.98	42.48	2.334
BROC9	Corona del Mar	2010	Mid-Intertidal	Rock	15.52	38.72	1.715
CDMD1	Corona del Mar	1958	“Intertidally exposed position”	Rock	40.2	20.4	0.8744
CDMD2	Corona del Mar	1958	“Intertidally exposed position”	Rock	37.9	21.7	0.755

CDMD3	Corona del Mar	1959	“Intertidally exposed position”	Rock	48	26.6	1.3604
CDMD4	Corona del Mar	1959	“Intertidally exposed position”	Rock	38.9	26.5	1.28
CDMD5	Corona del Mar	1959	“Intertidally exposed position”	Rock	32.4	28.6	1.4034
CDMD6	Corona del Mar	1960	“Intertidally exposed position”	Rock	26.6	25.5	0.8463
CDMD7	Corona del Mar	1960	“Intertidally exposed position”	Rock	32.4	27.3	1.105
CDMD8	Corona del Mar	1959	“Intertidally exposed position”	Rock	33.4	67.3	7.3
CDMD9	Corona del Mar	1959	“Intertidally exposed position”	Rock	29.3	63.2	4.91
CDMD10	Corona del Mar	1959	“Intertidally exposed position”	Rock	26.3	54	3.19
CDMD11	Corona del Mar	1959	“Intertidally exposed position”	Rock	33.3	48.8	3.39
CDMD12	Corona del Mar	1959	“Intertidally exposed position”	Rock	30.3	44.5	2.67
CDMD13	Corona del Mar	1959	“Intertidally exposed position”	Rock	28.1	42.4	1.31
CDMD14	Corona del Mar	1959	“Intertidally exposed position”	Rock	32.9	32.8	0.81
AVB1	Avila Beach	2018	Pier pilings (mid portion)	Wood	11.7	70.76	7.526
AVB2	Avila Beach	2018	Pier pilings (mid portion)	Wood	14.53	37.56	1.849
AVB3	Avila Beach	2018	Pier pilings (mid portion)	Wood	14.26	24.41	0.487
AVB4	Avila Beach	2018	Pier pilings (mid portion)	Wood	12.54	34.52	1.36
AVB5	Avila Beach	2018	Pier pilings (mid portion)	Wood	16.21	38.91	1.258
AVB6	Avila Beach	2018	Pier pilings (mid portion)	Wood	16.85	47.57	3.601
AVB7	Avila Beach	2018	Pier pilings (mid portion)	Wood	13.68	48.16	2.544
AVB8	Avila Beach	2018	Pier pilings (mid portion)	Wood	13.29	61.15	4.794
AVBD1	Avila Beach	1958	Pier pilings (mid portion)	Wood	22.7	69.2	9.48

AVBD2	Avila Beach	1958	Pier pilings (mid portion)	Wood	20.9	60.1	9.2
AVBD3	Avila Beach	1958	Pier pilings (mid portion)	Wood	23	47.6	5.25
AVBD4	Avila Beach	1958	Pier pilings (mid portion)	Wood	19.6	47	4.21
AVBD5	Avila Beach	1958	Pier pilings (mid portion)	Wood	26.4	39	2.69
AVBD6	Avila Beach	1958	Pier pilings (mid portion)	Wood	24.9	35.7	1.92
AVBD7	Avila Beach	1958	Pier pilings (mid portion)	Wood	26.6	34.2	1.79
AVBD8	Avila Beach	1958	Pier pilings (mid portion)	Wood	34.5	24.4	0.753
CC1	Crescent City	2017	Mid-Intertidal	Rock	21.08	59.98	7.756
CC2	Crescent City	2017	Mid-Intertidal	Rock	10.86	60.02	8.803
CC3	Crescent City	2017	Mid-Intertidal	Rock	18.28	52.32	5.227
CC4	Crescent City	2017	Mid-Intertidal	Rock	17.63	54.24	7.364
CC5	Crescent City	2017	Mid-Intertidal	Rock	14.33	63.79	9.506
CC6	Crescent City	2017	Mid-Intertidal	Rock	16.82	58.42	6.482
CC7	Crescent City	2017	Mid-Intertidal	Rock	23.38	64.25	10.731
CC8	Crescent City	2017	Mid-Intertidal	Rock	10.96	62.74	8.968
CC9	Crescent City	2017	Mid-Intertidal	Rock	8.34	67.62	10.359
CCD1	Crescent City	1959	Mid-Intertidal	Rock	42.9	44.5	3.37
CMW1	Chilean Memorial	2017	Mid-Intertidal	Rock	16.64	54.93	3.674
CMW2	Chilean Memorial	2017	Mid-Intertidal	Rock	27.15	56.72	5
CMW3	Chilean Memorial	2017	Mid-Intertidal	Rock	9.23	54.85	3.971
CMW4	Chilean Memorial	2017	Mid-Intertidal	Rock	23.87	58.8	3.496
CMW5	Chilean Memorial	2017	Mid-Intertidal	Rock	19.73	57.58	4.883
CMW6	Chilean Memorial	2017	Mid-Intertidal	Rock	13.39	59.09	4.613
CMW7	Chilean Memorial	2017	Mid-Intertidal	Rock	23.16	57.26	4.245
CMW8	Chilean Memorial	2017	Mid-Intertidal	Rock	22.94	52.74	2.801
CMW9	Chilean Memorial	2017	Mid-Intertidal	Rock	11.36	57	5.078
CMW10	Chilean Memorial	2017	Mid-Intertidal	Rock	18.12	56.61	4.636

WCD1	Westport	1958	“Intertidally exposed position”	Rock	31.9	60.2	8.67
WCD2	Westport	1958	“Intertidally exposed position”	Rock	28.4	55.2	7.94
WCD3	Westport	1958	“Intertidally exposed position”	Rock	31	50.2	5.12
WCD4	Westport	1958	“Intertidally exposed position”	Rock	30.6	46.5	3.7
WCD5	Westport	1958	“Intertidally exposed position”	Rock	34.5	32.3	1.3
WCD6	Westport	1958	“Intertidally exposed position”	Rock	34.1	27.3	0.739
WCD7	Westport	1958	“Intertidally exposed position”	Rock	34.8	22.3	0.578
WOD1	Waldport	1958	“Intertidally exposed position”	Rock	17.5	55.3	4.91
WOD2	Waldport	1958	“Intertidally exposed position”	Rock	20.1	45.7	2.87
WOD3	Waldport	1958	“Intertidally exposed position”	Rock	21.7	42.6	2.01
WOD4	Waldport	1958	“Intertidally exposed position”	Rock	19.8	38.5	1.56
WOD5	Waldport	1958	“Intertidally exposed position”	Rock	19.7	35.4	1.29
WOD6	Waldport	1958	“Intertidally exposed position”	Rock	16.4	31.2	0.771
WOD7	Waldport	1958	“Intertidally exposed position”	Rock	21.7	23.9	0.612
HWD1	Hoh	1958	“Intertidally exposed position”	Rock	20.5	64.2	8.11
HWD2	Hoh	1958	“Intertidally exposed position”	Rock	22	47.8	3.52
HWD3	Hoh	1958	“Intertidally exposed position”	Rock	22.1	45.7	3.48
HWD4	Hoh	1958	“Intertidally exposed position”	Rock	22.9	41.5	2.85

HWD5	Hoh	1958	"Intertidally exposed position"	Rock	26.5	39.5	1.94
HWD6	Hoh	1958	"Intertidally exposed position"	Rock	14.6	37.1	2.14
HWD7	Hoh	1958	"Intertidally exposed position"	Rock	26	36.5	1.37

SI References

1. L. Sahagún, Crowds removing sea creatures from San Pedro tide pools put delicate ecosystem at risk. *Los Angeles Times* (2020). Available at: https://www.latimes.com/environment/story/2020-07-17/unprecedented-crowds-are-harvesting-sea-creatures-from-san-pedros-famous-tide-pools

Acknowledgements

Chapter 1, in full, is a reprint as it appears in Bullard et al. 2021. Bullard, E.M, Torres, I., Ren, T., Graeve, O.A., Roy, K. 2021. Shell mineralogy of a foundational marine species, *Mytilus californianus*, over half a century in a changing ocean. *PNAS*, 118 (3), 1-5. The dissertation author was the primary investigator and author of this paper.

CHAPTER 2

Functional consequences of changing shell calcification traits in response to anthropogenic climate change in a foundational marine bivalve.

Abstract

Marine mollusks are potentially at great risk under ocean warming and acidification (OA) as their calcium carbonate exoskeletons make them vulnerable to dissolution. While there is a growing body of literature assessing how individual traits in mollusks, like shell calcification and mortality, respond to increasing temperature and OA on both short-term and decadal to centennial scales, we are still limited in our understanding of how multiple, interacting traits change across a species' range in response to these stressors. Two key traits that have received little attention but are integral to shell function, namely strength and toughness, are internal shell organics and shell structure (shape). Here, we assess how shell organics and shell structure respond to changing temperature and pH regimes across twelve populations of the foundational species, *Mytilus californianus*, from the Oregonian and Californian provinces of the eastern Pacific and quantify the impact of these changes on shell strength and toughness. We find that not only do our data not support the hypotheses that shell organics offset dissolution and increase toughness, but Oregonian samples are more calcified and have a greater shell volume than their Californian counterparts despite a more acidified environment. We also show that Californian shells are still stronger than Oregonian despite this difference in shell volume and no significant difference in shell organic weight percent between the provinces and suggest this is due to differences in shell structure, namely compacity index, and a greater endolithic parasite load in the Oregonian populations. Finally, we show that internal organic content does not differ

between the different polymorphs of calcium carbonate within the mussel shell and qualitatively suggest that this relationship of organics between polymorphs as well as shell organic weight percent has potentially changed through time. This work highlights the power of multi-population field analyses assessing how different anthropogenic drivers influence multiple traits and their relationships to shell function.

Introduction

The impacts of anthropogenic stressors, particularly warming and ocean acidification (OA), on organisms that precipitate calcium carbonate ($CaCO_3$) exoskeletons has garnered considerable attention in recent years. There is now a growing body of literature ranging from short-term tank experiments (Kroeker et al. 2010) to decadal and centennial comparisons (Pfister et al. 2016, Cross et al. 2018, Bullard et al. 2021) assessing how these two stressors may impact calcification-related traits and ultimately the health of marine calcifiers. Results of both short and long-term assessments can be varied (Ries et al. 2009, Pfister et al. 2016, Cross et al. 2018), but generally show negative impacts on traits ranging from physiology (Kroeker et al. 2013, Figuerola et al. 2021) to inhibition of shell growth (Kroeker et al. 2010, Figuerola et al. 2021) and function (Fitzer et al. 2015a). While past studies have provided a wealth of knowledge on how OA and temperature (and their interaction) can impact certain traits in individual organisms, we still lack robust data on how multiple traits change and interact under different temperature and pH regimes and how this may impact the overall functionality of the exoskeleton. For example, recent work on a mixed-mineralogy foundational marine mussel, *Mytilus californianus*, assessing multiple populations along the northeast Pacific over the last half century, showed that this species has shifted its mineralogy from the stronger but more soluble aragonite to the weaker

but less soluble calcite over the last 60 years (Bullard et al. 2021), but whether or not other traits are changing and how those interacting changes may influence shell strength and toughness in this species remain unknown.

As mineralogy (i.e., aragonite:calcite ratio) has already been assessed in *M. californianus* and has been shown to no longer be significantly different along the west coast of the U.S., we use *M. californianus* as a model to assess the response of additional traits, namely shell organics and shell structure, to different temperature and pH regimes. Shell organics are hypothesized to aid in stopping shell dissolution (Harper 2000, Telesca et al. 2019) as well as increasing shell toughness (Meyers et al. 2008, Lopez et al. 2014). They are known to vary in weight percentage in different species, mineralogy polymorphs, and structural types (Hudson 1967, Taylor and Layman 1972), though how they vary under different environmental conditions and among multiple populations of a species remains significantly less explored (but see (Welladsen et al. 2010, Telesca et al. 2019)). Shell structure, or shell shape, can be impacted by a myriad of drivers from wave energy (Pfister et al. 2016), to predation pressure (Pfister et al. 2016), and even food availability(Pfister et al. 2016). While some studies assessing how different morphometric measurements are tied to strength (e.g., thickness, length, etc.) (Zuschin et al. 2017), only theoretical assessments of how different shell structures correspond to increasing or decreasing strength currently have been conducted (Johnson 2020).

To assess how multiple traits important to shell function are changing under increasing temperature and OA as well as conduct a test of the theoretical work assessing the relationship between different shell structures and strength, we used twelve populations of *M. californianus*, from the Oregonian (cooler, lower pH waters) and Californian (warmer, higher pH waters) provinces along the northeastern Pacific coast. Using these twelve populations existing under

different temperature and pH regimes (Hauri et al. 2009, Feely et al. 2016), we explicitly test the following four hypotheses: i) Cooler, lower pH waters negatively impact shell calcification, and smaller, thinner shells are less strong. Due to more corrosive waters, Oregonian samples should have a lower shell volume and be weaker than their Californian counterparts., ii) Organics buffer against low pH and increase shell toughness. Lower pH in the Oregonian province should mediate higher organic content than Californian counterparts and this increase in organics should make Oregonian samples tougher than Californian., iii) Shells with similar biomaterials can still have different strength and toughness measurements because of difference in shell structure. More elongated, inflated, and higher compacity index shells will be stronger (and tougher)., and iv) Nacre (aragonite) has a significantly higher organic content than prismatic (calcite) so the nacreous portions of an individual *M. californianus* shell should be higher than the prismatic.

Methods

Specimen Collection & Morphometric Analysis

We collected individuals of *M. californianus* in 2017-2018 from twelve sites (Fig. 1, Table S1). At each locality, we collected individuals from wave-exposed sites in the middle portion of the mussel zone (Supplemental Methods). We targeted a similar body size range at each site, and when available, sampled an ontogenetic sequence. Each site was sampled once in either 2017 or 2018 except Cayucos, where samples from both 2017 and 2018 are available and La Jolla where samples were collected in both July and September 2018 (site details in Supplemental Methods).

We measured shell length (perpendicular to umbo), height (parallel to umbo), and width (base of a valve to most protruding point across the lateral plane) of individual valves with electronic calipers. Shell thickness was measured using an electronic micrometer across seven

points along the central portion of the valve following the growth trajectory from the beak to the posterior margin of each individual. We then averaged these measurements to get a mean thickness for each individual valve. Measurements were taken from a single valve for each individual with left or right valves chosen randomly.

We used shell length, height, width, and mean thickness measurements to calculate shell volume and three additional shell traits: elongation index (Johnson 2020), compacity index (Caill-Milly et al. 2012), and inflation index (Johnson 2020) (Fig. 2). All measurements and their explanations can be found in Table 1.

Table 1. Equations for each structural and organic measurement included in analyses.

Structure Measurement	Equation	Explanation
Shell Volume	$V = 4/3\prod(abc – (a-t)(b-t)(c-t))$	a = length, b = height, c = width, and t = thickness
Elongation Index	EI = a/b	a = length (perpendicular to umbo) and b = height
Compacity Index	CI: c/a	c = width and a = length
Inflation Index	I: b/c	b = height and c = width
Internal organics	Initial valve weight with periostracum removed – burned valve weight	Calculated amounts are converted to percentages and used as such in analyses.

Quantifying shell organics

Bulk measurement: We used two different but complimentary approaches to quantify the organic content of the shell. First, we weighed each valve, removed the periostracum using a Dremel drill tip, re-weighed the valve and combusted it in a muffle furnace at 450°C for 48 hours following long established published protocols (Goulletquer and Wolowicz 1989). The resulting ash-free dry weight was used to calculate both a fraction and percentage of internal and external shell organics (Table 1). As the periostracum is highly variable and can be damaged during transportation and handling, we did not include it in our analyses.

DSC/TGA: For a subset of the individuals (two per population of equivalent size), we also measured organics for the calcitic and aragonitic components of an individual shell using

differential scanning calorimetry (DSC) and thermal gravimetric analysis (TGA). DSC/TGA is more accurate than bulk organics as it gives estimates devoid of shell water burn off and provides a more in-depth picture of how organics vary between different polymorphs of calcium carbonate spatially in the shell. For each sample, two samples of calcite and two samples of aragonite were carefully removed using a diamond tipped Dremel hand saw along the growth axis in approximately the same location for each individual for a total of four samples per individual. We ran each sample, heating samples in air with a heating rate of 5K/min until 700°C following published protocols (Telesca et al. 2019). We calculated percent organics within each polymorph by assessing weight changes in the material between 150°C and 500°C, as anything before the former temperature should be the burn off of water and anything past 500°C should be the burn off of calcium carbonate (Telesca et al. 2019).

Shell Strength & Toughness Determination

The strength and toughness of each shell was measured following published protocols (Burnett and Belk 2018). Briefly, after cleaning each shell of epibionts, one valve was placed in an Instron material-testing machine to measure the load, time, and mechanical work that is required to fracture a valve when placed horizontally (to mimic crab predation) (Burnett and Belk 2018).

We defined shell strength as the maximum load a shell could withstand before complete failure (peak load) while shell toughness is the work needed to cause a shell to fail. Toughness was calculated by integrating under the curve of shell load (N) until the point of failure.

Statistical Analysis

All analyses were carried out in R (4.0.2) (R Core Team 2018). As morphometric data is often non-normally distributed, we first used the Shapiro-Wilk test to test for normality of the data as well as Bartlett's test for homogeneity of variance. Shell volume and each of the shell structure metrics (EI, CMI, I) were natural log transformed prior to analyses. To account for differences in thickness and internal organics that could be influenced by size and age of individuals, we constrained the data analyzed here to a similar size range.

To test our hypotheses around differences in traits and shell function between the cooler and lower pH Oregonian and warmer, higher pH Californian we used Wilcoxon rank-sum tests. We also used these tests to evaluate differences in percent organics within aragonitic and calcitic portions of the shell.

We used multivariate regressions to test our hypotheses around how structural traits and organics influence shell strength and toughness and to determine which traits matter most. As many of the structural measurements are correlated, multi-collinearity was high in models that included all structural calculations. We ran iterations of models and chose the best fit models using Akaike Information Criterion (AIC). Final models included evaluating strength and toughness as a function of shell volume, compacity index, elongation index, and percent shell organics and set locality as a random effect.

To test whether or not Oregonian and Californian populations have distinct phenotypes as a function of environmental differences, we used an unweighted paired group method with arithmetic mean (UPGMA) cluster analysis to visualize spatial differences among the sites. We then conducted permutational multivariate analysis of variance (PERMANOVA) tests at both site and biogeographic province level.

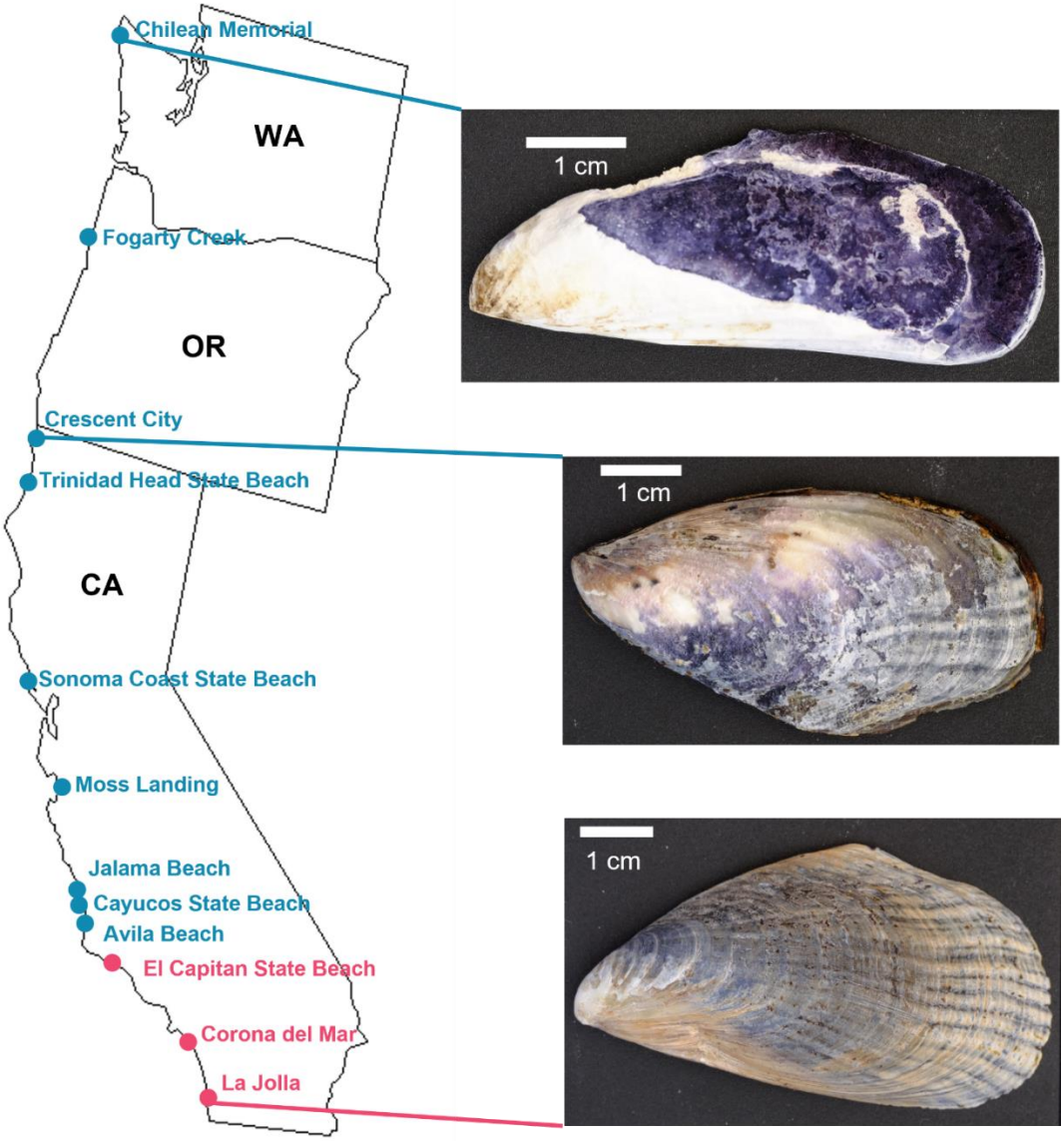

Figure 1. Locality map showing sampling locations. Shell images correspond to different sites and show differences in the quality of the shell.

Results & Discussion

Hypothesis 1: Cooler, lower pH waters negatively impact shell calcification, and smaller, thinner shells are less strong. Due to more corrosive waters, Oregonian samples should have a lower shell volume and be weaker than their Californian counterparts.

Sites in the Oregonian province have lower temperatures, but more importantly, lower pH and carbonate saturation state than our Californian sites (Hauri et al. 2009, Feely et al. 2016).

Studies on *M. edulis* in the Baltic have shown that populations of mussels in cooler, lower pH environments tend to produce thinner shells in more corrosive waters (Telesca et al. 2019); a finding in-line with many short-term tank experiments assessing the impact of OA on calcification (Kroeker et al. 2010). Additionally, assessments on the strength of *M. edulis* shells grown under different pCO_2 conditions showed that shells calcifying under high OA scenarios tend to produce weak and brittle shells as compared to those grown in less acidified water (Fitzer et al. 2015b).

Despite the cooler waters and lower pH, we found that not only are Oregonian shells thicker than Californian (Fig. 2d, Table 2), they also have a higher shell volume (Fig. 2c, Table 2). These results are in direct opposition to what has been observed in the Baltic (Telesca et al. 2019) and suggests a strong imprint of evolutionary history on present day relationships between shell calcification and environmental conditions. Furthermore, these results also suggest that responses of marine mussels to future climate change are likely to be species-specific.

Given our results of thinner, lower shell volumed shells in the Californian, we expected southern populations to have weaker shells. While we did indeed find a strong, positive relationship between shell volume (Fig. 3a) (and thickness, Fig. S1a, Table S2) and strength and toughness (Fig. 3a,b, Table 3), we still found that Californian shells are significantly stronger than Oregonian despite being thinner with lower shell volumes (Fig. 2a, Table 2). While past studies have suggested that shell thickness is the strongest correlate of strength (Zuschin et al. 2017), our results indicate that simply assessing thickness or shell volume does not always give you an accurate idea of an individual or population's strength.

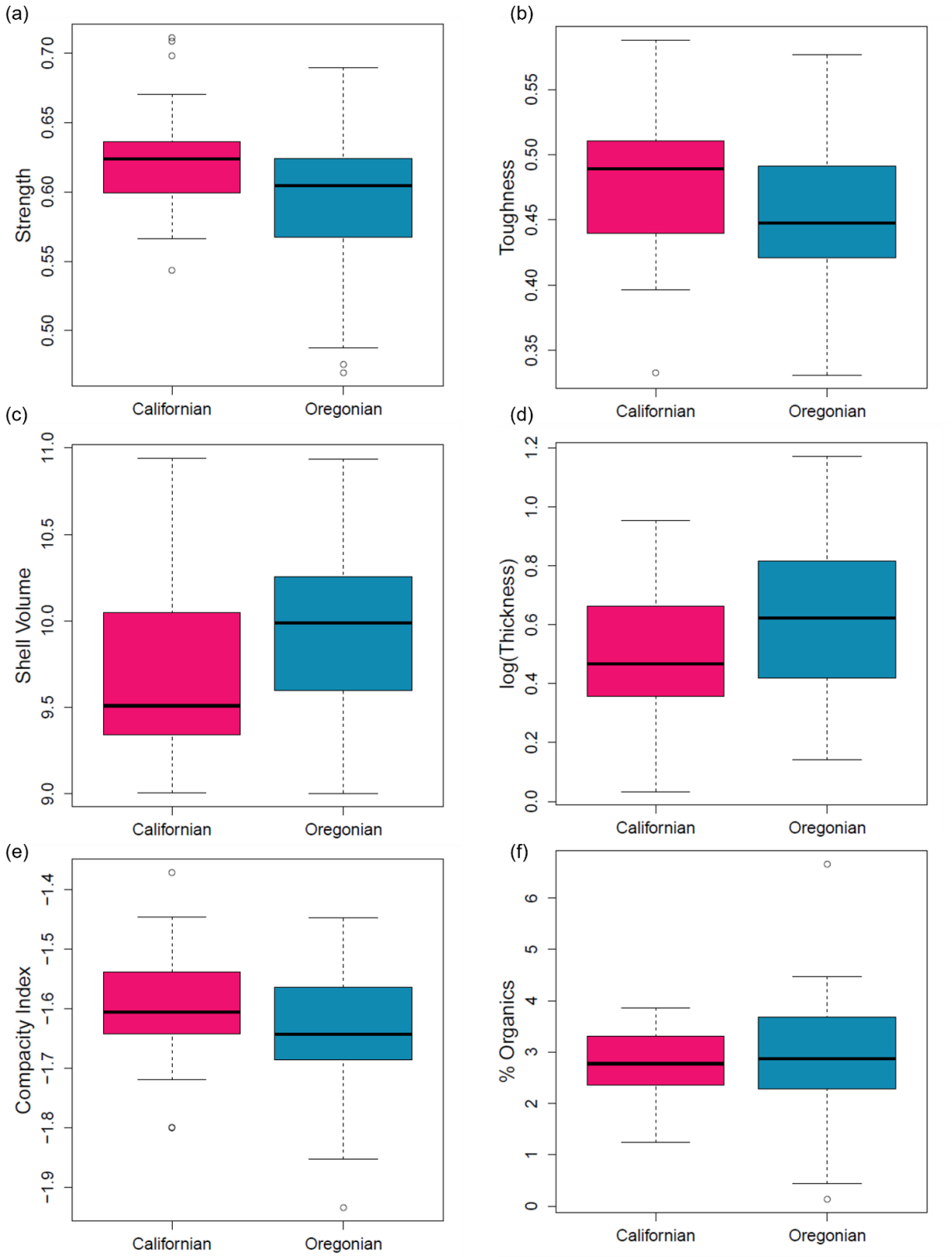

Figure 2. Boxplots showing differences between the Californian and Oregonian provinces for a) strength, b) toughness, c) shell volume, d) thickness, e) compacity index, and f) percent organics. Wilcoxon rank-sum test results recorded in Table 2.

Table 2. Wilcoxon rank-sum tests showing differences in structural and functional traits as well as thickness and percent organics between the Californian and Oregonian provinces.

Trait	Results
Strength	$p = 0.023$*
Toughness	$p = 0.072$
Thickness	$p = 0.025$*
Shell Volume	$p = 0.0059$*
% Organics	$p = 0.54$
Compacity Index	$p = 0.088$
Elongation Index	$p = 0.36$

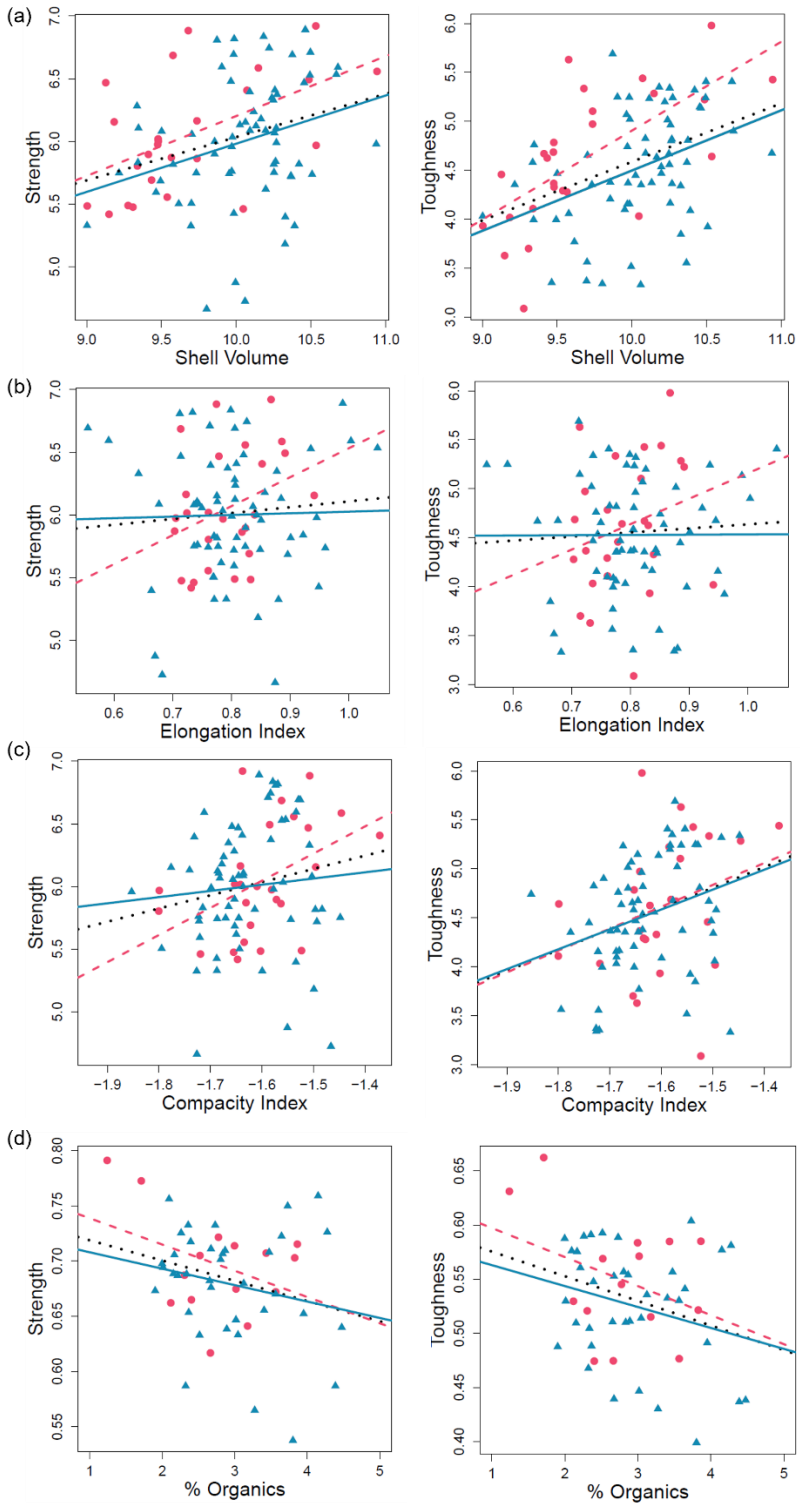

Figure 3. Strength and toughness measurements as influenced by different traits. The left column is strength and the right is toughness. Red circles and line represent Californian province samples while blue triangles and line represent Oregonian. The black line is the pattern for the whole dataset. Multivariate analysis recorded in Table 3. a) Strength and toughness vs. shell volume, b) vs. elongation index, c) vs. compacity index, d) vs. percent internal organic content.

Table 3. Multiple regression results for which traits significantly influence strength and toughness. Inflation index was not included in the final model for rank deficiency and multicollinearity reasons. Regressions were run for i) the total dataset, ii) Californian province, and iii) Oregonian province.

Measure	Province	Trait	Estimate	Std. Error	df	t value	P value
Strength	Total	Shell Volume	162.75	60.75	44.01	2.68	0.01*
		Elongation Index	-131.16	354.44	44.33	-0.37	0.71
		Compacity Index	907.33	283.36	41.04	3.2	0.0026*
		Organics	17.95	29.31	41.09	0.61	0.54
	Californian	Shell Volume	191.48	63.02	8.15	3.04	0.016*
		Elongation Index	-37.67	704.01	8.15	-0.054	0.96
		Compacity Index	1009.96	330.83	8.03	3.05	0.016*
		Organics	84.3	43.14	8.17	1.95	0.086
	Oregonian	Shell Volume	158.42	96.8	31.78	1.64	0.11
		Elongation Index	-200.86	454.81	31.87	-0.44	0.66
		Compacity Index	825.33	428.72	30.26	1.93	0.064
		Organics	8.44	38.46	28.01	0.22	0.83
Toughness	Total	Shell Volume	46.12	17.6	46.46	2.62	0.012*
		Elongation Index	-30.27	102.53	46.65	-0.3	0.77
		Compacity Index	284.51	83.44	42.46	3.41	0.0014*
		Organics	-0.89	8.63	42.2	-0.1	0.92
	Californian	Shell Volume	88.99	23.19	8.22	3.84	0.0047*
		Elongation Index	-313.85	259.02	8.23	-1.21	0.26
		Compacity Index	443.01	121.94	8.051	3.63	0.0066*
		Organics	43.94	16.87	8.25	2.77	0.024*
	Oregonian	Shell Volume	36.57	24.27	29.51	1.51	0.14
		Elongation Index	-44.2	113.84	29.64	-0.39	0.7
		Compacity Index	255.72	110.65	32.00	2.31	0.027*
		Organics	-6.73	10.21	29.56	-0.66	0.51

Hypothesis 2: Organics buffer against low pH and increase shell toughness. Lower pH in the Oregonian Province should mediate higher organic content than Californian counterparts and this increase in organics should make Oregonian samples tougher than Californian.

Internal shell organics have long been hypothesized to protect against shell dissolution (Harper 2000). A recent analysis on *M. edulis* looking at how internal shell organics change from temperate to polar regions found that mussel populations in polar waters contained far more shell organics than those in temperate (Telesca et al. 2019). However, a short-term tank experiment on

a mixed-mineralogy pearl oyster grown under different pCO_2 regimes found no impact of pH on internal shell organics (Welladsen et al. 2010), suggesting that pH alone may not be mediating the increase in internal shell organics observed in the field study.

We found no significant difference in internal shell organics between the Californian and Oregonian populations despite different temperature and pH regimes (Fig. 2, Table 2). While our results are more in-line with the experimental study, it is important to note that we do not know whether this spatial pattern has always existed or is already the product of an impacted environmental system. For example, a recent study on *M. californianus* mineralogy in response to warming and acidifying oceans found that populations today are secreting more calcite than 60 years ago in response to OA (Bullard et al. 2021). This study also showed that the well-documented spatial relationship showing an increase in the amount of aragonite in southern populations of *M. californianus* as compared to northern from the 1950's no longer exists today. If Bullard et al. (Bullard et al. 2021) had only assessed the modern day, the present-day results would suggest no relationship between mineralogy and OA. It is only within the context of historical data that the real impact of OA on mineralogy had been illustrated. While multiple population baseline data looking at internal shell organics does not exist, a study on the weight percent of internal shell organics in *M. californianus* from the 1960's does show that *M. californianus* from Corona del Mar have a mean of 2.96% carbon:nitrogen organics ratio (Hudson 1967) while modern day mussels have an average of 2.27% internal shell organics calculated using DSC/TGA at this site. While it's impossible to say if this pattern of possible organic decrease holds for other sites, the direction of a decrease in percent shell organics could suggest that shell organics have been decreasing through time in response to different anthropogenic factors. For example, changing temperature and OA, among other environmental

drivers, have been shown to increase metabolic stress as it becomes more and more difficult to calcify under new conditions (Sanders et al. 2018) and shell organics have been estimated to be a large part of the metabolic budget of marine mollusks (Palmer 1983). As OA and temperature continue to impact this species across its range, it's possible that spatial patterns could have become more and more muted in response to these environmental changes, similar to what has been observed in mineralogy through time in this species (Bullard et al. 2021).

Future studies assessing this hypothesis of a change through time in internal shell organics would be incredibly powerful to address whether or not the shell organic results seen here are truly already influenced by anthropogenic impacts and if past gradients have been erased by current environmental effects.

On top of protecting against shell dissolution, experimental studies have also shown that shell organics are an important component of shell toughness (Meyers et al. 2006, 2008, Lopez et al. 2014). Shell organics are hypothesized to increase the flexibility of the shell, contributing to the shell's ability to bend and withstand deformation (Meyers et al. 2006) as well as keep crystals properly sorted, equidistant, and similar-sized, all of which can help contribute to overall shell strength and toughness (Currey and Taylor 1974). They are also hypothesized to aid in crack propagation, re-directing cracks as they move through the shell and allowing the shell to avoid failure (Currey and Taylor 1974, Meyers et al. 2006). However, our data document a negative relationship between percent internal shell organics and toughness (Fig. 3, Table 3). It is possible that internal shell organics are only helpful up to a certain point and beyond that they can have a negative impact. Many incredibly strong molluscan species with similar mineralogy types (i.e., nacreous or prismatic) have internal shell organic weight percentages well below what we have recorded here for *M. californianus* (Currey and Taylor 1974, Meyers et al. 2006). It is

also possible that our multi-population analysis, a different approach to individual assessment in a lab, simply does not show support for this hypothesis.

Hypothesis 3: Shells with similar biomaterials can still have different strength and toughness measurements because of difference in shell structure. More elongated, inflated, and higher compacity index shells will be stronger (and tougher).

While much work has been done to assess how different biomaterials impact shell strength and toughness, less work has been done on how shell structure impacts shell function. Johnson (Johnson 2020) recently conducted a theoretical experiment that 3D printed different shell morphologies while keeping the biomaterial (plastic) constant to assess how shell shape can mediate shell strength. They found that simply by elongating and inflating the shell, even if the shell composite was identical to all others assessed, they could significantly increase shell strength (Johnson 2020). While not included in the Johnson (Johnson 2020) analysis, we also looked at another shell structure metric, compacity index (Caill-Milly et al. 2012), though how it ties to strength has not been previously assessed. As we document no difference in percent shell organics between the Californian and Oregonian provinces (Fig. 2, Table 2) and Bullard et al. (Bullard et al. 2021) showed a convergence of aragonite:calcite ratios across *M. californianus* range, we were able to test the theoretical models put forward by Johnson (Johnson 2020) as well as determine the impact of compacity index on strength and toughness.

When we assessed all structural traits as well as internal shell organics and their impact on strength and toughness, we found that only increasing shell volume and compacity index showed a positive, significant relationship with shell strength and toughness (Fig. 3, Table 3). This is potentially driven by the fact that neither elongation index nor inflation index are significantly different between the provinces (Fig. 2, Table 2) but compacity index is marginally

significantly higher in the Californian than Oregonian (Fig. 2, Table 2). It's possible that in order for significant differences in strength and toughness to be mediated by these structure measurements, much larger variation in elongation index and inflation index than what is currently documented in *M. californianus* populations must be achieved. In fact, when assessing whether or not there is a significant difference in the phenotype for each province using a PERMANOVA, we found no statistical difference (Table 4) and sites do not group cleanly into Oregonian and Californian provinces based on these traits in a dendrogram (Fig. 4).

While it is fascinating to see that shell volume and compacity index mediate such a significant influence over strength and toughness, the fact that shell volume is higher in the Oregonian than Californian and compacity index is only marginally significantly higher in the Californian than Oregonian suggests that another driver has to be at play to cause the significant difference in strength and marginal difference in toughness between the two provinces. We propose that another factor outside of biomaterials and structure, endolithic parasites, could be contributing to this marked difference in shell function between the two provinces. A recent study assessing shell strength differences in a close relative, *M. galloprovincialis*, found that shells parasitized by endolithic fungi and cyanobacteria exhibited significantly weaker shells than those that didn't (Marquet et al. 2013). While we currently have no quantitative data to support whether or not fungi and cyanobacteria are playing a role in decreasing shell strength and toughness between the Californian and Oregonian, qualitative data assessing differences in shell endolithic parasite load can clearly be seen in Fig. 1. Northern populations of shells are often severely compromised with almost no periostracum, the outer organic coating that protects the shell from being parasitized, other than around the edges of each valve. In contrast, southern populations, like La Jolla, are fully covered by the periostracum and have no visible impacts to

the shell. A study conducted on endolithic parasitism's impact on *M. californianus* in northern California also documented high endolithic cyanobacterial loads (Gehman and Harley 2019), further supporting this hypothesis. Interestingly, this same study suggested that while the cyanobacteria do decrease the strength of the shell, they help to mitigate overheating through the removal of the dark periostracum and decreased mussel mortality following thermal events (Gehman and Harley 2019). This suggests that there may be some mutualism between the endolithic parasites and the mussels, and that a tradeoff exists between surviving warmer and warmer water and maintaining shell strength. Future studies taking these complex interactions between changing environments, traits, and biotic interactions and how they intersect to impact shell function will be necessary to make more accurate predictions around marine calcifier susceptibility moving forward.

Table 4. PERMANOVA for determining the difference in sites and provinces based on trait data (strength, toughness, shell volume, elongation index, compacity index, percent shell organics) for each population of *M. californianus*.

Test	**Results**
Province	$F_{(1, 50)} = 2.87$, $p = 0.1$
Sites	$F_{(10, 41)} = 4.89$, $p = 0.002$*

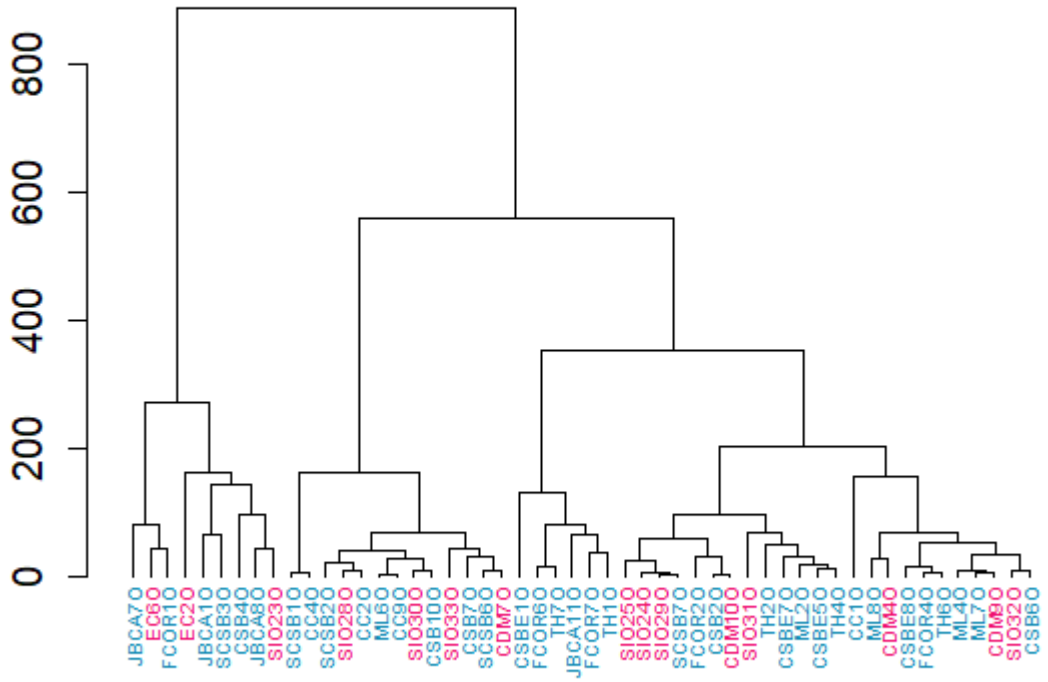

Figure 4. UPGMA showing clustering of sites. Red-hued sites belong to the Californian province while blue-hued sites belong to Oregonian. A PERMANOVA shows there is no significant difference between provinces but there is for sites (Table 4).

Hypothesis 4: Nacre (aragonite) has a significantly higher organic content than prismatic (calcite) so the nacreous portions of an individual Mytilus shell should be higher than the prismatic.

Bullard et al. (Bullard et al. 2021) showed that mussels today are secreting more calcite in their shells than during the 1950's. Work assessing different mineralogy and structural types has shown that nacreous species often exhibit much higher percentages of internal shell organic matrix than prismatic species (Hudson 1967, Taylor and Layman 1972), though material balance composition of the nacreous (aragonitic) and prismatic (calcitic) portions of *M. californianus*

from Corona del Mar in the 1960's shows that the mean weight percent carbon to nitrogen ratio of the aragonitic portion of the shell is a comparable 3.1 % to the 2.8 % for the calcitic portion (Hudson 1967). Still, if calcite holds less organic content than aragonite and calcite precipitation has significantly increased over the last 60 years, then we should expect to find significantly less internal organics in shells today than the past.

Using more advanced, but comparable for qualitative assessment, methods than the 1950's, we determined that the average weight percent of shell organics within the nacreous portion of the shell at Corona del Mar in present day is 1.73% and the prismatic portion is 2.81%. These organic weight percent measurements for present day Corona del Mar are in the opposite direction of what is expected based off past literature suggesting that either past shell organic material trends do not hold in today's oceans or there is far more variation in internal shell organic content than what was previously thought. Additionally, when we compare the weight percent of internal shell organics in the calcitic vs. aragonitic portions of all the individuals analyzed in this study, we find no significant difference between the aragonitic and calcitic parts of the shell (Fig. 5, Table 5). This suggests that interspecific differences in internal shell organic content do not hold within a species, even within different mineralogical polymorphs within the shell. It also suggests that the increase in calcite over the last 60 years is not solely responsible for the potential decrease in internal shell organics at Corona del Mar as both mineralogy types are not statistically different and both aragonite and calcite portions appear to be decreasing in organic content through time.

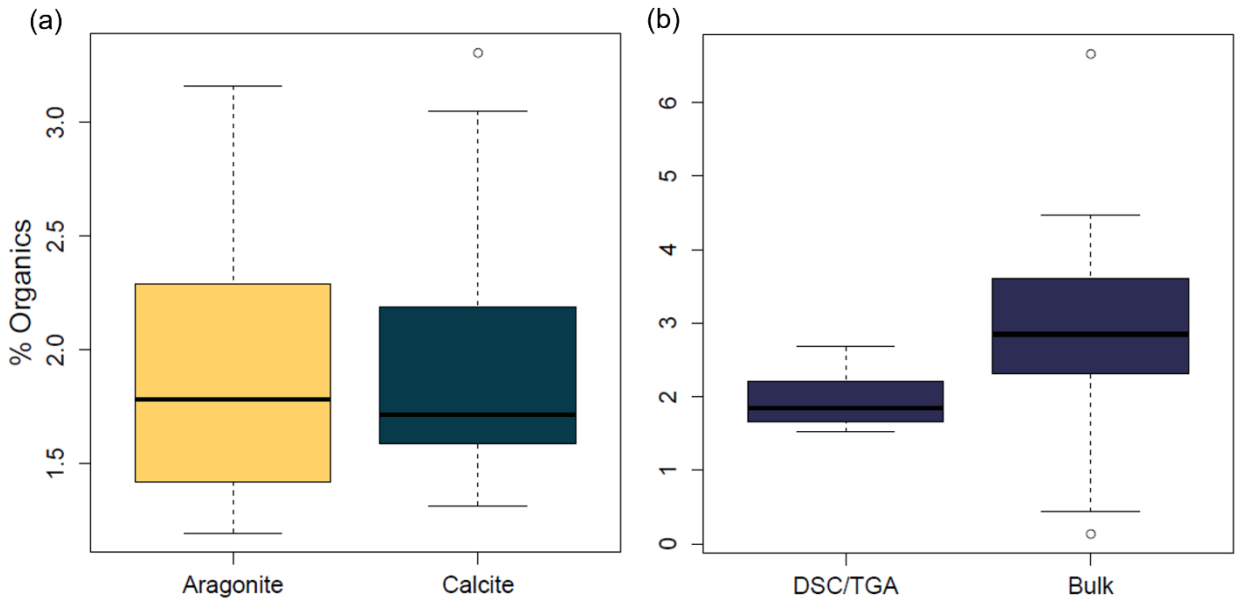

Figure 5. Comparison of internal organics a) using DSC/TGA and comparing the two mineral polymorphs within the shell and b) comparing organics determined through both DSC/TGA and muffle furnace (bulk) methods. Results of statistical comparisons are reported in Table 2.

Table 5. Wilcoxon rank-sum tests showing differences between DSC/TGA organic results and average percent DSC/TGA organics vs. bulk organics with standard deviations.

Comparison	**Result**
DSC/TGA Aragonite vs. Calcite	$p = 0.87$
%DSC/TGA organics vs. % bulk organics	%DSC/TGA = 1.97% +/- 0.35% %Bulk = 2.93% +- 1.02%

Conclusion

Here we have assessed multiple trait changes and their impact on shell strength and toughness for twelve populations of *M. californianus* from the eastern Pacific. While there is great variation in all traits assessed here at each locality and no significant difference in phenotype between the two provinces when assessing the combination of all traits (Fig. 3, Table 3), we still document a significant difference in shell strength and a marginal difference in toughness between the Californian and Oregonian populations (Fig.2, Table 2). Additionally, the patterns we document here don't match other calcification and organic spatial assessments of other Mytilid species in locations like the Baltic (Telesca et al. 2019) and serve as excellent

examples of both complex species-environment interactions and the likelihood of modern-day spatial patterns already being influenced by long-term anthropogenic impacts.

Finally, this study shows the importance of assessing multiple traits and their effect on strength and toughness as different anthropogenic drivers, like OA and temperature, can influence traits in opposite directions and mediate tradeoffs that have direct implications for shell functional success. For example, while Oregonian shells have traits that are useful adaptations under OA and usually positively associated with shell strength, (i.e., increased calcification and shell volume) other complex interactions, such as endolithic parasitism that confer potential positive tradeoffs for decreasing mortality under increased warming, may be dampening the effectiveness of these traits on shell function.

This study has shown the power of assessing multiple traits ranging from biomaterials to structure as well as the complex interactions of other biological processes, like parasitism, within multiple populations along a temperature and pH gradient. We have rejected three key hypotheses relating to how shell calcification and organics respond to changing ocean chemistry and how they impact shell function in a mixed-mineralogy species from the eastern Pacific and have conducted a practical test of the theoretical mediation of shell structure on strength and toughness. We hope the work we have presented here can serve as an example for future studies looking to combine multiple pieces of data to truly understand the functional consequences on marine calcifiers in a changing ocean.

Supplemental Materials

Tables

Table 1. Meta-data for samples collected from twelve locations along the eastern Pacific coast.

Locality	Province	# of Samples
Chilean Memorial	Oregonian	10
Fogarty Creek	Oregonian	10
Crescent City	Oregonian	9
Trinidad Head State Beach	Oregonian	10
Sonoma Coast State Beach	Oregonian	10
Moss Landing	Oregonian	8
Jalama Beach	Oregonian	5
Cayucos	Oregonian	14
Avila Beach	Oregonian	3
El Capitan State Beach	Californian	9
Corona Del Mar	Californian	8
La Jolla	Californian	9

Table 2. Linear Models & ANCOVA showing the relationship between different traits & strength + toughness.

Comparison	Strength			Toughness		
	Californian	Oregonian	Total	Californian	Oregonian	Total
Shell Volume	$p = 0.0058$* $AR^2 = 0.25$	$p = 0.021$* $AR^2 = 0.067$	P: $p = 0.081$ SV: $p = 0.0023$* (+)	$p < 0.001$* $AR^2 = 0.41$	$p = 0.0012$* $AR^2 = 0.14$	P: $p < 0.001$* SV: $p = 0.0098$* (+)
Elongation Index	$p = 0.1$ $AR^2 = 0.072$	$p = 0.85$ $AR^2 = -0.015$	P: $p = 0.63$ EI: $p = 0.44$	$p = 0.23$ $AR^2 = 0.021$	$p = 0.97$ $AR^2 = -0.016$	P: $p = 0.52$ EI: $p = 0.59$
Compacity Index	$p = 0.02$* $AR^2 = 0.17$	$p = 0.51$ $AR^2 = -0.009$	P: $p = 0.87$ CI: $p = 0.071$	$p = 0.13$ $AR^2 = 0.057$	$p = 0.017$* $AR^2 = 0.073$	P: $p = 0.85$ CI: $p = 0.0034$* (+)
Inflation Index	$p = 0.016$* $AR^2 = 0.19$	$p = 0.5$ $AR^2 = 0.0084$	P: $p = 0.76$ I: $p = 0.054$ (-)	$p = 0.1$ $AR^2 = 0.071$	$p = 0.059$ $AR^2 = 0.041$	P: $p = 0.65$ I: $p = 0.0091$* (-)
% Internal Organics	$p = 0.15$ $AR^2 = 0.017$	$p = 0.21$ $AR^2 = 0.017$	P: $p = 0.34$ %O: $p = 0.054$ (-)	$p = 0.18$ $AR^2 = 0.06$	$p = 0.12$ $AR^2 = 0.04$	P: $p = 0.21$ %O: $p = 0.028$* (-)
Thickness	$p < 0.001$* $AR^2 = 0.45$	$p = 0.098$ $AR^2 = 0.03$	P:T: $p = 0.049$* T: $p = 0.004$	$p < 0.001$* $AR^2 = 0.40$	$p = 0.01$* $AR^2 = 0.08$	P:T: $p = 0.035$* T: $p < 0.001$

Table 3. Linear Models & ANCOVA showing the relationship between different traits and each other sorted by province (Californian, Oregonian) and total pattern. P = province, EI = elongation index, SV = shell volume, CI = compacity index, I = inflation, IO = internal organics.

Comparison	Californian	Oregonian	Total
Thick vs. Length	$p = 0.045$* $AR^2 = 0.12$	$p < 0.001$* $AR^2 = 0.24$	P: $p = 0.064$ TL: $p < 0.001$*
EI vs. SV	$p = 0.16$ $AR^2 = 0.04$	$p = 0.27$ $AR^2 = 0.0032$	P: $p = 0.75$ EI: $p = 0.087$
CI vs. SV	$p = 0.97$ $AR^2 = -0.042$	$p = 0.015$* $AR^2 = 0.062$	P: $p = 0.041$* CI: $p = 0.13$
I vs. SV	$p = 0.55$ $AR^2 = -0.022$	$p = 0.0032$* $AR^2 = 0.096$	P: $p = 0.17$ I: $p = 0.014$*
IO vs. SV	$p < 0.001$* $AR^2 = 0.7$	$p = 0.0022$* $AR^2 = 0.16$	P: $p = 0.092$ IO: $p < 0.001$*
% Organics vs. Shell Volume	$p = 0.98$ $AR^2 = -0.077$	$p = 0.44$ $AR^2 = -0.0081$	P: $p = 0.46$ SV: $p = 0.55$

Figures

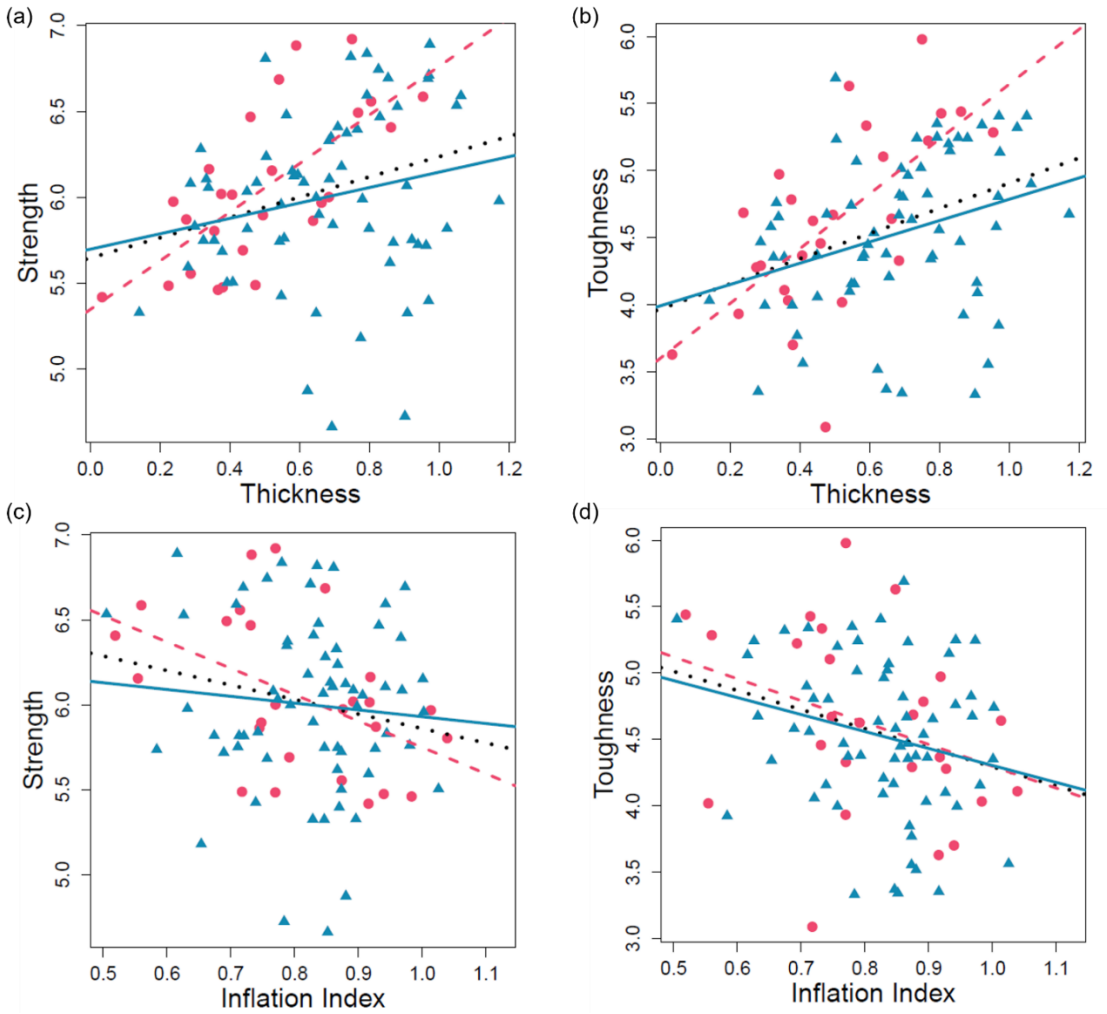

Figure 1. Relationship between a) strength and thickness, b) toughness and thickness, c) strength and inflation index, and d) toughness and inflation index.

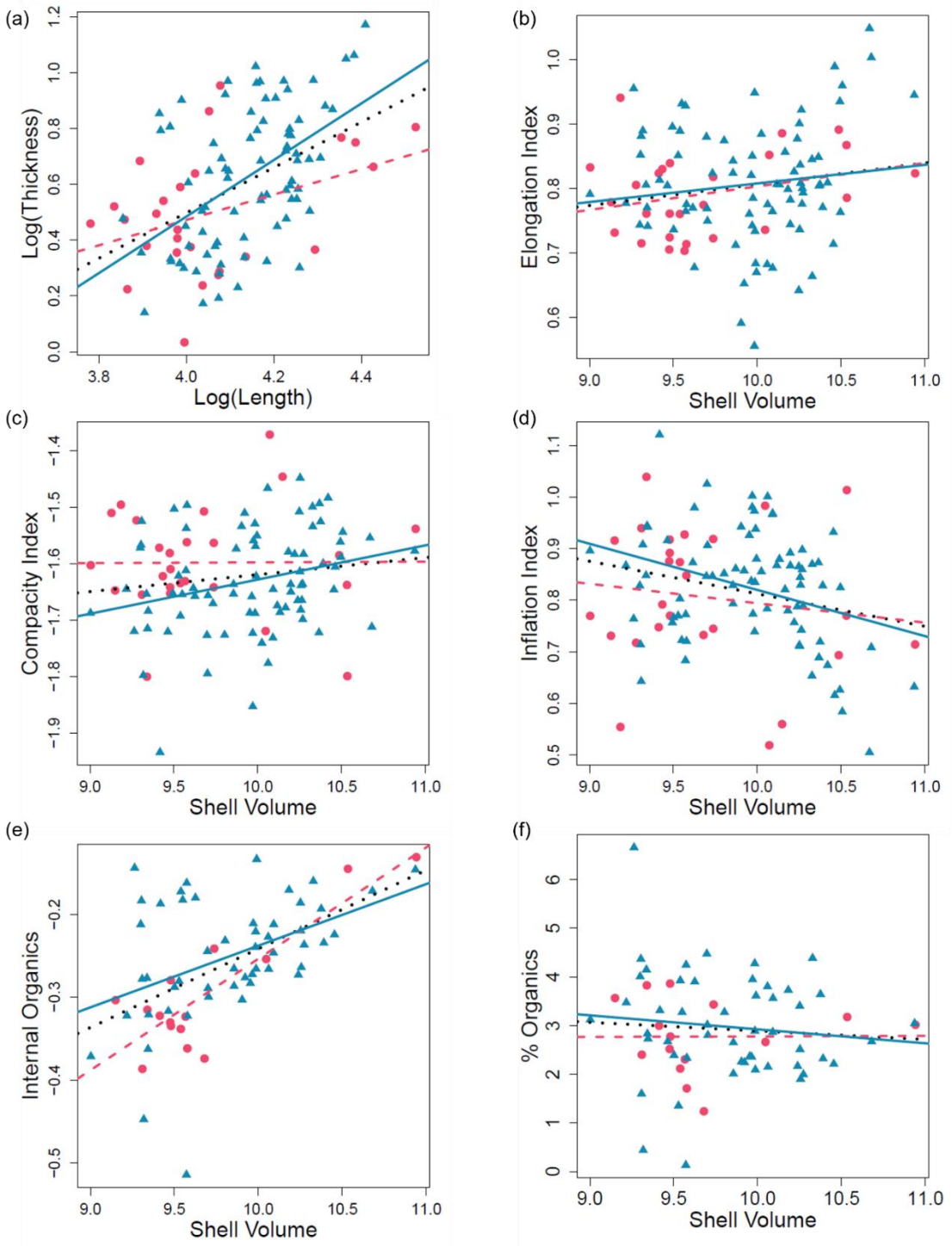

Figure 2. Traits vs. traits. Red circles and line are samples from the Californian province while blue triangles and line are Oregonian samples. The black line indicates the whole dataset pattern. a) Shell thickness vs. length, b) elongation index vs. shell volume, c) compacity index vs. shell volume, d) inflection index vs. shell volume, e) internal organics amount vs. shell volume, f) percent internal organics vs. shell volume.

Acknowledgements

Chapter 2, in part, is currently being prepared for submission for publication of the material. Bullard, E.M., Abi Ghanem, M., Yazdani, A., Allein, F., Graeve, O.A., Boechler, N., Roy, K. Functional consequences of changing shell calcification traits in response to anthropogenic climate change in a foundational marine bivalve. The dissertation author was the primary researcher and author of this material.

CHAPTER 3

Temporal trends in shell calcification of venerid bivalves: using paleontological baselines to understand species-specific responses in a changing ocean.

Abstract

Understanding and predicting species' response to anthropogenic climate and environmental change is of utmost importance. Marine species currently face threats such as ocean warming and ocean acidification (OA) along with other environmental changes such as eutrophication and human harvesting. OA is of particular concern for marine calcifiers, like bivalves, whose calcium carbonate exoskeletons are potentially vulnerable to current and future changes in pH and carbonate saturation state. While there is a growing body of research on longer-term (millenial to decadal) and greater spatial scale responses of marine calcifiers to OA, warming, and other changes, we still know very little about how temporal trajectories in shell calcification over longer, evolutionary timescales, especially across closely related species. Here, we use the Pleistocene fossil record from San Diego County, CA as a pristine, human-free baseline to quantify regional changes in shell calcification traits of five different species of venerid bivalves since the last interglacial period. Our results show that despite close phylogenetic affinities, changes in species-level shell calcification rates from the Pleistocene to present in San Diego County are individualistic with only two species, *Chione californiensis* and *Tivela stultorum*, showing significant reduction in this trait through time. In addition, comparisons of Pleistocene and recent populations from more southern biogeographic provinces that are environmentally analogous to San Diego Pleistocene assemblages show additional variation in calcification response with southern *C. californiensis* maintaining calcification traits observed in the Pleistocene but *T. stultorum* significantly thinning through time across its range.

Overall, our results suggest that the Pleistocene fossil record can provide a useful pre-human baseline for evaluating the effects of anthropogenic global change on marine calcifiers.

Introduction

Understanding species response to future climate change is of utmost importance in today's world. In the marine realm, ocean warming and ocean acidification (OA) have emerged as two of the most pressing issues (Poloczanska et al. 2013, 2016). OA results from the increase in dissolved anthropogenic carbon dioxide (pCO_2), and is of concern for marine calcifiers, such as bivalves and gastropods, whose calcium carbonate skeletons are potentially vulnerable to reduced pH and carbonate saturation state (Cooley and Doney 2009, Findlay et al. 2010, Kroeker et al. 2010). OA can negatively impact marine calcifiers through multiple processes including effects on metabolic activity (Kroeker et al. 2010, Figuerola et al. 2021), reduced shell calcification and/or increased dissolution (Kroeker et al. 2010, Figuerola et al. 2021), as well as increasing mortality (Soon and Zheng 2020). Likewise, warming has been shown to both negatively impact species' metabolism (Matoo et al. 2021) as well as exacerbate the impacts of OA (Findlay et al. 2010) though variable responses to both stressors have been shown across different species (Ries et al. 2009, Waldbusser et al. 2011, Matoo et al. 2021). Most of our existing insights on how species are likely to respond to these stressors come from laboratory experiments involving individual species (Kroeker et al. 2010, Alma et al. 2020) although there is a growing body of literature using comparative approaches and longer-term historical and archaeological data to evaluate long term trends in calcification in natural populations (Pfister et al. 2016, Cross et al. 2018, McCoy et al. 2018, Telesca et al. 2019, Bullard et al. 2021) (Pfister et al. 2016, McCoy et al. 2018). While such longer-term perspectives using natural experiments are needed to compliment and test the insights from short-term laboratory experiments, such

information is still scarce for most marine species. Furthermore, available long-term data on calcification rates do not include pre-human baselines, something that is needed to fully understand the plasticity in calcification traits as well as how modern-day trait values compare to those unaffected by human impacts.

The Pleistocene marine fossil record provides a rich archive of calcification related traits of many species and populations that were free of human impacts but experiencing major changes in the global climate during the glacial and interglacial cycles. Thus, comparative analyses of Pleistocene data in conjunction with samples from living populations can not only provide information about how calcification traits of individual species have been affected by human impacts, but also provide important insights into the level of plasticity in calcification traits. While extending our comparisons further back in time into the fossil record is powerful, it is important to keep in mind that the further back we go, the more difficult it is to get robust estimates of environmental parameters that could help us elucidate distinct anthropogenic drivers' impact on species. Despite this limitation, we argue that even without explicit estimates of environmental and climatic parameters and the disentangling of specific drivers, the recent fossil record is helpful because it provides us with the bounds of plasticity present in a species' functional traits that existed in a completely human free baseline – something we currently lack in the OA literature. The Pleistocene provides us this unique opportunity, not to necessarily disentangle specific drivers, but to determine the degree of variance for traits that can exist in our species of interest when the environment is fluctuating between glacial and interglacial cycles, and how these traits change when human impacts are introduced. Results derived from this type of analysis can then be used to further explore those specific drivers; allowing us to pinpoint

species where deeper evaluations of what is mediating trait changes would be the most meaningful.

Here we use the Pleistocene fossil record in San Diego, CA as our human-free baseline and compare shell morphometric and calcification trait changes in five species of eastern Pacific bivalves of varying relatedness from the Veneridae (Chen et al. 2011) to assess how traits specifically impacted by warming, OA, and other human impacts change from pre-human Pleistocene baselines to the human-altered Holocene. This system has three distinct advantages to help augment the information available from previous studies: i) utilizing multiple species of varying evolutionary relatedness allows for a test of generality of responses to anthropogenic induced change, ii) allows us to quantify baseline trait distributions in habitats devoid of any anthropogenic alterations (e.g., climatic, environmental, human harvesting) and iii) focusing on a single region from the Pleistocene to present gives us the ability to assess populations of the same species to different climatic and environmental changes through time. We specifically test the following three hypotheses using these Pleistocene baselines and Holocene data: i) Human impacts, like OA, negatively affect shell calcification through time causing modern-day shells to be significantly smaller and thinner than fossil shells., ii) Southern biogeographic province samples grown in warmer waters with higher pH will have larger, thicker shells and be more similar to Pleistocene fossil samples than northern populations., and iii) Shell calcification response is phylogenetically controlled so close relatives will have similar patterns through space & time.

Methods

Geographical and environmental setting

San Diego County, California, U.S.A. (32.72°, 117.16°) is located in the southern portion of California, U.S.A. (Fig. 1). The coastal ocean in this region is characterized by seasonal wind-driven upwelling, causing changes in the temperature and pH structure of surface water (Chan et al. 2017). These fluctuations in pH and temperature are exacerbated by changes in upwelling intensity following El Niño, La Niña cycles (Nam et al. 2011). Over the last century, ocean temperatures in this region have increased from a yearly average of 15.6°C in 1916 to 18.4°C in 2020 ("Southern California Coastal Ocean Observing System" n.d.), but salinity, another potential driver of changes in calcification has changed relatively little ("Southern California Coastal Ocean Observing System" n.d.). Few long-term data on changes in ocean pH and carbonate saturation state exist, but estimates show a mean decrease in Ω_{arag} (aragonite saturation state) by 0.3-0.4 since pre-industrial times within the California Current large marine ecosystem (CCLME) of which San Diego is a part of (Chan et al. 2017).

Pleistocene sample sites

Marine terrace Pleistocene assemblages were targeted for this study. Reliable dates for the Pleistocene terraces of California remain sparse, and the available data do not always permit resolving the chronology of many terraces. Similarly, paleoclimatic reconstructions and estimates of paleotemperatures for these terraces remain poorly constrained. Because of these constraints, we only targeted interglacial terraces for which dating is available and their potential age equivalents, namely the Nestor Terrace – dated to around 120,000 ± 10,000 yr or Marine Isotope Stage (MIS) 5e (Ku and Kern 1974) the Bird Rock Terrace – dated to between 70,000-90,000 yr or MIS5a (Kern 1977, Kern and Rockwell 1992), and dated portions of the Broadway Faunal horizon with some portions potentially being age equivalents to the Nestor Terrace (Kern

1977). All terraces are characterized by unconsolidated medium to course grained sand and gravel and represent a shoreline with water depths estimated to be no more than 10m deep (Kern 1977). While predominantly representing an interglacial period, the Nestor terrace does contain both a mixture of some northern and primarily southern extralimital species (Valentine 1960) or species which today only exist either north or south of where their range previously extended during the Pleistocene (i.e., north or south of San Diego). While it is unknown what contributed to this mixing of both interglacial and glacial species, the two most likely explanations are either a cool climatic flicker, or quick change in climatic conditions, (Roy et al. 1996) or a mixing of faunas from 100 ka which was a cooler water period (capturing the northern extralimitals) and the warmer 120 ka which has been shown to be even warmer than today (Muhs et al. 2006, 2014, Muhs 2022). The Bird Rock Terrace, while still part of the interglacial MIS5 period, has been suggested to be a slightly cooler environment than today, most likely due to an increase in strength from the California Current resulting in increased upwelling of cooler, lower pH bottom waters (Muhs et al. 2006). This is reflected in the paleontological assemblage as there is an increase in northern extralimital species but no southern extralimital species in the Bird Rock Terrace (Kern 1977).

When working with any fossil data, the impact of sampling and taphonomic bias must be considered. One of the clearest patterns in taphonomy, both for marine and terrestrial environments, is the preservation of larger, thicker individuals (Behrensmeyer et al. 2000). In general, the fossil record tends to be biased against smaller, thinner shelled species and individuals due to easier dissolution of the shell and situations conducive to shell destruction (Behrensmeyer et al. 2005). One way to evaluate the fidelity of the fossil record is to evaluate how many juveniles and small, thin shelled species are present. In our assemblages a diverse

range of ontogenetic stages is present for all of our target species, and two of the species abundant in these assemblages, *Leptopecten latiaruatus* and *Laevicardium substriatum*, are both small and thin-shelled. This suggests that the focal assemblages for this study are adequate for the temporal comparisons undertaken here.

Sampling

We sampled multiple individuals of each of five species of venerid bivalves (Table S1) within San Diego, County, California (Fig. 1). For each species, individuals were sampled from at least one interglacial Pleistocene assemblage as well as historical collections ranging from 1900 to 2010 and living populations collected during 2017-2019. For historical and Pleistocene samples, we used collections at the San Diego Museum of Natural History (SDMNH), the Natural History Museum of Los Angeles County (LACM), and the Santa Barbara Museum of Natural History (SBMNH). Live individuals were collected from around San Diego County, CA (SI Appendix, Methods).

We targeted interglacial Pleistocene assemblages where we could sample a minimum of 25 individuals per faunal horizon (Table S1). As discussed above, these were the Nestor Terrace, Bird Rock Terrace, the Spanish Bight Faunal Horizon, and portions of the Broadway Faunal Horizon

We measured historical samples for each species from the SDMNH, LACM, and SBMNH as well as archived shells at the University of California at San Diego (UCSD). Historical samples ranged in age from early 1900s to early 2000s and were originally collected from all around San Diego County (Table S1, SI Appendix, Methods). Similar to Pleistocene sampling, we targeted a minimum of 25 individuals from time periods across the last century to

measure for our historical component. We then lumped historical and live samples to create a larger time-averaged assemblage for comparison with Pleistocene samples. These live individuals were collected from multiple locations in San Diego, CA, but the majority of samples were taken from around Mission Bay and habitats around Scripps Institution of Oceanography (SIO) (SI Appendix, Methods). In areas where members of our focal species were abundant, a range of size classes were collected to account for any impacts of size on calcification. Recently dead individuals with fresh tissue still attached to the shell were collected along with live individuals and used in analyses.

Historical samples for two species, *C. californiensis* and *T. stultorum* were additionally collected for assessment of trait variations across their geographic distributions for comparison with fossil samples from San Diego, CA to evaluate if trait values found in the fossil assemblages but absent in San Diego today, can be still found in other parts of each species' range. These samples were also collected from the early 1900's to 2000's from the SDMNH, LACM, and SBMNH. As the stable isotope data for our fossil assemblages suggests that the portions of the Pleistocene we are assessing are potentially warmer than today (Muhs et al. 2006, 2014), we focus primarily on the southern portion of each species range for a more relevant comparison based on climate, so ranges for both species are restricted to Californian provinces well as the Surian and Panamic provinces (Fig. 1, Table S1). This analysis allows us to test our hypotheses around spatial calcification patterns and to see how traits of populations living under modern environmental conditions similar to Pleistocene San Diego compare to the past. This spatial assessment also serves as an additional test of whether or not taphonomy could be driving our through time results; if we document similar sized individuals in southern populations as our Pleistocene samples it lends credence to our through time patterns being a true biological signal.

It is important to note here that both the fossil and Holocene collections represent time-averaged assemblages, but on different scales. Time-averaging is the accumulation of specimens from different time periods in the death assemblage. An excellent example of this in our data is the likely presence of individuals from both 100 ka and 120 ka in the Nestor terrace. Time averaging is especially powerful when establishing baselines for trait distributions, since the accumulation of different individuals living under different environmental conditions through time can capture any plastic responses and thus provide a more complete estimate of trait variations compared to single temporal snapshots. In recognizing the disparity in time-averaging between our Pleistocene and Holocene assemblages and how that can impact statistical trait variation differences between our assemblages, we focus on assessing changes in the slope and intercept of the relationship between size and thickness and changes in median trait values for size and thickness in same sized individuals. This approach provides greater confidence to interpretation of results, especially if we see clear differences in slope and intercepts between Pleistocene and Holocene assemblages.

Shell characteristics

We investigated trends in two key traits - size and calcification - from the Pleistocene to present in San Diego, CA. We define size here as the geometric mean of length x height x width to avoid any impact of shell shape changes through time (Roy et al. 2000). We measured shell length, height, and width of individual valves with electronic calipers. Shell thickness was measured using an electronic micrometer across seven points along the central portion of the valve following the growth trajectory from the beak to the ventral margin of each individual. We then averaged these measurements to get a mean thickness for each individual valve. All the

species evaluated here have symmetrical valves. We measured only one valve per individual, ensuring that there were no duplicates by meticulously matching up valves pre-measuring and removing valves that were potentially matches from the sampling pool to ensure no double measuring. We alternated between measuring left and right valves of individuals and determined that there is no significant difference in size or thickness for left and right valves for any of our five species (Table S2). For this reason, we combined all left and right valves when doing our analyses.

Statistical analyses

All analyses were carried out in R (4.0.2) (R Core Team 2018). We first used the Shapiro-Wilk test to determine normality of the size and thickness data as well as Bartlett's test for homogeneity of variance. Data were not always normally distributed, so we used a natural log transformation. In addition, since variances were also not always equal, we primarily used non-parametric tests.

We used linear models to quantify the relationship between subsets of same-sized individuals using the natural logarithm of mean thickness and size (the geometric mean of length x height x width) for each species within a time period (e.g., Pleistocene.). We used analysis of co-variance (ANCOVA) on models that account for temporal autocorrelation to test for changes in the relationship between thickness and size between time periods (i.e., Pleistocene vs. Holocene). First, we tested for temporal autocorrelation using the Durbin Watson test (Durbin and Watson 1971) in the lmtest package (Zeileis and Hothorn 2002). To account for any observed autocorrelation, we used the Cochrane-Orcutt method (Koenig and Liebhold 2016) on a base linear model assessing average thickness as a function of time and the geometric mean of

length, height, and width using the Orcutt package in R (Stefano et al. 2018). For determining temporal differences in same-sized subsets' median size and thickness between epochs (e.g., Pleistocene, Holocene), we used Wilcoxon-rank sum tests, and we used F-tests to assess changes in trait variance between Pleistocene and Holocene assemblages.

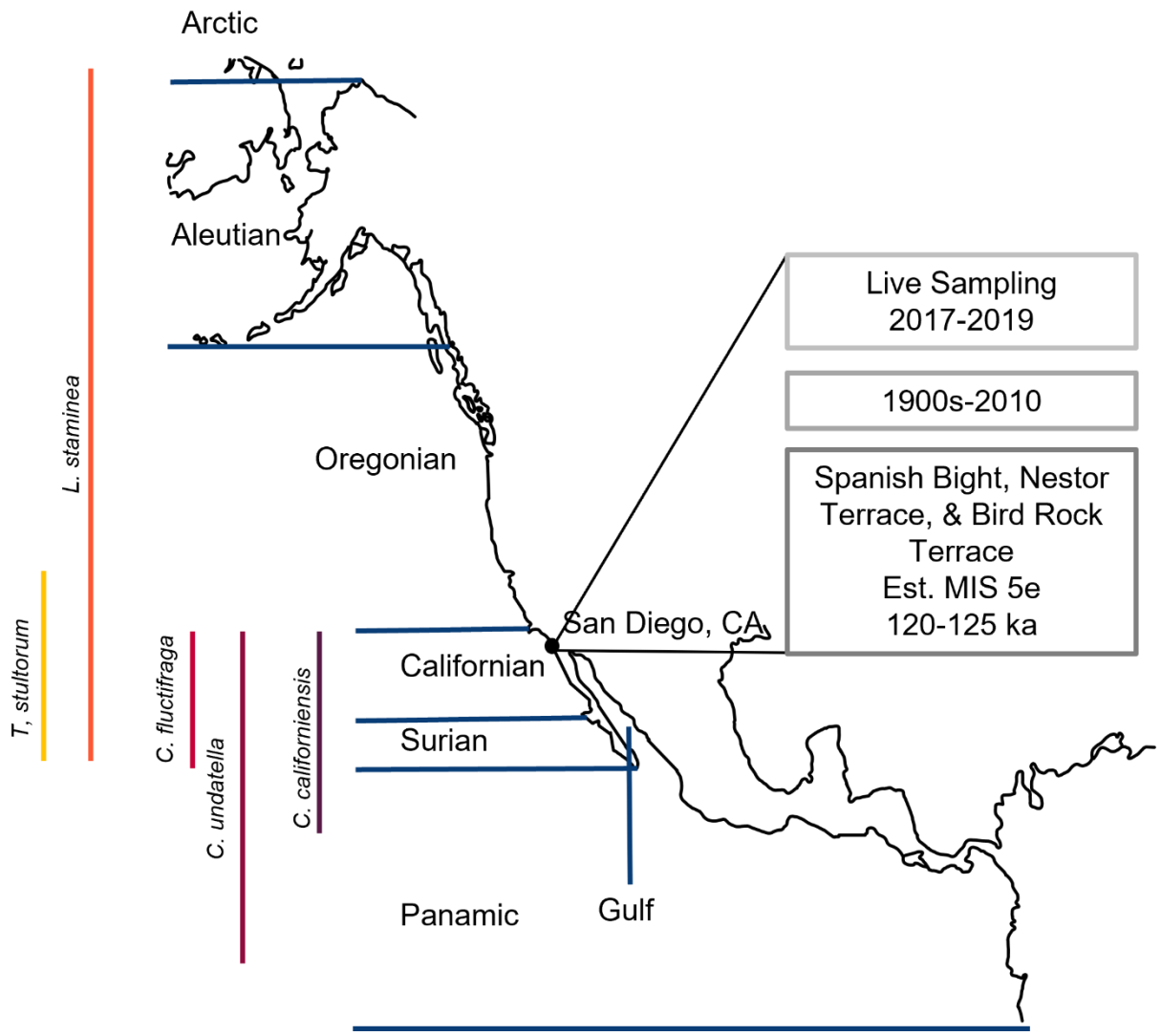

Figure 1. Map of the eastern Pacific with biogeographic provinces, geographic ranges of each species, and through time-sampling scheme in San Diego, California. Limits of each biogeographic province is indicated by the blue line. The faunal horizons and sampling scheme for the through time assessment at San Diego is organized with the oldest assemblages, the Pleistocene terraces, being at the bottom and the most recent live-collected sampling at the top.

Results & Discussion

Through Time Analysis

Much of the work assessing how marine calcifiers, like mollusks, will respond to increased ocean warming and acidification comes from short-term tank experiments (Kroeker et al. 2010). Some longer-term assessments ranging from half a century (Bullard et al. 2021), to a century (Cross et al. 2018), and even to archaeological times (Pfister et al. 2016, McCoy et al. 2018) have recently been conducted, but these types of analyses still remain relatively rare and have only been performed on individual species. Short-term tank experiments overwhelmingly report decreased calcification in response to OA (Kroeker et al. 2010). While some of the longer-term assessments, like an archaeological study assessing decreases in shell calcification in *Mytilus californianus* in Washington State (Pfister et al. 2016), supports these findings, some variation in calcifier response has been documented. For example, a short-term tank experiment assessing different marine calcifier responses to OA (e.g., crustaceans, corals, urchins, bivalves, etc.) found that there was variation in how different groups responded to decreasing aragonite saturation state (Ries et al. 2009). While bivalves and gastropods were primarily severely impacted by decreasing aragonite saturation state, crustaceans were not and actually performed better under OA conditions (Ries et al. 2009). However, this variation was greatest between phyla (i.e., crustacean vs. mollusk), with variation, while present, occurring less between bivalves and gastropods suggesting that more closely related species will have more similar responses.

We tested the hypotheses generated from these short-term tank experiments and millennial assessment that we should see similar decreasing patterns in shell calcification for five

related venerids through time, and we reject both. While in two of the six venerid species (*C. californiensis* & *T. stultorum*), calcification and body size do decrease from the Pleistocene to the modern (Table 1, Fig. 2), the three other species do not show this same temporal pattern. *C. undatella, C. fluctifraga*, and *L. staminea* showed no temporal change in size, and *C. undatella* and *L. staminea* both increase their calcification rate from Pleistocene to now with Holocene individuals being significantly thicker than Pleistocene (Fig. 2, Table 2).

These results on closely related species (Chen et al. 2011) occupying similar habitats with similar life histories truly supports the idea that responses to changing ocean conditions will be species-specific and can't be predicted simply by looking at phylogeny, mineralogy, environment, etc. Though variation in calcification response to temperature and OA has been documented previously in short-term tank experiments (Ries et al. 2009) and centennial studies (Cross et al. 2018), these results are not common. Our results, however, suggest that longer-term analyses that utilize pristine fossil baselines, and thus capture the amalgamation of evolutionary and environmental changes over multiple populations, and how that impacts calcification through time could be suggesting a slightly different story than the vast majority of short-term tank experiments focusing on one driver impacting individuals. While it's true that we have two species following the traditional pattern of decreasing calcification through time, we also document three unexpected patterns (Tables 1,2), contributing to the possibility that variation in calcification response through time may be more common than previously documented. We propose that while we have used short-term assessments to drive our hypotheses for this study, it may be beneficial to instead use long-term assessment results to drive hypotheses for future short-term tank experiments and as a first order assessment to identify potential species at risk of decreasing calcification due to an amalgamation of anthropogenic impacts.

Table 1. Temporal patterns for size and thickness of subsetted data for each species from the Pleistocene to Holocene. Size and thickness code: + = increase from the Pleistocene to Holocene, / = no change (stasis), - = decrease from the Pleistocene to Holocene.

Life Habit	Mineralogy	Species	Size	Thickness
Shallow infaunal. Sand/Mud	Aragonite	*C. californiensis*	-	-
Shallow infaunal Sand/Mud	Aragonite	*C. undatella*	/	+
Shallow infaunal Sand/Mud	Aragonite	*C. fluctifraga*	/	/
Shallow infaunal Sand/Mud	Aragonite	*L. staminea*	/	+
Infaunal Sand	Aragonite	*T. stultorum*	-	-

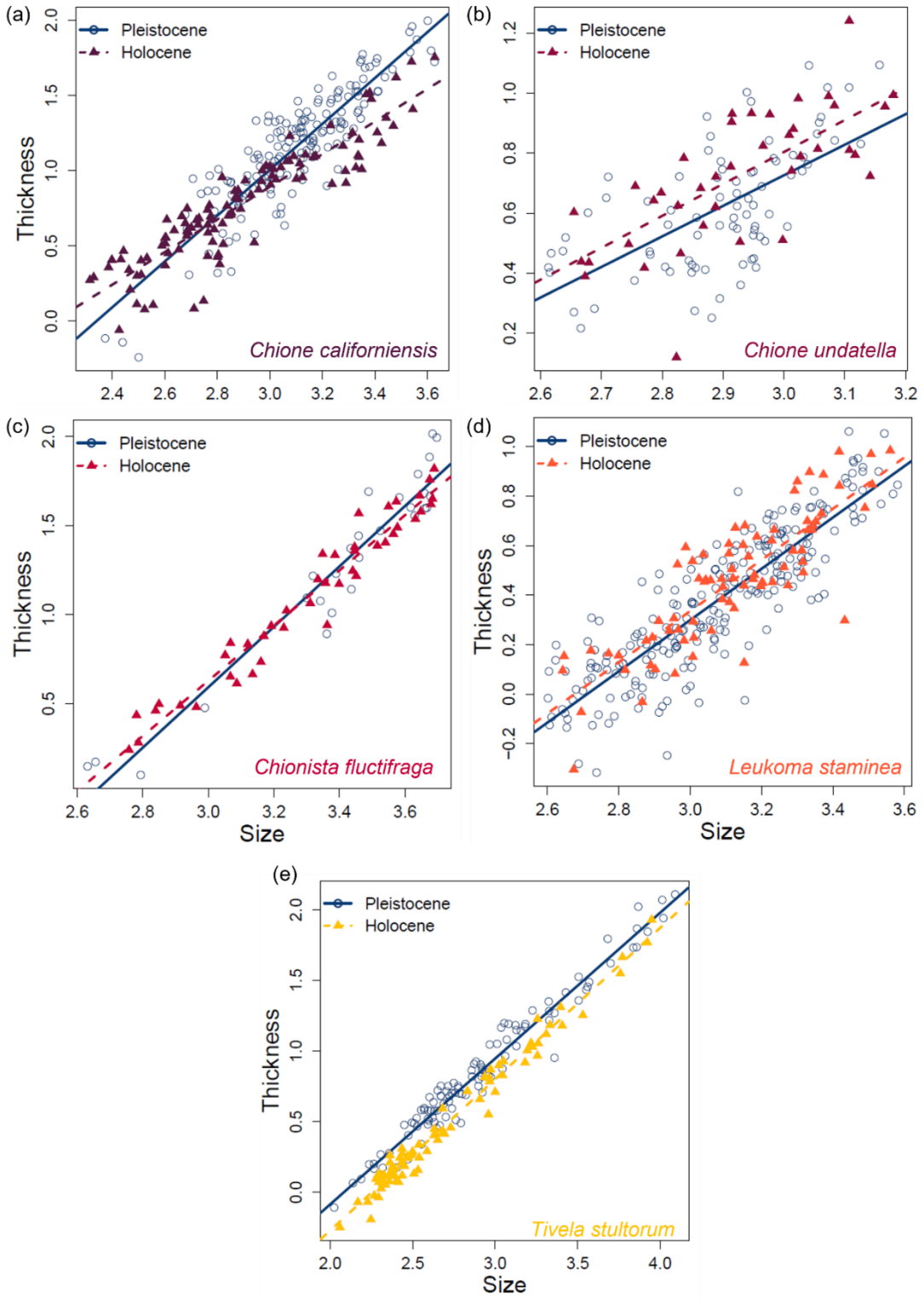

Figure 2. Changes in size (geometric mean of length x height x width) and mean shell thickness for same sized data from the Pleistocene to Holocene in five species of venerids. a) *C. californiensis*, b) *C. undatella*, c) *C. fluctifraga*, d) *L. staminea*, e) *T. stultorum*. Results of linear models for each time period and ANCOVA for slope and intercept comparisons in Table 2.

Table 2. Statistical results from trait comparisons between Pleistocene and Holocene assemblages for five species using same sized data. Significant *p*-values at alpha = 0.05 are denoted by an (*). ANCOVA assessing changes in shell thickness as a function of size and time conducted using temporal-autocorrelated corrected models. Median difference determined by a Wilcoxon-rank sum test, variance using an F-test. Code: '-' = smaller/thinner in Holocene, '+' = bigger/thicker in Holocene.

Species	ANCOVA	Size	Thickness
C. californiensis	Time p =<0.001* Size p < 0.001* Time:Size p < 0.001* AR^2 = 0.75 $F_{(2, 262)}$ = 266.4	Median: p < 0.001* (-) Variance: p < 0.01* (+)	Median: p < 0.001*(-) Variance: p = 0.74
C. undatella	Time p = 0.047* Size p < 0.001* AR^2 = 0.41 $F_{(2, 116)}$ = 42.1	Median: p = 0.38 Variance: p = 0.13	Median: p = 0.01* (+) Variance: p = 0.64
C. fluctifraga	Time p = 0.65 Size p = 0.001* AR^2 = 0.94 $F_{(2, 66)}$ = 552.9	Median: p = 0.068 Variance: p = 0.75	Median: p = 0.061 Variance: p = 0.27
L. staminea	Time p = 0.13 Size p = 0.001* AR^2 = 0.72 $F_{(2, 309)}$ = 402.2	Median: p = 0.14 Variance: p = 0.28	Median: p = 0.023* (+) Variance: p = 0.43
T. stultorum	Time p = 0.001* Size p = 0.001* AR^2 = 0.97 $F_{(2, 182)}$ = 3373.1	Median: p = 0.0032* (-) Variance: p = 0.93	Median: p < 0.001* (-) Variance: p = 0.86

Through space analysis:

A recent trend has been observed in mixed mineralogy bivalves suggesting that shell calcification, namely the thickening of aragonite, is higher in warmer, higher pH waters (Telesca et al. 2019) (though see Chapter 2 for example of how this doesn't always hold true). Studies on the climate during MIS 5e (Pleistocene) in southern California suggest that sea surface temperatures (SST) could be as much as 4°C warmer than current ocean conditions (Muhs et al. 2006, 2014, Muhs 2022) though saturation state and pH are still relatively unknown. This suggests that San Diego County may not be the best environmental analgoue to what existed during the Pleistocene and that more southern biogeographic provinces, like the Surian and Panamic, could be more similar environments to what existed in the past. Thus, we use Holocene spatial calcification data for the two species that showed a decrease in calcification through time, *C. californiensis* and *T. stultorum*, to test hypotheses around shell calcification increasing in warmer, higher pH waters and a phylogenetic signal in spatial calcification responses and assess

whether or not modern analgoues to Pleistocene trait distributions exist in warmer, southern bivalve populations.

We found that *C. californiensis* fossil assemblages from San Diego, CA are statistically indistinguishable for size and thickness to Surian Holocene samples with Holocene Panamic size being significantly larger than Pleistocene (Table 3). *T. stultorum* Surian size is also statistically indistinguishable from San Diego Pleistocene, but thickness in the fossil record is greater in fossil assemblages than Holocene Surian (Fig. 3, Table 3). Again, we document variation in spatial calcification response where *C. californiensis* follows the predicted calcification increase with warmer waters and southern populations acting as trait analogues to the Pleistocene assemblage, but *T. stultorum* shows significant thinning across its entire range. These results further support the idea of species-specific responses to current and future change, not just through time but in regard to space as well.

The addition of a spatial component to this analysis further powers our understanding of these through time patterns in two main ways: i) helps us to eliminate the possibility that our through time results are driven by taphonomy in the fossil record and ii) illustrates that temporal patterns don't always equal regional-scale patterns. The first aspect is important as a decrease in size and thickness is in-line with what would be expected if taphonomy was at play in our fossil assemblage, and while we've constrained our size range to be equivalent for both Pleistocene and Holocene to combat this, the fact that we see similar sized Holocene individuals in southern biogeographic provinces to Pleistocene samples further confirms that our temporal pattern is not because of taphonomy but is a true biological signal. The second aspect that temporal patterns don't always equal regional scale patterns is fascinating in that it suggests that different populations along a species range may be experiencing different levels of vulnerability to

changing conditions through time. While San Diego, County *C. californiensis* have a significant decrease in size and calcification from the Pleistocene to present, Surian and Panamic still show trait values in-line with what existed pre-human impacts. These results are akin to areas of refugia under Pleistocene glacial-interglacial cycles (Jones et al. 2020) and give hope to these traits being retained in these areas moving forward and even possible recovery.

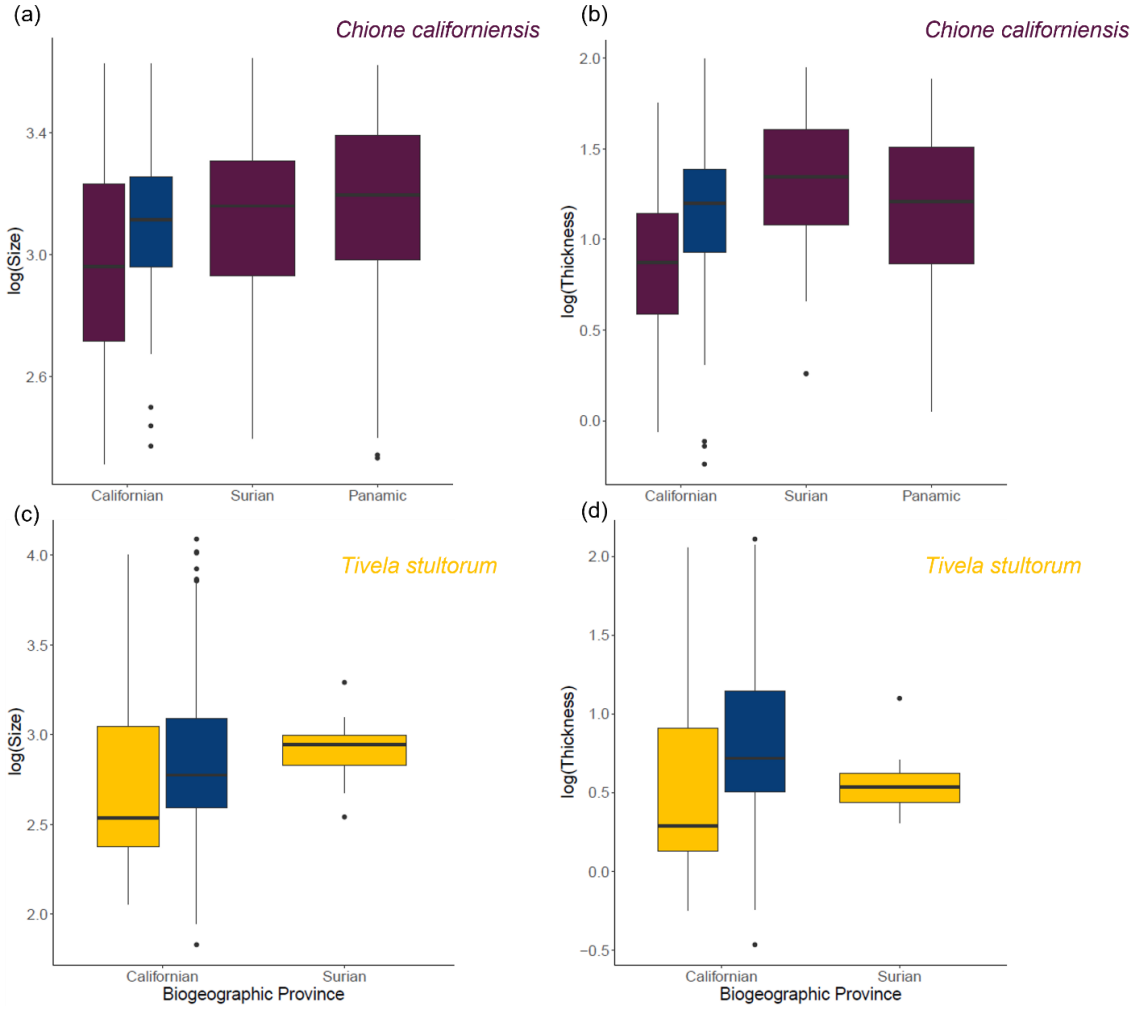

Figure 3. Fossil samples plotted with Holocene samples across *C. californiensis* and *T. stultorum* modern southern range. a) *C. californiensis* size, b) *C. californiensis* thickness, c) *T. stultorum* size, d) *T. stultorum* thickness. Even when Pleistocene *T. stultorum* samples are constrained to the same size range, Surian thickness is still significantly lower when using a Wilcoxon rank sum test to compare medians ($p < 0.001$).

Table 3. Wilcoxon-rank sum test establishing how fossil samples compare to Holocene along *C. californiensis*' and *T. stultorum*'s modern range. Code: P = Pleistocene, '+' = Holocene bigger/thicker than fossil, '-' = Holocene smaller/thinner

Species	Size	Thickness
C. californiensis	P to Surian: $p = 0.45$ P to Panamic: $p = 0.019$* (+)	P to Surian: $p = 0.058$ P to Panamic: $p = 0.99$
T. stultorum	P to Surian: $p = 0.14$	P to Surian: $p = 0.006$ (-)

Conclusion

Here we have utilized fossil trait baselines devoid of human impacts to assess how shell size and calcification has changed through time in five closely related venerids. We have shown that calcification response through time is variable despite relatedness and doesn't always fit expected patterns hypothesized from shorter-term assessments. Additionally, we have documented this same variation in calcification response through space in two temporally impacted species, *C. californiensis* and *T. stultorum*, and shown that temporal patterns don't always match regional scale patterns.

Finally, we illustrate the power of comparing modern data, both within a constant location and across a species range, to un-altered fossil baselines as a first order assessment to determine potential species vulnerability. As species responses through time and space appear to be species-specific and can elicit unexpected patterns, using this type of assessment pairing fossil and Holocene data could be valuable to identify species for further analysis and to develop more targeted hypotheses to use in short-term tank experiments.

The fossil record provides us an unparalleled tool for determining the impacts of anthropogenic climate change, envioronmental change, and other human impacts (Lockwood and Mann 2019) on key species. Using the powerful data preserved for us in the recent fossil record, we can not only better understand our current species susceptibilty, but make more accurate and informative predictions for our future.

Supplemental Materials

Detailed description of live sampling sites

Below we provide more detailed descriptions of each of the sampling sites used in this study.

Smiley Lagoon: Smiley Lagoon is our only lagoon site (32.7552° N, 117.2471° W). We entered the lagoon from the parking lot near the dog beach. We walked east along the edge flush with the Ocean Beach Athletic Area until we reached sandy channels. We then collected clams at low tide from these channels. The horn snail *Cerithideopsis californica* and razor clams dominate the lagoon. The environment is primarily mud and standing water with sandy mud channels where the clams were found.

Crown Point Beach: Crown Point Beach is one of our Mission Bay localities (32.7876° N, 117.2334° W). This is a long stretch of sand in the bay nestled against Kendall-Frost Mission Bay Marsh Reserve and dominated by *Chiones*. We sampled Crown Point Beach in two zones: from the edge adjacent to Kendall-Frost Marsh south until the bridge (large structure covered with oysters and rich in *Argopecten ventricosus* on the mud flats) and then from just south of the bridge until where the boats are docked (*Chione* abundance dramatically decreased from the bridge southward).

Mission Point Park: Mission Point Park (32.7612° N, 117.2459° W) is situated at the Entrance of the Channel into Mission Bay. We parked in the park and headed north to sample Mission Point Beach. This locality is a combination of sandy beach in the southern portion with extensive muddy tidal flats at the northernmost stretch flush with Bonita Cove. This area is rich in *Chiones* with *Leptopecten latiauratus* in the eel grass exposed during low tide.

La Jolla Shores: La Jolla Shores Beach (32.8577° N, 117.2529° W) is a long expanse of sandy beach ending in rocky intertidal shoreline just north of the Ellen Browning Scripps Memorial Pier on the Scripps Institution of Oceanography campus. Tivela stultorum is the only species found from this locality and can be found during extreme low tides just north and south of the pier.

Tables

Table 1. Specimen collection info. PlT = total samples from the Pleistocene of San Diego, Co., PlS = subset used for main analyses, HT = total Holocene of San Diego Co., HS = subset used for main analyses, CT = Total Californian biogeographic province (BP), CS = subset used for analyses, ST = Total Surian BP, SS = subset used for analyses, PT = Total Panamic BP, PS = subset used for analyses.

Family	Species	PlT	PlS	HT	HS	CT	CS	ST	SS	PT	PS
Veneridae	*Chione californiensis*	316	315	113	108	163	140	38	25	73	72
Veneridae	*Chione undatella*	168	150	79	72	n/a	n/a	n/a	n/a	n/a	n/a
Veneridae	*Chionista fluctifraga*	78	52	46	43	n/a	n/a	n/a	n/a	n/a	n/a
Veneridae	*Leukoma staminea*	269	235	84	78	n/a	n/a	n/a	n/a	n/a	n/a
Veneridae	*Tivela stultorum*	112	107	85	79	93	83	19	18	0	0

Table 2. Wilcoxon rank-sum test evaluating left vs. right valve size & thickness for each species.

Species	Size	Thickness
Chione californiensis	$p = 0.093$	$p = 0.16$
Chione undatella	$p = 0.95$	$p = 0.73$
Chionista fluctifraga	$p = 0.67$	$p = 0.9$
Leukoma staminea	$p = 0.73$	$p = 0.61$
Tivela stultorum	$p = 0.89$	$p = 0.65$

Acknowledgements

Chapter 3, in part, is currently being prepared for submission for publication of the material. Bullard, E.M., & Roy, K. Temporal trends in shell calcification in the Veneridae: using paleontological baselines to understand species-specific responses in a changing ocean. The dissertation author was the primary researcher and author of this material.

REFERENCES

Alma, L., K. E. Kram, G. W. Holtgrieve, A. Barbarino, C. J. Fiamengo, and J. L. Padilla-Gamiño. 2020. Ocean acidification and warming effects on the physiology, skeletal properties, and microbiome of the purple-hinge rock scallop. Comparative Biochemistry and Physiology -Part A : Molecular and Integrative Physiology 240.

Behrensmeyer, A. K., F. T. Fürsich, R. a. Gastaldo, S. M. Kidwell, M. a. Kosnik, M. Kowalewski, R. E. Plotnick, R. R. Rogers, and J. Alroy. 2005. Are the most durable shelly taxa also the most common in the marine fossil record? Paleobiology 31:607–623.

Behrensmeyer, A. K., S. M. Kidwell, and R. A. Gastaldo. 2000. Taphonomy and paleobiology. Source: Paleobiology 26:103–147.

Beniash, E., A. Ivanina, N. S. Lieb, I. Kurochkin, and I. M. Sokolova. 2010. Elevated level of carbon dioxide affects metabolism and shell formation in oysters Crassostrea virginica. Marine Ecology Progress Series 419:95–108.

Bullard, E. M., I. Torres, T. Ren, O. A. Graeve, and K. Roy. 2021. Shell mineralogy of a foundational marine species, Mytilus californianus, over half a century in a changing ocean 118:2021.

Burnett, N. P., and A. Belk. 2018. Compressive strength of Mytilus californianus shell is time-dependent and can influence the potential foraging strategies of predators. Marine Biology 165:1–9.

Caill-Milly, N., N. Bru, K. Mahé, C. Borie, and F. D'Amico. 2012. Shell Shape Analysis and Spatial Allometry Patterns of Manila Clam (Ruditapes philippinarum) in a Mesotidal Coastal Lagoon . Journal of Marine Biology 2012:1–11.

Chan, F., J. A. Barth, C. A. Blanchette, R. H. Byrne, F. Chavez, O. Cheriton, R. A. Feely, G. Friederich, B. Gaylord, T. Gouhier, S. Hacker, T. Hill, G. Hofmann, M. A. McManus, B. A. Menge, K. J. Nielsen, A. Russell, E. Sanford, J. Sevadjian, and L. Washburn. 2017. Persistent spatial structuring of coastal ocean acidification in the California Current System. Scientific Reports 7.

Chen, J., Q. Li, L. Kong, and X. Zheng. 2011. Molecular phylogeny of venus clams (Mollusca, Bivalvia, Veneridae) with emphasis on the systematic position of taxa along the coast of mainland China. Zoologica Scripta 40:260–271.

Cooley, S. R., and S. C. Doney. 2009. Anticipating ocean acidification's economic consequences for commercial fisheries. Environmental Research Letters 4.

Cross, E. L., E. M. Harper, and L. S. Peck. 2018. A 120-year record of resilience to environmental change in brachiopods. Global Change Biology 24:2262–2271.

Cross, E. L., E. M. Harper, and L. S. Peck. 2019. Thicker Shells Compensate Extensive Dissolution in Brachiopods under Future Ocean Acidification. Environmental Science and Technology 53:5016–5026.

Currey, J. D., and J. D. Taylor. 1974. The mechanical behaviour of some molluscan hard tissues. Journal of Zoology 173:395–406.

Dodd, J. R. 1961. Paleoecological Implications of the Mineralogy, Structure, and Strontium and Magnesium Contents of Shells of the West Coast Species of the Genus Mytilus. California Institute of Technology.

Durbin, J., and G. S. Watson. 1971. Testing for serial correlation in least squares regression III. Biometrika 58:1–19.

Feely, R. A., S. R. Alin, B. Carter, N. Bednaršek, B. Hales, F. Chan, T. M. Hill, B. Gaylord, E. Sanford, R. H. Byrne, C. L. Sabine, D. Greeley, and L. Juranek. 2016. Chemical and biological impacts of ocean acidification along the west coast of North America. Estuarine, Coastal and Shelf Science 183:260–270.

Fenberg, P. B., and K. Roy. (n.d.). Anthropogenic Harvesting Pressure and Changes in Life History: Insights from a Rocky Intertidal Limpet. 180.

Figuerola, B., A. M. Hancock, N. Bax, V. J. Cummings, R. Downey, H. J. Griffiths, J. Smith, and J. S. Stark. 2021, January 29. A Review and Meta-Analysis of Potential Impacts of Ocean Acidification on Marine Calcifiers From the Southern Ocean. Frontiers Media S.A.

Findlay, H. S., M. A. Kendall, J. I. Spicer, and S. Widdicombe. 2010. Relative influences of ocean acidification and temperature on intertidal barnacle post-larvae at the northern edge of their geographic distribution. Estuarine, Coastal and Shelf Science 86:675–682.

Fitzer, S. C., V. R. Phoenix, N. A. Kamenos, M. Cusack, W. Zhu, and K. E. Tanner. 2015a. Ocean acidification alters the material properties of Mytilus edulis shells. Journal of the Royal Society Interface 12.

Fitzer, S. C., W. Zhu, K. E. Tanner, V. R. Phoenix, N. A. Kamenos, and M. Cusack. 2015b. Ocean acidification alters the material properties of Mytilus edulis shells. Journal of the Royal Society Interface 12.

Gehman, A. L. M., and C. D. G. Harley. 2019. Symbiotic endolithic microbes alter host morphology and reduce host vulnerability to high environmental temperatures. Ecosphere 10.

Goulletquer, P., and M. Wolowicz. 1989. The shell of cardium edule, cardium glaucum and ruditapes philippinarum: Organic content, composition and energy value, as determined by different methods. Journal of the Marine Biological Association of the United Kingdom

69:563–572.

Harper, E. M. 2000. Are calcitic layers an effective adaptation against shell dissolution in the Bivalvia? Journal of Zoology 251:179–186.

Hauri, C., N. Gruber, G. Plattner, S. Alin, R. A. Feely, B. Hales, and P. A. Wheeler. 2009. Ocean in the California Current System 22:60–71.

Hudson, J. D. 1967. The elemental composition of the organic fraction, and the water content, of some recent and fossil mollusc shells. Geochimica et Cosmochimica Acta 31:2361–2378.

Johnson, E. H. 2020. Experimental tests of bivalve shell shape reveal potential tradeoffs between mechanical and behavioral defenses. Scientific Reports 10:1–12.

Jones, J. R., A. B. Marín-Arroyo, L. G. Straus, and M. P. Richards. 2020. Adaptability, resilience and environmental buffering in European Refugia during the Late Pleistocene: Insights from La Riera Cave (Asturias, Cantabria, Spain). Scientific Reports 10:1–17.

Jones, S. J., F. P. Lima, and D. S. Wethey. 2010. Rising environmental temperatures and biogeography: Poleward range contraction of the blue mussel, Mytilus edulis L., in the western Atlantic. Journal of Biogeography 37:2243–2259.

Kern, P. J. 1977. Origin and history of upper Pleistocene marine terraces, San Diego, California. Geological Society of America Bulletin 88:1553–1566.

Kern, P. J., and T. K. Rockwell. 1992. Chronology and deformation of quaternary marine shorelines, San Diego County, California. Society for Sedimentary Geology 48:377–382.

Koenig, W. D., and A. M. Liebhold. 2016. Temporally increasing spatial synchrony of North American temperature and bird populations. Nature Climate Change 6:614–617.

Kroeker, K. J., R. L. Kordas, R. Crim, I. E. Hendriks, L. Ramajo, G. S. Singh, C. M. Duarte, and J. P. Gattuso. 2013. Impacts of ocean acidification on marine organisms: Quantifying sensitivities and interaction with warming. Global Change Biology 19:1884–1896.

Kroeker, K. J., R. L. Kordas, R. N. Crim, and G. G. Singh. 2010. Meta-analysis reveals negative yet variable effects of ocean acidification on marine organisms. Ecology Letters 13:1419–1434.

Ku, T.-L., and P. J. Kern. 1974. Uranium-Series Age of the Upper Pleistocene. Geological Society of America Bulletin 85:1713–1716.

Lischka, S., and U. Riebesell. 2012. Synergistic effects of ocean acidification and warming on overwintering pteropods in the Arctic. Global Change Biology 18:3517–3528.

Lockwood, R., and R. Mann. 2019. A conservation palaeobiological perspective on Chesapeake

Bay oysters. Philosophical Transactions of the Royal Society B: Biological Sciences 374.

Lopez, M. I., P. E. Meza Martinez, and M. A. Meyers. 2014. Organic interlamellar layers, mesolayers and mineral nanobridges: Contribution to strength in abalone (Haliotis rufescence) nacre. Acta Biomaterialia 10:2056–2064.

Lowenstam, H. A. 1954. Factors Affecting the Aragonite : Calcite Ratios in Carbonate-Secreting Marine Organisms. The Journal of Geology 62:284–322.

Marquet, N., K. R. Nicastro, M. Gektidis, C. D. Mcquaid, and G. A. Pearson. 2013. Comparison of phototrophic shell-degrading endoliths in invasive and native populations of the intertidal mussel Mytilus galloprovincialis:1253–1272.

Matoo, O. B., G. Lannig, C. Bock, and I. M. Sokolova. 2021. Temperature but not ocean acidification affects energy metabolism and enzyme activities in the blue mussel, Mytilus edulis. Ecology and Evolution 11:3366–3379.

McCoy, S. J., N. A. Kamenos, P. Chung, T. J. Wootton, and C. A. Pfister. 2018. A mineralogical record of ocean change: Decadal and centennial patterns in the California mussel. Global Change Biology 24:2554–2562.

Meyers, M. A., A. Y. M. Lin, P. Y. Chen, and J. Muyco. 2008. Mechanical strength of abalone nacre: Role of the soft organic layer. Journal of the Mechanical Behavior of Biomedical Materials 1:76–85.

Meyers, M. A., A. Y. M. Lin, Y. Seki, P. Y. Chen, B. K. Kad, and S. Bodde. 2006. Structural biological composites: An overview. Jom 58:35–41.

Muhs, D. R. 2022. MIS 5e sea-level history along the Pacific coast of North America. Earth System Science Data 14:1271–1330.

Muhs, D. R., L. T. Groves, and R. R. Schumann. 2014. Interpreting the paleozoogeography and sea level history of the thermally anomalous marine terrace faunas: A case study from the last interglacial complex of San Clemente Island, California. Page Monographs of the Western North American Naturalist.

Muhs, D. R., K. R. Simmons, G. L. Kennedy, K. R. Ludwig, and L. T. Groves. 2006. A cool eastern Pacific Ocean at the close of the Last Interglacial complex. Pages 235–262 Quaternary Science Reviews.

Nam, S., H. J. Kim, and U. Send. 2011. Amplification of hypoxic and acidic events by la Nia conditions on the continental shelf off California. Geophysical Research Letters 38.

National Oceanic and Atmospheric Administration’s National Data Buoy Center. Center of Excellence in Marine Technology. (n.d.). . https://www.ndbc.noaa.gov/.

Palmer, A. R. 1983. Relative cost of producing skeletal organic matrix vs. calcification: evidence from marine gastropods. Marine Biology 75:287–292.

Pfister, C. A., K. Roy, J. T. Wootton, S. J. McCoy, R. T. Paine, T. H. Suchanek, and E. Sanford. 2016. Historical baselines and the future of shell calcification for a foundation species in a changing ocean. Proceedings of the Royal Society B: Biological Sciences 283:20160392.

Poloczanska, E. S., C. J. Brown, W. J. Sydeman, W. Kiessling, D. S. Schoeman, P. J. Moore, K. Brander, J. F. Bruno, L. B. Buckley, M. T. Burrows, C. M. Duarte, B. S. Halpern, J. Holding, C. V. Kappel, M. I. O'Connor, J. M. Pandolfi, C. Parmesan, F. Schwing, S. A. Thompson, and A. J. Richardson. 2013. Global imprint of climate change on marine life. Nature Climate Change 3:919–925.

Poloczanska, E. S., M. T. Burrows, C. J. Brown, J. G. Molinos, B. S. Halpern, O. Hoegh-Guldberg, C. V. Kappel, P. J. Moore, A. J. Richardson, D. S. Schoeman, and W. J. Sydeman. 2016. Responses of marine organisms to climate change across oceans. Frontiers in Marine Science 3:1–21.

R Core Team. 2018. R: A language and environment for statistical computing. R Foundation for statistical computing. Vienna, Austria.

Ries, J. B., A. L. Cohen, and D. C. McCorkle. 2009. Marine calcifiers exhibit mixed responses to CO2-induced ocean acidification. Geology 37:1131–1134.

Roy, K., D. Jablonski, and K. K. Martien. 2000. Invariant size-frequency distributions along a latitudinal gradient in marine bivalves. Proceedings of the National Academy of Sciences 97:13150–13155.

Roy, K., J. W. Valentine, D. Jablonski, and S. M. Kidwell. 1996. Roy et al. 1996 Scales of climatic variability and time avergaing in Pleistocene biotas Implications for ecology and evolution.pdf. Trends in Ecology and Evolution 11:458–463.

SAHAGÚN, L. 2020, July 17. Crowds removing sea creatures from San Pedro tide pools put delicate ecosystem at risk. Los Angeles Times. Los Angeles.

Salas, A., F. Díaz, A. D. Re, C. E. Galindosanchez, E. Sanchez-Castrejon, M. González, A. Licea, A. Sanchez-Zamora, and C. Rosas. 2014. Preferred temperature, thermal tolerance, and metabolic response of tegula regina (Stearns, 1892). Journal of Shellfish Research 33:239–246.

Sanders, T., L. Schmittmann, J. C. Nascimento-Schulze, and F. Melzner. 2018. High Calcification Costs Limit Mussel Growth at Low Salinity. Frontiers in Marine Science 5:1–9.

Soon, T. K., and H. Zheng. 2020. Climate Change and Bivalve Mass Mortality in Temperate Regions. Pages 109–129 Reviews of Environmental Contamination and Toxicology.

Springer New York LLC.

Southern California Coastal Ocean Observing System. (n.d.). . http://sccoos.org/data/autoss/.

Stefano, S., M. Quartagno, M. Tamburini, and D. Robinson. 2018. _orcutt: Estimate procedure in case of first order autocorrelation_.

Taylor, J. D., and M. Layman. 1972. The mechanical properties of bivalve (Mollusca) shell structure.

Telesca, L., L. S. Peck, T. Sanders, J. Thyrring, M. K. Sejr, and E. M. Harper. 2019. Biomineralisation plasticity and environmental heterogeneity predict geographic resilience patterns of foundation species to future change. Global Change Biology Accepted:1–15.

Valentine, J. W. 1960. Habitats and sources of Pleistocene mollusks at Torrey Pines Park, California. Ecology 91:161–165.

Waldbusser, G. G., E. P. Voigt, H. Bergschneider, M. A. Green, and R. I. E. Newell. 2011. Biocalcification in the Eastern Oyster (Crassostrea virginica) in Relation to Long-term Trends in Chesapeake Bay pH. Estuaries and Coasts 34:221–231.

Welladsen, H. M., P. C. Southgate, and K. Heimann. 2010. The effects of exposure to near-future levels of ocean acidification on shell characteristics of Pinctada fucata (Bivalvia: Pteriidae). Molluscan Research 30:125–130.

Zeileis, A., and T. Hothorn. 2002. lmtest.

Zuschin, M., R. J. Stanton, and M. Zuschin. 2017. Experimental Measurement of Shell Strength and Its Taphonomic Interpretation Published by : SEPM Society for Sedimentary Geology Stable URL : http://www.jstor.org/stable/3515527 Linked references are available on JSTOR for this article : Experimental Meas 16:161–170.